Integrated Masters in Chemical Engineering

Packed Bed Membrane Reactor for the Water-Gas Shift Reaction: Experimental and Modeling Work

Masters Thesis

of

Joel Alexandre Moreira da Silva

Developed in the framework of the course of dissertation

performed at

Multiphase Reactors Group, Department of Chemical Engineering & Chemistry, Eindhoven University of Technology

Supervisor at TU/e: **Eng. Arash Helmi, Dr. Fausto Gallucci and Dr. Martin Van Sint Annaland**

Chemical Engineering Department

July of 2013

Acknowledgements

I would like to deeply thank Engineer Arash Helmi for all the advice, patiente, support, encouragement and dedication to this project. His help was fundamental to this project.

I would also like to thank Doctor Fausto Gallucci for all the good advices given and all the help provided during this project.

I would also like to thank Doctor Martin Van Sint Annaland for all the suggestions made regarding the scope of my project and for making this project possible to happen.

Also a special thanks to Masters student Rogelio González for all the help while using the phenomenological models that he was developing.

Also a very special thanks to Joris for the technical support provided to the set-up I used and for all the technical advices.

I would like to thank all SMR group members for making this group such a good one, with such a good environment.

Finally I would like to thank my family and friends for their encouragement and support. They played undoubtedly a very important role during this dissertation project.

Abstract

The main goal of this work was to perform the experimental study of a water-gas shift (WGS) reaction and produced hydrogen separation unit using a Pd membrane. By combining both elements in a single unit it is expected to obtain conversions that go beyond the thermodynamic equilibrium, for a specific operating temperature and feed stream composition, due to the selective removal of hydrogen in the reaction media. It is also expected to obtain a highly pure hydrogen stream that can be used in systems that are highly sensitive to CO poisoning for example. The second main goal of this work was to validate both 1D and 2D pseudo-homogeneous models for the permeation of hydrogen through the Pd membrane and later for the WGS reaction inside the packed bed membrane reactor (PBMR). The possible demonstration of the existence of the concentration polarization effect, considered in the 2D model, was one of the aspects of more focus.

A lab set-up that is continuously available for permeation tests was used. In a first stage this set-up was used to perform the characterization of the permeation of hydrogen through several Pd membranes and in a later stage the set-up was modified so that it would be possible to study the performance of the WGS reaction inside a PBMR. Regarding the catalyst characterization, since it had been already done by a PhD student it wasn't part of the scope of this project. Regarding the activation of the catalyst used, which in this case was $0.5Pt/6CeTiO_2$, it was performed in a lab set-up that is continuously available for kinetics tests. Finally both 1D and 2D models, developed in Delphi 7, which simulate the WGS reaction inside a PBMR were used to simulate the permeation of hydrogen through the Pd membrane used in the membrane reactor. The comparison between the results obtained using both models and the experimental results as well as the quantification of the concentration polarization effect were done.

It can be concluded that the Pd-Ag membrane reactor allowed the conversion of CO beyond the thermodynamic equilibrium, as expected, and simultaneously produce a highly pure hydrogen stream that meets the requirements of the polimer electrolyte membrane fuel cells. It was also possible to validate both phenomenological models for the permeation of hydrogen through the Pd-Ag membrane and verify that the concentration polarization effect is not negligible for some of the conditions tested.

Keywords: hydrogen; water-gas shift; packed bed membrane reactor; concentration polarization.

Resumo

O principal objetivo deste trabalho foi efetuar o estudo experimental de uma unidade de reação de gás-de-água (water-gas shift, WGS) e de separação do hidrogénio produzido por via de uma membrane de Pd. Ao combinar ambos os elementos numa única unidade espera-se conseguir obter conversões que vão além do equilíbrio termodinâmico, para uma determinada temperatura de operação e composição da corrente de alimentação, devido à remoção seletiva do hidrogénio presente no meio reacional. Espera-se também a obtenção de uma corrente de hidrogénio de elevada pureza que possa ser utilizada em sistemas altamente sensíveis ao envenenamento por CO por exemplo. O segundo grande objetivo deste trabalho foi a validação de ambos os modelos pseudo-homogéneos 1D e 2D para a permeação de hidrogénio através da membrana de Pd e posteriormente para a reação de WGS no interior de um reator de membrana de leito fixo. A possível demonstração da existência do efeito da polarização da concentração, tido em conta pelo modelo 2D, foi um dos aspetos ao qual foi dada mais atenção.

Para isto foi utilizada uma instalação laboratorial que está continuamente disponível para testes de permeação. Numa primeira fase esta instalação foi utilizada para efetuar a caracterização da permeação de hidrogénio através de várias membranas de Pd e numa fase posterior a instalação foi alterada para que se pudesse estudar a reação de WGS no interior de um reator de membrana de leito fixo. Em relação à caracterização do catalisador, esta já tinha sido feita por um aluno de PhD sendo que não fez parte da ordem de trabalhos deste projeto. Relativamente à ativação do catalisador usado, que neste caso foi $0.5Pt/6CeTiO_2$, esta foi efetuada numa instalação laboratorial que está continuamente disponível para testes cinéticos. Por fim os modelos 1D e 2D, desenvolvidos no software Delphi 7, que simulam a reação de WGS no interior de um reator de membrana de leito fixo foram usados para simular a permeação de hidrogénio através da membrana de Pd usada no reator de membrana. A comparação entre os resultados obtidos usando os modelos e os resultados experimentais foi feita e a quantificação do efeito da polarização da concentração foi efetuada.

Concluíu-se que o reator de membrana de Pd-Ag permite converter CO para além do equilíbrio termodinâmico, tal como era suposto, e produzir em simultâneo uma corrente de hidrogénio altamente puro que vai de encontro ao requísitos das células de combústivel de membrana eletrolítica polimérica. Foi também possível validar ambos os modelos fenomenológicos para a permeação de hidrogénio através da membrana de Pd-Ag e verificar que o efeito da polarização da concentração não é desprezável para certas condições.

Palavras Chave: hidrogénio; water-gas shift; reator de membrana de leito fixo; polarização da concentração.

Declaration

I declare under oath that this work is original and that all non-original contributions were adequately referenced with the reference identification.

Syllabus

Notation and Glossary

C_H	Concentration of atomic hydrogen at the spacial position x along the membrane thickness	mol·m^{-3}
D_H	Effective diffusion coefficient of atomic hydrogen	m^2·s^{-1}
d_t	Diameter of the membrane tube	m
E_a	Apparent activation energy	kJ·mol^{-1}
$E_{a,Pd}$	Apparent activation energy of the Pd membrane	kJ·mol^{-1}
J	Atomic hydrogen diffusion flux through the metal lattice	mol·m^{-2}·s^{-1}
J_{H_2}	Flux of H_2 through the membrane	mol·m^{-2}·s^{-1}
$J'_{H_2,calc.}$	Predicted total flux of H_2 through the Pd-Ag membrane	mol· s^{-1}
k	Forward reaction rate constant	mol·g_{cat}^{-1}·h^{-1}·Pa^{-2}
k^+	Forward reaction rate constant	mol·g_{cat}^{-1}·h^{-1}·Pa^{-1}
k^-	Reverse reaction rate constant	mol·g_{cat}^{-1}·h^{-1}·Pa^{-1}
k_0	Pre-exponential factor	s^{-1}
K_{CO}	Langmuir's adsorption constant for CO	Pa^{-1}
K_{eq}	Equilibrium constant	
k_f	Forward reaction rate constant	mol·g_{cat}^{-1}·h^{-1}·Pa$^{-(a+b+c+d)}$
K_i	Equilibrium adsorption constant of species i	Pa^{-1} or Pa$^{-1.5}$
k_{Pd}	Membrane constant	mol·m^{-1}·s^{-1}·Pa^{-x}
L	Membrane length	m
$n_{H_2,in}$	Molar flow of H_2 in the feed stream	mol·h^{-1}
$n_{H_2,permeate}$	Molar flow of H_2 in the permeate outlet	mol·h^{-1}
$n_{H_2,retentate}$	Molar flow of H_2 in the retentate outlet	mol·h^{-1}
P_{CO}	Partial pressure of CO	Pa
$P_{H_2,permeate}$	Partial pressure of H_2 in the permeate side	Pa
$P_{H_2,retentate}$	Partial pressure of H_2 in the retentate side	Pa
P_i	Partial pressure of component i	Pa
P_{Pd,H_2}	Permeability of the Pd-Ag membrane to H_2	mol·m^{-1}·s^{-1}·Pa^{-1}
P^0_{Pd,H_2}	Pre-exponential factor	mol·m^{-1}·s^{-1}·Pa^{-1}
$Q^{Permeate}_{H_2,out}$	Volumetric flow of H_2 at the permeate outlet	mL$_N$·min^{-1}
$Q^{Retentate}_{CO,in}$	Volumetric flow of CO at the retentate inlet	mL$_N$·min^{-1}
$Q^{Retentate}_{CO,out}$	Volumetric flow of CO at the retentate outlet	mL$_N$·min^{-1}
$Q^{Retentate}_{H_2,out}$	Volumetric flow of H_2 at the retentate outlet	mL$_N$·min^{-1}
r	Experimental reaction rate	mol·g_{cat}^{-1}·h^{-1}
R	Ideal gas constant	kJ·K^{-1}·mol^{-1}
Re_{H_2}	H_2 recovery	
R_f	Forward reaction rate	mol·$g_{cat}^{-1\cdot h\text{-}1}$
R_{f_0}	Pre-exponential factor	mol·g_{cat}^{-1}·h^{-1}
S	Sorption coefficient of hydrogen in the metal lattice	mol·m^{-3}·Pa$^{-0.5}$
T	Absolute temperature	K
X_{CO}	CO conversion	
$X_{CO,eq}$	Conversion of CO at the equilibrium	
$y_{i,in}$	Molar fraction of the component i at the reactor inlet	

Greek letters

α	H_2 permeance reduction factor	
β	Approach to equilibrium	
δ	Pd-Ag membrane thickness	m
$\Delta H_r^{298\ K}$	Reaction enthalpy at 298 K	kJ·mol^{-1}
ε	Relative error	

Superscripts

a, b, c, d	Forward reaction orders for H_2O, CO, H_2 and CO_2 respectively
x	Pressure exponent

List of acronyms

CSTR	Continuous Stirred-Tank Reactor
FBMR	Fluidized Bed Membrane Reactor
GHSV	Gas Hourly Space Velocity
MR	Membrane Reactor
PBMR	Packed Bed Membrane Reactor
PBR	Packed Bed Reactor
PEMFC	Polymer Electrolyte Membrane Fuel Cell
SRM	Steam Reforming of Methane
TR	Traditional Reactor
WGS	Water-Gas Shift
µ-GC	Micro Gas Chromatograph

Figures Syllabus

Tables Syllabus

1 Introduction

1.1 Framework and Project Presentation

For thousands of years humans have felt the need of using extracorporeal sources of energy simply to heat themselves, to pump water, to move a vehicle or to keep a television on in a rainy Saturday night. At first the human race resorted to the burning of wood and straw, later to the use of the energy of the wind and water, the use of engines based on the ability to harness the power of steam and for many years fossil fuels have been the source of energy on which the worldwide society has been relying the most. [1]

With all the environmental problems identified as a consequence of the use of fossil fuels and also with the still increasing consumption of fossil fuels and the therefore escalating prices of those, renewable energy sources like hydro energy, solar energy and wind energy are becoming more important. However, these renewable sources of energy are not enough to completely take over from the fossil fuels. Hydrogen as an energy carrier has been commonly thought to play an important role in the future in fuel cells as a substitute for conventional internal combustion engines and gas turbines because of, for example, it's higher power density and cleaner exhausts. [2]

Nowadays hydrogen is mostly used in petroleum refining processes such as hydrotreating and hydrocracking and in the petrochemical industry for the production of methanol, ammonia and hydrocarbon synthesis via the Fischer Tropsch process. There are many routes for hydrogen production being that the production processes can be categorized into five types: reforming, electrolysis, nuclear based, photo-catalytic and non-catalytic processes. Considering the feedstocks used, these hydrogen production processes can be divided into fossil based processes that use natural gas, coal, methanol and naphtha, and non-fossil based processes that use water and biomass. [2]

The fossil based routes are the most used for the industrial production of hydrogen, being that the steam reforming of methane (SRM) is responsible for almost 48% of the worldwide hydrogen production. The reforming of naphtha/ oil contributes with 30% and the coal gasification with 18%. [3] A traditional reforming process flow scheme for such a hydrogen plant is presented in Figure 1.

The traditional reforming process involves firstly a feed treatment in order to remove the impurities that are poisonous to the reforming and shift catalysts. The most important process step is the reforming section which can be divided in two sub-steps: the processing of

the feedstock by reforming or gasification and the water-gas shift (WGS) reaction that upgrades the carbon monoxide to hydrogen.

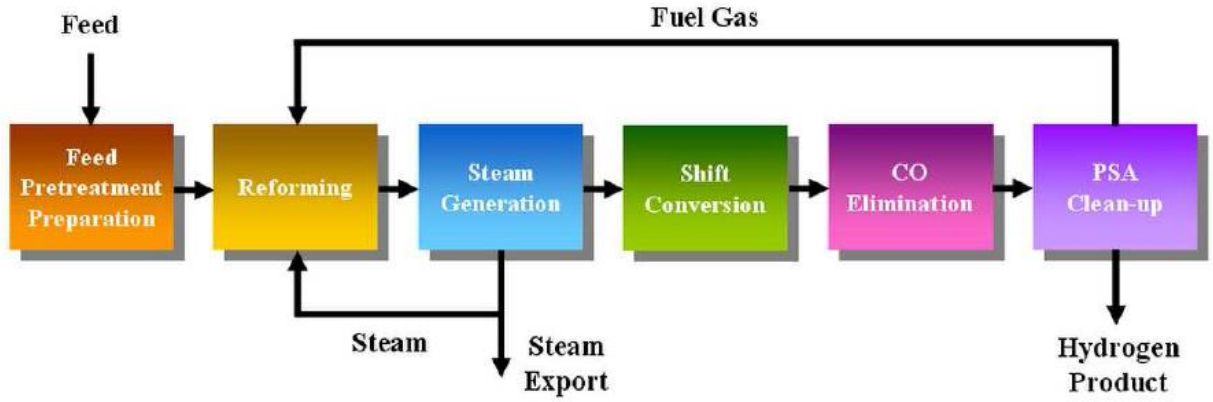

Figure 1 - Process flow in a typical fuel processor operating in the steam reforming mode. Taken from [4]

The basic reactions for the production of hydrogen from natural gas (primarily methane) are as follows:

Endothermic SRM

$$CH4 + H2O \leftrightarrow CO + 3H2 \qquad (\Delta H_r^{298\,K} = 206\ kJ{\cdot}mol^{-1}) \tag{1}$$

Exothermic WGS reaction

$$CO + H_2O \leftrightarrow CO_2 + H_2 \qquad (\Delta H_r^{298\,K} = -41.1\ kJ{\cdot}mol^{-1}) \tag{2}$$

The amount of carbon monoxide can still be decreased through catalytic methanation in the CO elimination step of Figure 1. After methanation other methods such as pressure swing adsorption (PSA), cryogenic distillation or membrane technology can be used to purify even more the hydrogen stream. [5]

Although the SRM is the best current option for hydrogen production, in the future the production of hydrogen may be done through the steam reforming of liquid fuels (e.g. ethanol and methanol obtained from biomass). [4]

As previously mentioned hydrogen fuel cells may take over the conventional internal combustion engines in the future because of being more environment friendly and more efficient. Polymer electrolyte membrane fuel cells (PEMFCs) can generate and deliver electric power in a wide range that can go from micro to mega-watt and because of that they are suitable for many different applications at many different scales (from mobile phones to stationary power stations). Besides that PEMFCs are compact, modular, operate at relative low temperatures (80-110 ºC), have high power density, present fast start-up and response time and have no shielding requirements for personal safety. However, PEMFCs applied to road vehicles still present some technological limitations associated to water management

and CO sensitivity of the anode catalyst. One of the main goals at the moment is to reduce the CO concentration in the H_2 stream fed to the fuel cells to a value lower than 0.2 ppm (ISO, 2008). By doing this it will be possible to avoid CO poisoning of the anode, to reduce the size and increase the efficiency of the PEMFCs. At the moment, the WGS reaction technology may be the most promising process to reduce the CO content in the H_2 streams and that's why it is such a hot topic. [4]

1.2 SMR Presentation

The research group Multiphase Reactors (SMR) is a part of the Faculty of Chemical Engineering at the Technical University of Eindhoven in the Netherlands. The research group SMR focusses on the fundamentals of the discipline of chemical reaction engineering. The main area of interest of SMR is the quantitative description of transport phenomena (including fluid flow) and the interplay with chemical transformations in multiphase chemical reactors. One of the main goals of SMR is the generation of new knowledge and the development of new reactor models with improved predictive capability for this industrially important class of chemical reactors. Through the intended co-operation with other (application oriented) research groups, both fundamental aspects and those closely related to applications are studied through concerted action. [6]

1.3 Work Contributes

In this project a highly permeable Pd-based membrane for hydrogen permeation and a highly active Pt-based catalyst are integrated into a packed bed membrane reactor (PBMR) in order to analyse the performance of the reactor at different operating conditions: temperature, gas hourly spacial velocity (GHSV) and carbon/steam ratio. The experimental data obtained is used to validate both existing 1D and 2D phenomenological models. For the 2D model there is a special attention on the possible verification of the existence of the concentration polarization effect, which is considered by the model.

1.4 Thesis Organization

This Masters dissertation is divided in 4 chapters, being that the first chapter encompasses an introduction to the subject of this project as well as a short presentation of the research group SMR in which all the work was developed and the main goals of the project. The second chapter is called "Context and State of the Art" and consists on a literature review about the current state of all the important subjects addressed.

Chapter 3 is divided in 4 sub-chapters. The sub-chapter 3.1 is called "Membrane characterization" and includes a description of the set-up used for the permeation tests as

well as a list with all the permeation tests performed and the respective results. A discussion of these results is also included. Sub-chapter 3.2 encompasses a description of the PBMR set-up and the list of WGS experiments performed on it as well as the respective results and discussion. Sub-chapter 3.3 includes a short description of both 1D and 2D phenomenological models developed by another Masters student in parallel with the experimental work reported in this thesis. A comparison between the experimental results and the phenomenological models predictions is as well included in order to verify if both models describe adequately the PBMR system, with special focus on the 2D model in order to verify if indeed there is concentration polarisation inside the PBMR. A discussion of the results is included.

In the fourth chapter there are included all the conclusions of the work and in the fifth chapter there are presented all the achieved goals, the limitations of the work, possibilities for future work and a final appreciation of this dissertation project.

2 Context and State of the Art

2.1 History of Hydrogen and the WGS Reaction

Hydrogen has been target of interest by a huge scientific community in the last decades. However it was way before the 20th or 21st century that hydrogen was subject of research. Sometimes the first discovery of hydrogen gas is attributed to the Swiss alchemist Philippus Aureolus Paracelsus in 1520. Paracelsus firstly described a gaseous substance arising as iron that was dissolved in sulphuric acid. He described this substance as "an air which bursts forth like the wind". [7] In 1671 an English chemist and physicist called Robert Boyle published a paper called "New experiments touching the relation between flame and air" in which he described the reaction between iron filings and diluted acids which results in the formation of hydrogen. [8] However hydrogen was only identified as a distinct element by British scientist Henry Cavendish in 1766 after he has separated hydrogen gas by making metallic zinc react with hydrochloric acid. Cavendish demonstrated to the Royal Society of London that by applying a spark to hydrogen gas (in the presence of air) it is possible to produce water. This led him to discover that water is made of hydrogen and oxygen.

In 1783 Jacques Alexander Cesar Charles launched the first hydrogen balloon flight and the name hydrogen was given to the gas by Antoine Lavoisier in 1788. In 1800 William Nicholson and Sir Anthony Carlisle discovered the water electrolysis process. Later in 1839 a Swiss chemist called Christian Friedrich Schoenbein discovered the fuel cell effect which consists on combining hydrogen and oxygen to produce water and an electric current. This discovery was later demonstrated by Sir William Grove on a practical scale through the creation of a "gas battery". For this achievement he gained the title of "Father of the Fuel Cell". In the 1920s Rudolf Erren converted the internal combustion engines of trucks, buses and submarines to use hydrogen or hydrogen mixtures and J.B.S. Haldane introduced the concept of renewable hydrogen. In 1958 the United States formed the National Aeronautics and Space Administration (NASA) and currently NASA's space program use the most liquid hydrogen worldwide, primarily for rocket propulsion and as a fuel for fuel cells. One year later Francis T. Bacon built the first practical hydrogen-air fuel cell with a power of 5kW. Later that year Harry Karl Ihrig demonstrated the first fuel cell vehicle: a 20-horsepower tractor. Hydrogen fuel cells based on Bacon's design have been used to generate on-board electricity, heat and water for astronauts aboard all the space shuttle missions after Apollo spacecraft.

In 1974 it was formed the International Association for Hydrogen Energy (IAHE) and in 1977 the International Energy Agency (IEA) was established in response the global oil market

disruptions. The activities performed in IEA included the research and development of hydrogen energy technologies. During the year of 1990 the world's first solar powered hydrogen production plant became operational. In 1991 Georgetown University in Washington, D.C began developing three 3—foot Fuel Cell Test Bed Buses as part of their Generation I Bus Program. Ten years later they finished their Generation II Bus which uses hydrogen from methanol to power a 100kW fuel cell "engine". During the year of 1998 Iceland unveiled a plan to create the first hydrogen economy by 2030. In 1999 the first European hydrogen fuelling stations were opened in Hamburg and Munich and two years later Ballard Power Systems lunched the world's first volume-produced proton exchange membrane fuel cell system designed with the aim of being integrated into a wide variety of industrial and consumer end-product applications. In 2003 U.S.A. announced an investment of $1.2 billion in a hydrogen fuel initiative to develop the technology for commercially viable hydrogen-powered fuel cells and in the following year a $350 million investment on hydrogen research and vehicle demonstration projects was also done. [9]

However, despite all the applications hydrogen has been used for, a simple question has to be answered: how has hydrogen been produced? As mentioned before, there are many ways to produce hydrogen being that the most used process is the reforming of methane. This process can be divided in two steps: the SRM and the WGS. On this thesis the WGS reaction will be the target of research.

The WGS reaction has been researched for many decades and because of that a vast amount of knowledge about it has been gathered. Ever since its first industrial application considerable research regarding reaction catalyst, process configuration, reactor design, reaction mechanisms and kinetics has been done.

The WGS reaction was observed for the first time in 1780 by Felice Fontana. At the time, Fontana observed that a combustible gas is produced when steam is passed through a bed of incandescent coke. On the following century Ludwig Mond developed the process to produce the so called "Mond gas" (the product of the reaction of air and steam passed though coal/coke – CO_2, CO, H_2, N_2, etc.), which turned to be the basis for future coal gasification processes. Mond and his assistant Carl Langer were the first to use the term "fuel cells" while performing experiments with the first ever working fuel cell using coal-derived "Mond gas". Their biggest difficulty was to feed pure hydrogen to the "Mond battery" because of the large quantities of carbon monoxide present in the "Mond gas", which poisoned the Pt electrode. In order to solve this problem Mond passed "Mond gas" and steam over finely divided nickel at 400 ºC, reacting carbon monoxide and steam to produce carbon dioxide and more hydrogen. After removing CO_2 with an alkaline wash, the hydrogen stream could be successfully fed to the hydrogen cell without poising its electrode. [4] Mond and Langer discovered and reported

for the first time in the literature the WGS reaction in 1888. The first industrial application of this reaction happened in 1913 for the production of synthesis gas, as a part of the Haber-Bosch process of ammonia manufacture. This reaction started being considered as a very important step when it was found that the Fe-based catalyst used in the ammonia synthesis process was polluted and therefore deactivated by carbon monoxide. This meant that the carbon monoxide had to be upgraded to hydrogen and carbon dioxide via the WGS reaction. The WGS reaction was firstly integrated on an industrial scale with the aim to convert the CO in the syngas produced and at that time the reaction was done in a single stage reactor that could reduce the CO level to around 10000 ppm (1%). Since the value was still high, a two-stage system combined with a better catalyst was adopted instead and it resulted in a CO level lower than 0,5%. The WGS reaction followed the increase of hydrogen demand for the production of mainly methanol and ammonia. Also the increasing interest in the production of hydrogen for fuel cells applications required continuous research on the WGS reaction because of the high purity hydrogen needed for these cells, which are highly sensitive to CO poisoning. [4,5,10]

2.2 Thermodynamics of the WGS Reaction

The WGS reaction is an equilibrium-limited reaction and since it is exothermic (equation (2)) the CO conversion and therefore hydrogen production are favoured at lower temperatures as can be seen in equation (3):

$$K_P = exp\left(\frac{4577.8}{T} - 4.33\right) \tag{3}$$

in which K_p is the equilibrium constant and *T* the absolute temperature. As the temperature increases, K_p decreases and consequently the CO conversion at the equilibrium also decreases, as can be seen in Figure 2. Also lower temperatures are favourable from steam economy's point of view. However, the WGS reaction is kinetics controlled at these conditions, consequently requiring highly active and stable WGS catalysts. Typically the WGS reaction is conducted in a two or three-stage converter rather than only one. This embodiment allows a smaller adiabatic temperature rise and a better steam management making the process more economical. The first stage is a high temperature converter that allows a fast CO consumption and the minimization of the catalyst bed volume. The next stages operate at lower temperatures in order to achieve higher conversions, which are limited by the reaction equilibrium. [5]

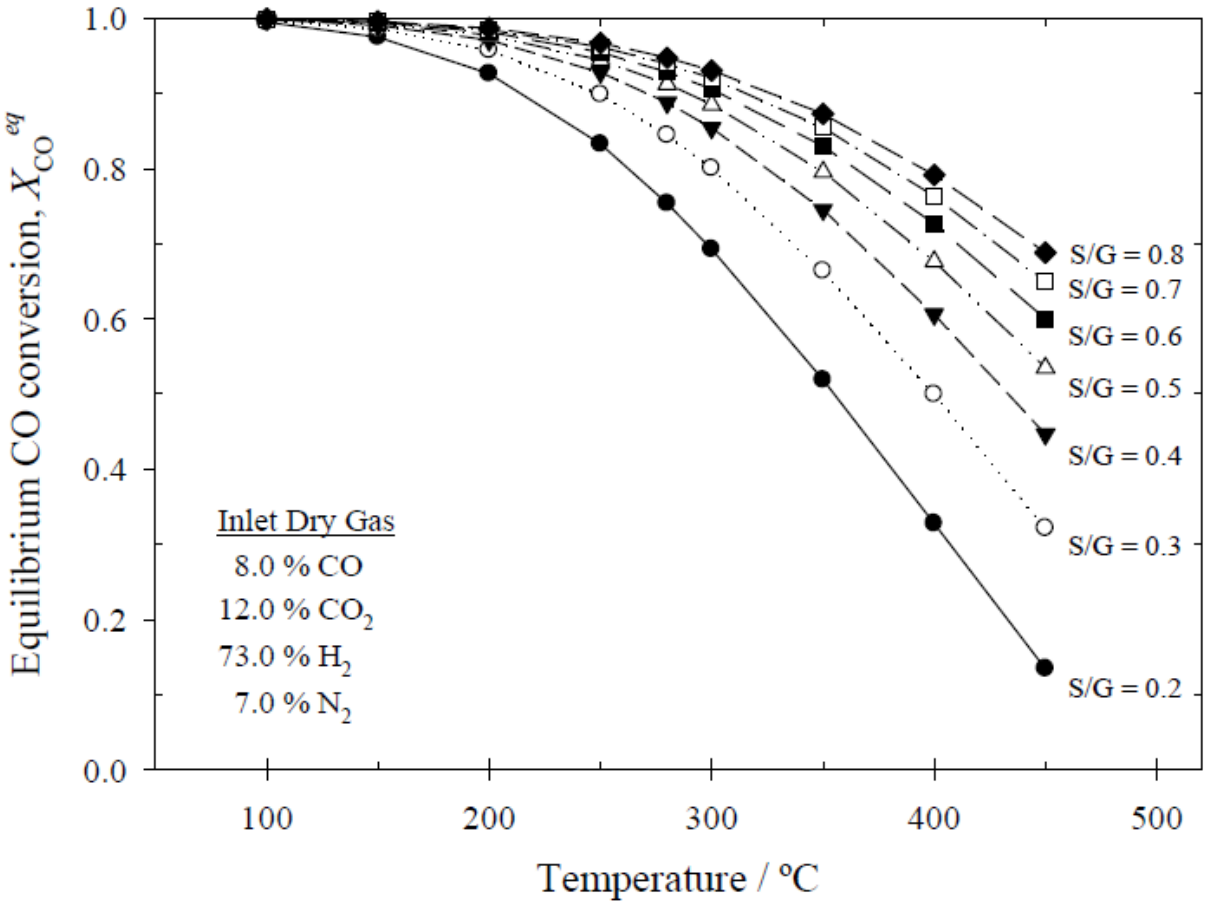

Figure 2 – CO equilibrium conversions of a typical reformate stream from a SRM process for different steam to dry gas (S/G) ratios. Taken from [5]

However, temperature is not the only parameter that affects the CO equilibrium conversion. As can be seen in Figure 2 the amount of steam that is fed to the WGS reactor also influences the CO conversion obtained at

he equilibrium, especially for temperatures higher than 150 ˚C. Of course the amount of steam added to the WGS reactor inlet stream must be decided taking into consideration the operating conditions, the catalyst capacity for H_2O activation, the CO composition desired at the end of the process and the steam available. The composition of the syngas fed to the WGS reactor also affects the CO conversion at the equilibrium ($X_{CO,eq}$), as expressed in equation (4):

$$K_{eq} = \frac{(y_{CO_2,in}+y_{CO,in}X_{CO,eq})(y_{H_2,in}+y_{CO,in}X_{CO,eq})}{[y_{CO,in}(1-X_{CO,eq})](y_{H_2O,in}-y_{CO,in}X_{CO,eq})} \quad (4)$$

being that $y_{i,in}$ is the molar fraction of species *i* at the reactor inlet.

Some of the typical WGS inlet stream compositions used by different authors for WGS tests are presented in Table 1.

Table 1 – Typical WGS inlet stream compositions (vol.%) reported in the literature for WGS tests.

Component	Kalamaras et al. [11][a]	Roh et al. [12][b]	González et al. [13][b]
CO	0.05-9.00	6.5	4.4
CO_2	0.00-18.00	7.1	8.7
H_2O	3.00-20.00	28.7	29.6
H_2	0.00-50.00	42.4	28.0
CH_4	-	0.7	0.1

[a] - Balanced with He.
[b] - Balanced with N_2.

2.3 Catalysts for the WGS Reaction

As mentioned before the catalyst plays a very important role in the WGS reaction. Fe-based catalysts, whether or not combined with Cr, were some of the earliest heterogeneous catalyst to be used in the industry for the WGS reaction. Maroño et al. [14] reported the catalytic activity of a Fe-Cr catalyst for the WGS reaction that allowed the attainment of a CO conversion of 93% at around 380 ˚C. For lower temperatures the CO conversion decreased very fast meaning that this catalyst is not completely suitable for low temperature WGS. In another work Maroño et al. [15] reported the performance of another Fe-Cr based WGS catalysts prepared by co-precipitation and oxi-precipitation. Both catalysts showed good WGS catalytic activity however, they require high temperatures. These catalysts were also compared with a commercial WGS catalyst which consisted on a mixture of iron, chromium and copper oxides. It was noticed that the commercial catalyst was able to catalyse the WGS reaction at lower temperatures probably because of the presence of copper in its composition. Mahadevaiah et al. [16] reported the catalytic activity of two new WGS catalysts: $Ce_{0.67}Fe_{0.33}O_{2-\delta}$ and $Ce_{0.65}Fe_{0.33}Pt_{0.02}O_{2-\delta}$. It was observed that the platinum catalyst presents much higher catalytic activity for the WGS reaction than the other one, even at medium temperatures (≈300 ˚C), due to the synergistic interaction of the Pt ion with Ce and Fe ions. The Fe-based catalysts are known to be cheap and stable but, as it has been concluded, only at high temperatures. The introduction of Cu-based catalysts in the WGS reaction was a very important step forward because of the higher CO conversion and yield in the production of H_2 that they allowed to obtain at lower temperatures, as seen in one of Maroño's work. [5] However, Cu-based catalysts are sensitive to sulphur and chlorine and so

the syngas needs to be properly cleaned before entering in the WGS reaction stage. Also, these catalysts normally only operate within a limited temperature range because of problems with Cu sintering. [5] Zhang et al. [17] showed the sensitivity that Cu-based catalysts show in the presence of H_2S. In their work Zhang's group analysed a series of Fe-based catalysts for the WGS reaction and characterized them after their exposure to H_2S. The Cu-containing catalysts showed a higher sensitivity to H_2S and faster deactivation kinetics than the Cu-free catalysts. This deactivation is probably due to the fact that the catalyst surface oxygen is partially replaced by sulphur, which results in pronounced changes in Fe and Cu coordination environment. [17]

The search for better catalysts that are not only active and stable but also resistant to impurities, like sulphur, continued and Co-based catalysts were found to fulfil all these requirements. However, these catalysts only work well at high temperatures and increase the production of by-products. [5] Au-based catalysts were thought to be promising because of their high activity at low temperatures. Gamboa-Rosales et al. [18] showed that the Au-Co_3O_4/CeO_2 bimetalic catalysts allow higher CO conversion and H_2 yield than the Co_3O_4/CeO_2 catalysts because of the higher dispersion of gold and reducibility. The gold catalysts also showed higher activity for lower temperatures. Sakurai et al. [19] verified that some gold catalysts, like Au (4.0 wt.%)/CeO_2, show high WGS activity at temperatures below 250 °C. However, gold catalysts in general were found to deactivate in a reasonable short period of time under WGS conditions. [5] There have been many explanations to describe de reasons for gold catalysts deactivation like sintering of the metal particles, "irreversible" over-reduction of the ceria support, loss of ceria surface area and blocking of the ceria surface by formation of surface carbonates and/or formats. However, there isn't still a totally coherent explanation for this activity reduction because of the many catalyst morphologies and surface compositions. [5] Pt-based catalysts are very similar to Au-based catalysts, which makes them very strong candidates as well. [5] Roh et al. [12] reported highly active nanosized (1 wt.% Pt/CeO_2) catalysts for the WGS reaction. During their synthesis a white precursor named cerium (III) carbonate precipitated and that precipitate was digested for 0-8 h. When there was no digestion or it was only 2 hours long the Pt catalysts showed lower CO conversion under medium temperatures than for the cases in which the digestion time was 4 and 8 hours. For a 4 hours digestion time the Pt catalyst presented the highest CO conversion (≈80%) and CO_2 selectivity (≈100%). [12] Jeong et al. [20] tested Pt catalysts over CeO_2, ZrO_2 and $Ce_{(1-x)}Zr_{(x)}O_2$ for a single stage WGS reaction. The Pt/CeO_2 catalyst presented a CO conversion of approximately 85% while the Pt/$Ce_{0.8}Zr_{0.2}O_2$ catalyst converted 80% of the CO approximately, both at the same temperature between 300 and 350 °C. The Pt/$Ce_{0.6}Zr_{0.4}O_2$ catalyst presented a CO conversion slightly lower than 80% for the same temperature while the Pt/$Ce_{0.4}Zr_{0.6}O_2$ catalyst only originated this conversion at a temperature slightly above 350 °C.

The other Pt catalysts with lower cerium content support (20% and no cerium) showed low CO conversions. Also the CeO_2 supported catalyst besides presenting a good stability was the one that presented the lowest activation energy. This makes Pt/CeO_2 a promising catalyst for single stage WGS reaction. [20] Also, González et al. [13] compared the performance of three different Pt catalysts supported on CeO_2, TiO_2 and $Ce\text{-}TiO_2$. The Pt catalyst supported on Ce-modified TiO_2 support was the one that presented the best activity and better stability at temperatures higher than 300 °C than that of the TiO_2 supported one. González et al. believe that the fact that the contact between Pt and Ce in the $Pt/Ce\text{-}TiO_2$ catalyst eases the reducibility of the ceria component in the support at lower temperatures is the cause for the better activity and stability of this catalyst for the WGS reaction. [13]

In order to decide what catalyst is going to be used some more aspects need to be considered. Has it is known, the presence of WGS products (H_2 and CO_2) is disadvantageous since they inhibit the WGS catalysts thus lowering the reaction rate. This inhibition effect depends not only on the nature of the catalyst that's used but also on the temperature range at which the reaction occurs. Consequently the reaction effectiveness can be highly improved when membrane reactors (MRs) are used instead of traditional reactors (TRs). For the case of using MRs for the WGS reaction two situations are possible depending on the nature of the membrane used. If a hydrogen perm-selective membrane is used, the concentration of CO_2 in the reaction medium will be higher, which affects the reaction rate. If a CO_2 perm-selective membrane is used, then the hydrogen concentration in the reactor medium will be high thus affecting also the reaction rate. For some Fe-based catalysts the presence of hydrogen at high concentrations is adverse since it over-reduces the magnetite active phase.

As can be seen in Table 2 Cu-based catalysts performance is slightly more affected in the presence of WGS products than Au or Pt catalysts, for similar temperatures, pressures and feed composition. By making a comparison between Pt and Au catalysts it may be fair to say that Pt-based WGS catalysts are one step ahead since they present lower inhibition by WGS products than Au-based catalysts (Table 2) and also, because the science of Au catalysis is relatively new and so there's a bigger know-how about Pt catalysts. Therefore a Pt-based catalyst is used in this project for the WGS reaction carried out inside a MR.

2.4 Mechanisms and Kinetics

In this section a small review on the WGS reaction kinetics and mechanisms is done. The reaction rate for the WGS reaction is normally written as follows:

$$r = R_f\,(1 - \beta) \tag{5}$$

$$R_f = R_{f_0} exp^{\left(-\frac{E_a}{RT}\right)} \quad (6)$$

$$\beta = \frac{P_{CO_2} P_{H_2}}{K_{eq} P_{CO} P_{H_2O}} \quad (7)$$

where r is the experimental reaction rate, R_f is the forward reaction rate, R_{f_0} is the pre-exponential factor, β is the approach to equilibrium, P_i is the partial pressure of component i, E_a is the apparent activation energy and R is the gas constant.

In Table 2 there are presented some important literature values of kinetic parameters obtained for some of the most relevant WGS catalysts. In terms of apparent activation energy, a comparison between both Fe_3O_4/Cr_2O_3 catalyst and 1% Pt/Al_2O_3 catalyst (higher temperatures) can be done being thus possible to notice that even without WGS products in the feed stream, the Fe-based catalyst presented a higher apparent activation energy than the Pt-based catalyst. This suggests that the reaction mechanism or the rate-determining step for the Fe catalyst may be different from that of the other catalysts. By making a comparison between the Al_2O_3 supported catalysts and the CeO_2 supported catalysts in terms of apparent activation energy, it is possible to conclude that overall the CeO_2 supported catalysts present lower apparent activation energy. In particular, the 8% CuO/15% CeO2/Al_2O_3 catalyst is the one that presents the lowest apparent activation energy. This might be due to the increase of the reducibility of the surface oxygen in the ceria support, which probably results from the addition of Cu. [5]

Normally the reaction rate data are fitted to a power-law with the following form:

$$r = k_f P_{H_2O}^a P_{CO}^b P_{H_2}^c P_{CO_2}^d (1 - \beta) \quad (8)$$

where $a - d$ are the forward reaction orders and k_f is the forward reaction rate constant. By analysing Table 2 once again it can be observed that for the Pt-based catalysts all the apparent reaction orders except the H_2O reaction order are very similar. Also, the apparent activation energies are quite close. In terms H_2O apparent reaction orders for Pt catalysts, the alumina-supported catalysts present values close to 1 while the ceria-supported ones present values near to 0.5. This difference suggests that different reaction mechanisms and/or different sites for H_2O activation may exist for these materials. Also by analysing the H_2O apparent reaction orders for both Au-based catalysts in Table 2 it can be concluded that the 4.5 wt% Au/CeO_2 catalyst, for which the H_2O concentration at the inlet stream was higher, presents a H_2O apparent reaction order higher than the 2.6 wt% Au/CeO_2 catalyst. This can be explained by the occurrence of H_2O dissociation on the catalyst surface, where OH groups react with hydrogen to produce water. This means that the WGS reaction is sensitive towards the partial pressure of water in the feed stream. Also, competitive adsorption between H_2O and H_2 may happen. [5]

Table 2 - Apparent activation energies and reaction orders for the forward WGS reaction.

Catalyst	Operating conditions[a]	E_a (kJ·mol^{-1})	Reaction order[b]				Reference
			H_2O	**CO**	**H_2**	**CO_2**	
1% Pt/Al_2O_3	1 atm, 285 ˚C	68	1.0 (10-46%)	0.06 (5-25%)	-0.44 (25-60%)	-0.09 (5-30%)	[21]
1% Pt/Al_2O_3	1 atm, 315 ˚C	84	1.1 (10-46%)	0.1 (5-25%)	-0.44 (25-60%)	-0.07 (5-30%)	[21]
1% Pt/CeO_2	1 atm, 200 ˚C	75	0.44 (10-46%)	-0.03 (5-25%)	-0.38 (25-60%)	-0.09 (5-30%)	[21]
2% Pt/CeO_2-ZrO_2	1.3 bar, 210-240 ˚C	71	0.67	0.07	-0.57	-0.16	[22]
2% Pt-1%Re/CeO_2-ZrO_2	1.3 bar, 210-240 ˚C	71	0.85	-0.05	-0.32	-0.05	[22]
4.5 wt% Au/CeO_2	1bar, 180 ˚C	-	1.0 (5-20 kPa)	1.0 (2-5 kPa)	-0.7 (50-78 kPa)	-0.5 (5-20 kPa)	[23]
2.6 wt% Au/CeO_2[c]	1bar, 180 ˚C	40	0.5 (0.7-10 kPa)	0.5 (0.2-2 kPa)	-0.5 (3.2-75 kPa)	-0.5 (1.2-3.4 kPa)	[24]
40% $CuO/ZnO/Al_2O_3$	1 bar, 190 ˚C	79	0.8 (10-46%)	0.8 (5-25%)	-0.9 (25-60%)	-0.9 (5-30%)	[25]
8% CuO/CeO_2	1 bar, 240 ˚C	56	0.4 (10-46%)	0.9 (5-25%)	-0.6 (25-60%)	-0.6 (5-30%)	[25]
8% CuO/Al_2O_3	1 bar, 200 ˚C	62	0.8 (10-46%)	0.9 (5-25%)	-0.8 (25-60%)	-0.7 (5-30%)	[25]
8% CuO/15% $CeO2/Al_2O_3$	1 bar, 200 ˚C	32	0.6 (10-46%)	0.7 (5-25%)	-0.6 (25-60%)	-0.6 (5-30%)	[25]
Fe_3O_4/Cr_2O_3	1 bar, 450 ˚C	118	0.0 (20-75%)	1.0 (10-40%)	-	-	[26]

[a] - Temperature and total pressure at which the reaction order experiments were carried out.
[b] - The values between brackets are the ranges of concentrations for each species in the feed, or their partial pressures.
[c] - The reaction orders for H_2O and CO were obtained in the absence of H_2 and CO_2 in the feed stream.

In terms of CO apparent reaction order, the values for Pt catalysts are close to zero (sometimes positive, sometimes negative). Since CO highly adsorbs on the Pt surface its coverage is close to saturation and thus, an increase in the CO partial pressure normally has no effect on the reaction rate or can even reduce it due to surface blocking, even at high pressures and low temperatures. For Au-based catalysts it can be seen that an increase in the CO partial pressure increases its apparent reaction order. This happens because CO adsorption on Au is very weak and so only a low coverage of the surface is obtained for lower pressures. [5]

Regarding the H_2 apparent reaction order for Pt catalysts it can be observed that H_2 highly adsorbs on Pt thus inhibiting the WGS reaction. This may be explained by the possibility that after CO has achieved the coverage saturation, the free Pt sites available for H_2O activation may be occupied by atomic hydrogen thus inhibiting the forward WGS reaction. The same situation can be observed for the case of Au catalysts. Finally, for the case of CO_2 partial reaction order the low values in Table 2 for Pt catalysts may be due to the weak interaction between CO_2 and Pt. On the other hand, for Au catalysts the inhibition effect is much more significant. This may be explained by the blocking of ceria surface sites and/or increase of the reverse reaction due to a higher amount of carbonate species adsorbed at the active sites. [5]

As mentioned before, Pt catalysts present different apparent reaction orders depending on, for example, the material used in the support. This suggests that there are different reaction mechanisms or rate-limiting steps for the WGS reaction over this kind of materials. Until now two main reaction mechanisms have been proposed: the regenerative mechanism and the Langmuir-Hinshelwood mechanism.

The regenerative mechanism, sometimes called oxidation-reduction cycle, encompasses first the dissociation of water on the catalyst surface producing H_2 and oxidizing the respective active site (*). In order to complete the cycle the reduction of the oxidized site is promoted by a CO molecule yielding CO_2. This two steps mechanism can be presented as follows [5]:

$$H_2O + (*) \leftrightarrow H_2 + (O) \tag{9}$$

$$CO + (O) \leftrightarrow CO_2 + (*) \tag{10}$$

Considering that equation (10) is the rate-limiting step, one of the earliest WGS reaction rate expression was proposed as follows:

$$r = k^{+} P_{CO} \left(\frac{P_{H_2O}}{P_{H_2}}\right)^{\frac{1}{2}} - k^{-} P_{CO_2} \left(\frac{P_{H_2}}{P_{H_2O}}\right)^{\frac{1}{2}} \tag{11}$$

where k^+ is the forward reaction rate constant and k^- is the rate constant of the reverse reaction.

The Langmuir-Hinshelwood mechanism involves 6 steps:

- Dissociative adsorption of water to form reactive hydroxyl groups;
- Adsorption of CO;
- Combination of the adsorbed CO with the reactive hydroxyl groups to form an intermediate structure that normally is a formate and/or carbonate;
- Decomposition of the intermediate structure into CO_2 and H_2.

$$H_2O + 2(*) \leftrightarrow H^* + OH^* \quad (12)$$

$$CO + (*) \leftrightarrow CO^* \quad (13)$$

$$OH^* + CO^* \leftrightarrow HCOO^* + (*) \quad (14)$$

$$HCOO^* + (*) \leftrightarrow CO_2(*) + H(*) \quad (15)$$

$$CO_2^* \leftrightarrow CO_2 + (*) \quad (16)$$

$$2H^* \leftrightarrow H_2 + (*) \quad (17)$$

A kinetic expression (equation (18)) for the WGS reaction rate over a Cu-based catalyst at low temperatures was proposed considering that the surface reaction between molecularly adsorbed reactants to form a formate intermediate and atomically adsorbed hydrogen is the rate-limiting step.

$$r = \frac{k\left(P_{CO}P_{H_2O} - \frac{P_{CO_2}P_{H_2}}{K_{eq}}\right)}{\left(1 + K_{CO}P_{CO} + K_{H_2O}P_{H_2O} + K_{H_2}^{0.5}P_{H_2}^{0.5} + K_{CO_2}P_{CO_2}P_{H_2}^{0.5}\right)} \quad (18)$$

Where k is the forward reaction rate constant and K_i is the equilibrium adsorption constant of species i. [5]

2.5 Hydrogen Purification

The purification of the hydrogen stream that comes either directly from the reactor or from the catalytic methanation process is a very important step towards the achievement of a final high pure hydrogen stream. There are different methods to purify hydrogen like PSA, cryogenic distillation, or membrane separation. Unlike traditional processes, which produce a stream with medium purity (94-97%) of hydrogen, the PSA process allows the attainment of 99,9% purity hydrogen. The PSA process has been used since the 1980's in almost all hydrogen plants not only because of the higher purification of hydrogen but also because it requires

less unit operations and consequently is less complex from the operational point of view. The PSA-based process needs only a high temperature WGS stage while the traditional process requires not only the high temperature stage but also the low temperature one. The PSA-based process is also advantageous because of the lower steam to carbon ratios that it requires and because it produces a hydrogen stream completely free of methane. [5] In Figure 3 there are presented the process schemes for both traditional and PSA-based hydrogen production and purification.

Besides the PSA process there is an even more promising purification process: membrane separation. The membrane separation process is based on the selective permeation of hydrogen through the membrane. Separation membranes have potential to be long-lasting and cheap what makes them highly attractive. The combination of membrane separation and the WGS reaction (as can be seen in Figure 3) became a very appealing subject because for the case of equilibrium-limited reactions, the continuous removal of hydrogen or carbon dioxide from the reaction medium, depending on the type of membrane used, allows the shifting of the reaction equilibrium towards the formation of products, in other words higher conversions. [5, 27]

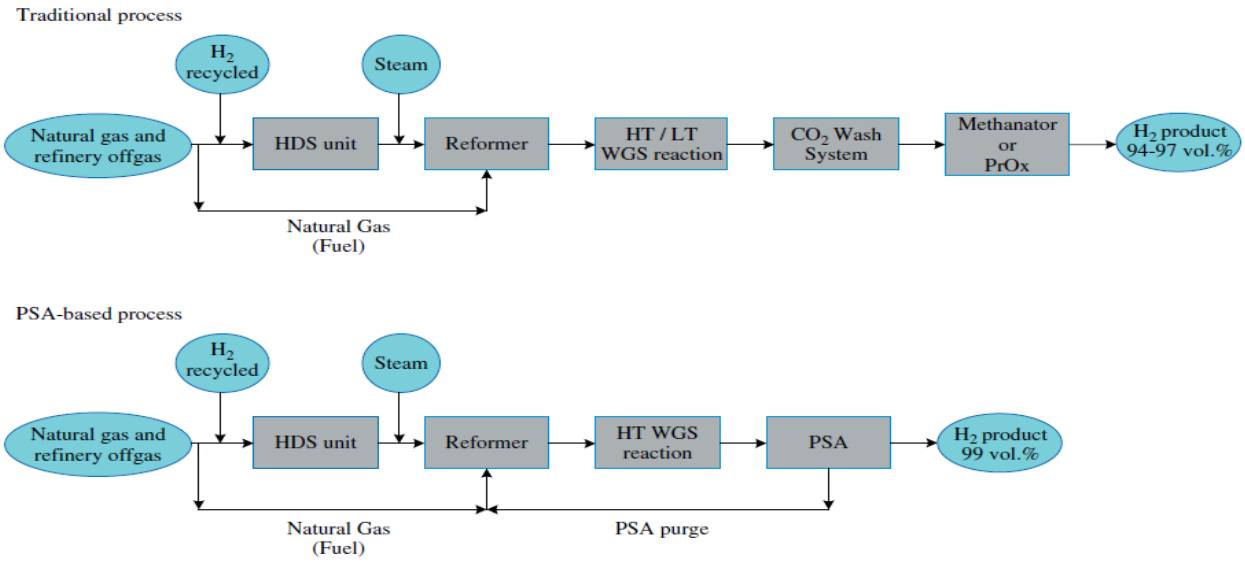

Figure 3 - Process schemes for the hydrogen production and purification; (a) traditional process considering an absorption and catalytic approach for hydrogen purification (b) PSA-based hydrogen purification. Taken from [5]

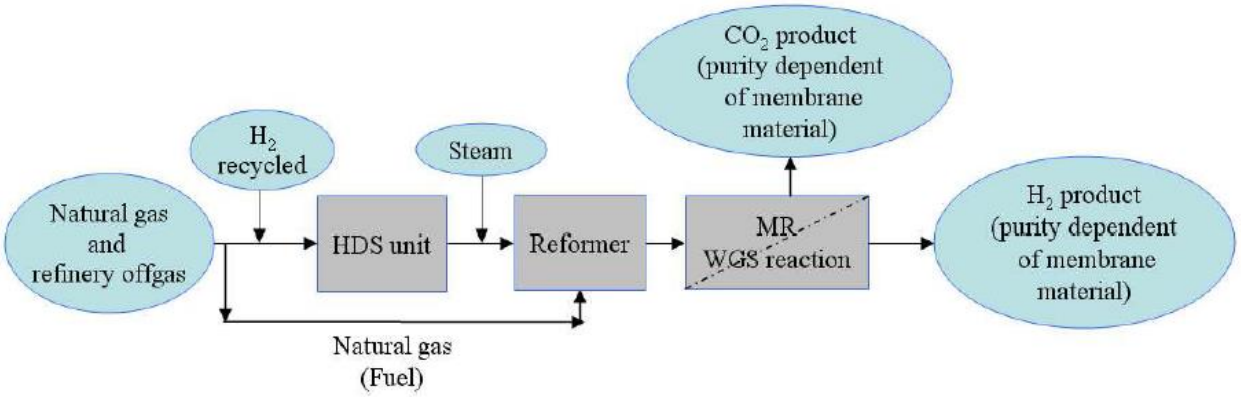

Figure 4 - Hydrogen production and purification based on the WGS MR unit. Taken from [5]

2.6 Membrane Reactors

A MR is a device for simultaneously carrying out a reaction and a membrane-based separation in the same physical device. Taken from [5] MRs present consequently many advantages when compared to TRs, being that the main ones are:

- Conversion enhancement of equilibrium-limited reactions;
- Enhancement of the hydrogen yield and hydrogen selectivity (in the case of hydrogen production);
- Attainment of the same performance obtained in the TR at milder operating conditions, meaning that it is possible to reduce material costs and because of the lower temperatures used new heat integration strategies must be adopted;
- Achievement of better performance at the same operating conditions as in the TR;
- Reduced capital costs due to the combination of reaction and separation in only one system. [5]

There are three main types of membranes: organic membranes, inorganic membranes and organic/inorganic hybrid membranes. Normally inorganic membranes present several advantages over the organic ones, like superior stability and good chemical and mechanical resistance at temperatures above 100 °C. [5] The inorganic membranes, in particular, can either be dense or porous, made from metals, carbon, ceramics or glass. Also inorganic membranes for MRs can be inert or catalytically active. Pd membranes and its alloys with Ni, Ru or Ag are dense inorganic membranes while alumina membranes, silica membranes, titania membranes, glass membranes and stainless steel membranes are porous membranes. Usually dense membranes present higher selectivities for a specific component than porous membranes. However, permeability is also a very important factor to have in consideration.

As expected dense membranes present lower trans-membrane fluxes than porous membranes.[2] Considering now the case of the WGS reaction and the attempt to produce hydrogen enough purified to be used in PEMFCs, it is possible to conclude that it is preferable to use H_2 perm-selective membranes in order to isolate H_2 instead of using CO_2 perm-selective membranes and having hydrogen mixed with steam and some unreacted CO. Also, since the purity of the hydrogen obtained is more important than its quantity, it is preferable to choose a high hydrogen selectivity membrane (dense inorganic membranes).

2.7 Dense H_2 Perm-Selective Membranes for Membrane Reactors

A new challenge that is encountered with MRs is the membrane itself. There are different types of membranes and the membrane to be used needs to be adjusted so that it can be used in a MR. Pd-based membranes are the most promising for the WGS MR technology because of the very high hydrogen selectivity that they present. This means that the permeate (the stream that goes through the membrane) contains almost pure hydrogen as can be seen in Figure 5, while the retentate contains all the substances that don't go through the membrane.

However, Pd membranes are sensitive to poisoning and can suffer some embrittlement in the presence of H_2 at low temperatures. When combined with other metals, like Ag or Cu

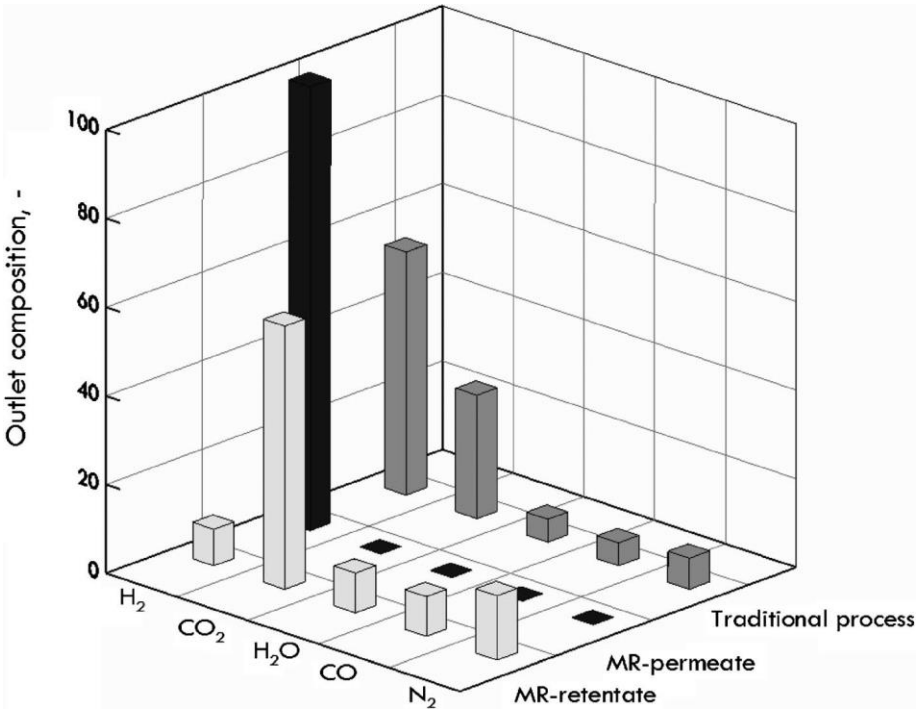

Figure 5 - Composition of the outlet stream of a MR and a traditional process with a typical composition of syngas coming out of a reformer and a H_2O/CO molar ratio of 1. Taken from [27]

among others, Pd-based membranes may get less susceptible to these effects. [28] Also it has been shown by Tosti et al. [29] that self-supported dense and thin wall Pd-Ag 23 wt% tubular membranes with finger-like configuration have high durability and reliability since complete hydrogen selectivity and none failure were observed after at least one year of thermal and hydrogenation cycles. These Pd-Ag 23 wt% membranes were also shown to be highly permeable to hydrogen. These characteristics all together with the reduced costs make this technology ready for being used in the production of highly pure hydrogen in energetic and industrial applications (PEMFCs for example). [29]

Normally it is considered that the permeability of hydrogen through a Pd-based membrane can be described by a solution-diffusion mechanism and the trans-membrane flux can be described by the following equation:

$$J_{H_2} = \frac{P_{Pd,H_2}}{\delta}\left(P^{x}_{H_2,retentate} - P^{x}_{H_2,permeate}\right) \quad (19)$$

where J_{H_2} is the hydrogen flux, P_{Pd,H_2} is the permeability of the membrane, δ is the thickness of the membrane, $P_{H_2,retentate}$ and $P_{H_2,permeate}$ are the partial pressures of H_2 in the retentate and in the permeate respectively and x is the pressure exponent. The ratio $\frac{P_{Pd,H_2}}{\delta}$ is normally termed permeance or pressure normalized flux. The pressure exponent varies between 0.5 and 1. This exponent is 0.5 (Sieverts' law) when the diffusion of atomic hydrogen through the metallic lattice of the membrane is the limiting step. The dependency on temperature of the permeability of the membrane is described below:

$$P_{Pd,H_2} = P^{0}_{Pd,H_2} exp\left(-\frac{E_{a,Pd}}{RT}\right) \quad (20)$$

where P^{0}_{Pd,H_2} is the pre-exponential factor and $E_{a,Pd}$ is the apparent activation energy of the Pd membrane.

In Table 3 a literature review on different Pd-based membranes that have been reported over the years is presented. Some parameters such as membrane thickness, hydrogen flux through the membrane, hydrogen permeability, ideal H_2/N_2 selectivity and apparent activation energy are compared.

By analysing Table 3 it can be concluded that thicker Pd-Ag membranes in general present a better combination of permeability and selectivity of hydrogen, mainly because of the infinite H_2/N_2 ideal selectivity, which is very important because of the desired purity for the hydrogen used in PEMFCs. However they are too thick to be industrially implemented because of the high costs that its implementation at a high scale would involve. Although thinner membranes are very promising in terms of permeability and also because of their low thickness and therefore potential for future industrial implementation, they still are quite limited in terms of selectivity and durability. In this project thin Pd membranes were initially

used because of the above mentioned potential. However, due to the problems previously stated a Pd-Ag membrane with a 50 μm thickness was finally selected.

Table 3 - Data for different Pd-based membranes from the literature.

Membrane	T (°C)	ΔP (kPa)	δ (μm)	Permeability to H_2 ($mol \cdot m^{-1} \cdot s^{-1} \cdot Pa^{-0.5}$)	Ideal Selectivity H_2/N_2	$E_{a,Pd}$ ($kJ \cdot mol^{-1}$)	Reference
Pd-Ag	200-300	10-150	50	5.74×10^{-9}[a]	∞	10.72	[4,30]
Pd-Ag	350-400	100-400	61	1.0×10^{-8}	∞	11,24	[29]
Pd-Ag	352	800	84	1.90×10^{-8}[a]	∞	2.92	[31]
Pd-Cu-Y	400	-	2.0	5.2×10^{-9}	>10000	-	[32]
Pd-Cu-Mo	400	-	2.0	3.5×10^{-9}	>10000	29.0	[32]
Pd-Au	400	-	2.0	1.1×10^{-8}	>10000	-	[32]

[a] - Calculated value.

2.8 The WGS Reaction in Packed Bed Membranes Reactors

There are two main types of MRs: PBMR and FBMR). In this thesis the focus is on the analysis of a PBMR.

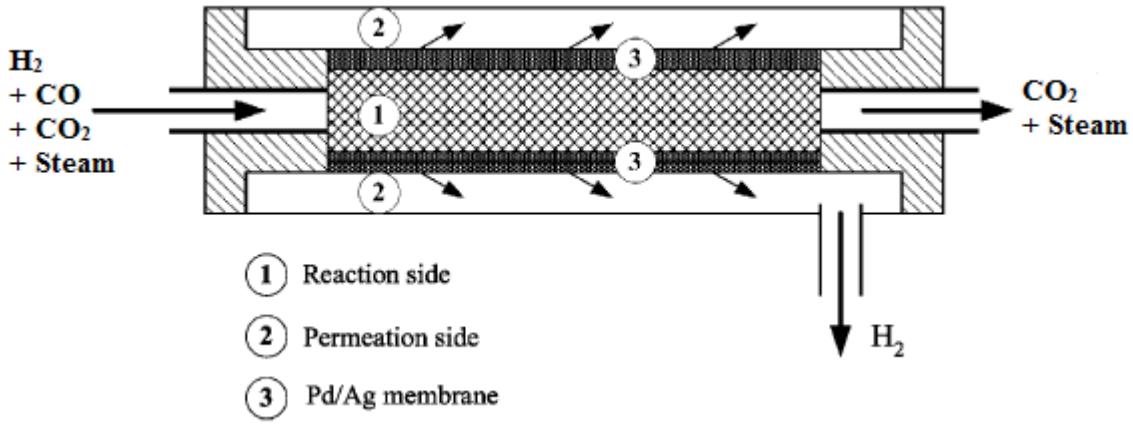

Figure 6 - Scheme of a PBMR for the WGS reaction. Adapted from [10]

With the membrane integrated in the packed bed reactor only one process unit is needed for the WGS. Normally Pd-based membranes are used, as mentioned before, so that a pure hydrogen stream can be produced. After being inserted in the reactor the Pd-based membrane is filled with a WGS catalyst (if the permeation occurs from the inside to the

outside of the membrane). At increased pressures it is possible to achieve almost complete conversion of CO. A particularity of PBMR is that there are mass transfer limitations from the catalyst bed to the membrane surface (concentration polarization) unless a sufficiently small tube diameter is used. However, decreasing the tube diameter implies using smaller catalyst particles whose minimum size is restricted by the pressure drop restrictions. [10, 33]

There are 4 important parameters that have always to be considered in a PBMR because of their influence on the CO conversion and H_2 recovery: operating temperature, retentate pressure, H_2O/CO ratio and the gas hourly space velocity.

Mendes et al. [34] showed that by performing the WGS reaction in a PBMR the equilibrium can be shifted resulting in a higher CO conversion. Also, for increasing temperatures it was verified that the CO conversion decreased while the H_2 recovery kept increasing. This happens because the permeability of the Pd membrane increases with increasing temperatures and on the other hand, since the WGS reaction is exothermic higher temperatures don't favour the CO conversion.

Mendes group also showed that for increasing GHSVs the CO conversion decreases, especially for lower temperatures. The hydrogen recovery is highly affected as well. Regarding the pressure influence it was verified that for higher retentate pressures both CO conversion and H_2 recovery increase since the driving force for hydrogen permeation through the membrane is higher and, consequently the equilibrium is more shifted towards higher conversions. [34]

In terms of H_2O/CO ratio Mendes group analysed the effect of both CO and steam inlet concentration on the performance of the PBMR. When the CO content is increased while keeping the steam concentration constant both CO conversion and H_2 recovery are negatively affected. This happens because higher concentrations of CO inhibit more the H_2 permeability of the Pd membrane and in some cases also because the catalyst is negatively affected because of the negative partial order with respect to CO. On the other hand by increasing the steam amount while keeping the CO content constant both CO conversion and H_2 recovery are enhanced. This can be explained by the fact that for some catalysts the amount of steam fed to the reactor is crucial for their performance (the Pt catalysts presented on Table 2 present this behaviour). Also the Le Chatelier's principle was verified for conversions beyond the thermodynamic equilibrium meaning that higher steam concentrations result in higher H_2 production. [34] Also, higher amounts of steam allow avoiding carbon deposition on the WGS catalyst.

2.9 Modeling Studies on the WGS Reaction Carried in Packed Bed Membrane Reactors

In the last decades there has been a huge effort on trying to simulate the WGS reaction in PBMRs as realistic as possible. There have been reported many 1D and 2D models for PBMRs considering many assumptions.

For 1D models normally the following assumptions are made:

- Steady-state and isothermal operation;
- Axially dispersed plug-flow pattern in the retentate side with pressure drop described by Ergun's equation;
- Radial temperature and concentration gradients are ignored;
- Ideal plug flow pattern in the permeate side without any pressure drops;
- Ideal gas behavior. [30, 33]

In the case of 2D models generally the following assumptions are comprised:

- The mass and energy transport in the gas phase is described as convective flow with axial and radial dispersion;
- The particle size is sufficiently small so that it can be considered that intra-particle mass and heat transfer limitations as well as external mass and heat transfer limitations from the gas bulk to the catalyst surface can be neglected;
- Homogenous gas phase reactions are ignored due to the relatively low temperatures;
- The gas bulk is described as an ideal Newtonian fluid. [2, 33]

Marín et al. [35] concluded that intra-particle mass transfer limitations are not negligible and so generalized Thiele modulus, apparent kinetic parameters or empirical fitting of external efficiency were proposed.

In this thesis project the validation of both 1D and 2D existing phenomenological models is done being that the main focus is on the validation of the radial dispersion, as known as concentration polarisation effect, considered in the 2D model, since until now it has seldom been done. Tiemersma et al. [10] reported a 2D model to study the performance of the autothermal reforming (ATR) of methane in a PBMR. This model included the assumption of the existence of the concentration polarization effect however, it was not validated with experimental data for the ATR of methane in a PBMR.

3 Technical Description

In this section it is made a description of all the tasks performed during this Masters thesis project. The main results obtained are presented and discussed as well.

3.1 Membrane Characterization

In this project two Pd membranes with 3.5-4.0 μm and 4.0-5.0 μm thickness, both supported on porous ceramic supports, developed at TECNALIA group were firstly used for H_2 permeation tests. Both membranes permeated hydrogen from the outside to the inside part. The thinner membrane was tested for a period of two weeks at the end of which started showing N_2 leaks (results showed in Appendix A). The second membrane started showing N_2 trans-membrane flows in the second day of experiments (results showed in Appendix A). For this reason a Pd-Ag membrane with a thickness of 50 μm developed at ENEA group was used to purify the H_2 generated during the WGS reaction. Unlike the other 2 membranes this one permeates hydrogen from the inside to the outside part. Before the incorporation of the membrane in the PBMR a set of permeation tests was performed with the aim of characterizing the permeation of H_2 through the membrane.

3.1.1 Experimental set-up

To feed pure H_2 or gas mixtures to the stainless steel tube in which the Pd membrane is encased four mass flow controllers (Brooks Smart Mass Flow II, model SLA) were used. The pure H_2 or gas mixture can either go to the stainless steel tube or bypass it and go straight to the ventilation or to the micro gas chromatograph (μ-GC) (Varian, CP-4900 series) equipped with two chromatographic Mol-sieve (5A) columns and a Poraplot Q (PPQ) column to analyse the gas streams. One of the Mol-sieve columns is used for the detection of N_2, CO, CH_4 and O_2, while the other is used for the detection of H_2 or He. The PPQ is used to measure the concentration of CO_2 and traces of water. More details regarding the analysis method can be found in Appendix B. The stainless steel tube is encased inside an electrical oven (Carbolite®, Type 3216|p1 p5) that is controlled by a programmable temperature controller. Two thermocouples were inserted through the top of the reactor for reading the temperature at the surface of the stainless steel tube, both distanced by a distance equivalent to the membrane length. This way it was possible to monitorize the maximum temperature difference at the outside surface of the metallic tube. Also a thermocouple was inserted inside the stainless steel tube in order to be close to the membrane surface. The pressures in the feed and in the retentate and permeate outlets were measured with three pressure transmitters (Druck, PTX 1400). The trans-membrane pressure was adjusted through a manual pressure control valve that on its hand controlled the retentate pressure. The permeate was

kept at atmospheric pressure. After the permeation process the permeate stream flow is measured by a mass flow meter (Brooks Smart Mass Flow II, model SLA). This mass flow meter is able to measure H_2 flows up to 500 $mL_N \cdot min^{-1}$. After being measured the permeate stream can be directed either to the ventilation or to the μ-GC in order to be analysed. The retentate stream can be as well directed either to the ventilation or to the μ-GC (If the permeate stream goes to the μ-GC then the retentate stream has to go to the ventilation and vice versa). A schematic overview of the experimental set-up described is depicted in Figure 7. The set-up is equipped with an emergency shutdown system and a pressure relief valve that are activated in the following situations:

- CO detection;
- H_2 detection;
- Temperature inside the stainless steel tube is higher than 1000 ˚C;
- Feed pressure is higher than 6 bar;
- Ventilation fail;
- PC failure.

The safe mode can also be activated manually through an emergency button.

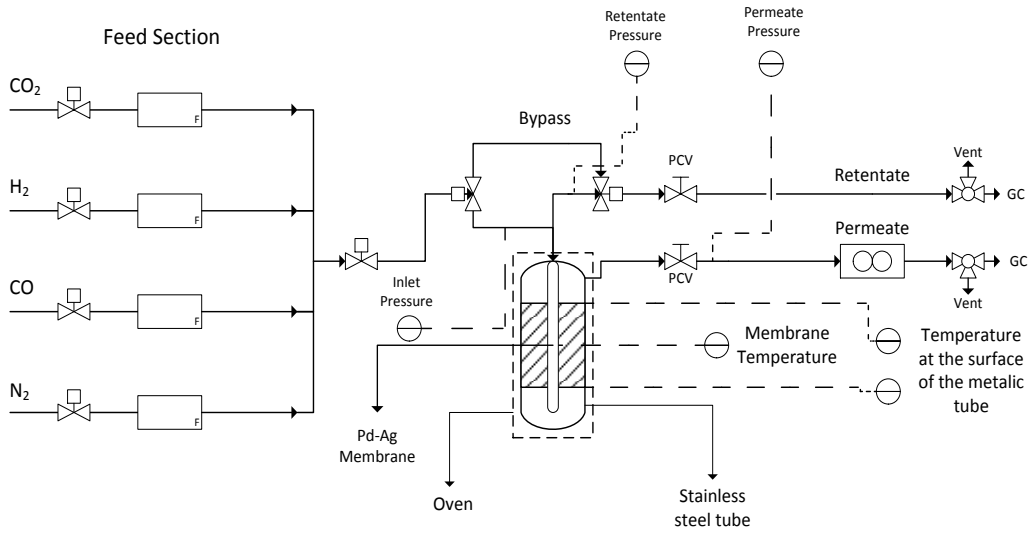

Figure 7 - Scheme of the experimental set-up for the Pd-based membrane testing.

3.1.2 Experiments performed

The Pd-Ag membrane was firstly introduced and fixed inside the stainless steel tube and then the tube was subsequently attached to the set-up. Once the set-up was completely attached a leak test at room temperature was performed with helium. The membrane was then heated up to the desired temperature (300-500 ˚C) under a continuous N_2 purge and was tested for gas leaks at the operating temperature using helium once again. In order to avoid

embrittlement, the membrane must not be exposed to pure hydrogen up to 300 ˚C. After the gas leaks tests, some hydrogen trans-membrane flux measurements were performed for each temperature at different H_2 partial pressures. In Table 4 is presented an overview of all the operating conditions investigated.

Table 4 - Overview of the operating conditions investigated.

Temperature (˚C)	Feed flow ($mL_N \cdot min^{-1}$)	Trans-membrane H_2 partial pressure difference (bar)	H_2 concentration (volume %)	Number of data points
300	94-470	0.5-2.5	100	5
400	188-518	0.5-2.5	100	5
500	188-565	0.5-2.5	100	5

In order to measure the N_2 flux through the membrane a feed of pure N_2 was fed to the membrane at each temperature and at a trans-membrane pressure difference of 2.5 bar. Also, in order to investigate the poisoning effect of CO on the permeability of the membrane to H_2, the flux of H_2 was measured before and after the membrane has been exposed to CO. An overview of the measurements of the CO poisoning effect performed is presented in Table 5

Table 5 - Overview of the operating conditions investigated regarding CO poisoning.

Temperature (˚C)	Feed flow ($mL_N \cdot min^{-1}$)	Trans-membrane H_2 partial pressure difference (bar)	H_2 concentration (volume %)	CO concentration (volume %)	Number of data points
400	188-518	1.0-2.5	85-95	5-15	5

The Pd membranes supplied by TECNALIA group were also tested for pure H_2 feeds and for mixtures of H_2 and CO in order to access the CO poisoning effect. Also, since the know-how about these relatively new membranes is still reduced the possible poisoning effect of CO_2 was evaluated as well. The list of experiments performed for these membranes is presented in Appendix A.

3.1.3 Results and discussion

The permeation of hydrogen through a dense Pd-based membrane follows a solution-diffusion mechanism as already stated. This mechanism can be divided in several steps [2]:

- Diffusion from the gas phase to the Pd surface on the feed side;
- Adsorption on the Pd surface and dissociation into atomic hydrogen;
- Diffusion of atomic hydrogen through the metal lattice;
- Regeneration of atomic hydrogen into hydrogen molecules and desorption from the Pd surface;
- Diffusion from the Pd surface into the permeate gas phase.

The diffusion of hydrogen through the metal lattice is usually the rate-limiting step in the process of mass transfer of hydrogen through a thick Pd membrane at high temperatures (>150 °C). [4] This process is described by Fick's law as follows:

$$J = -D_H \frac{dC_H}{dx} \tag{21}$$

where J is the atomic hydrogen diffusion flux through the metal lattice, D_H is the effective diffusion coefficient of atomic hydrogen and C_H is the concentration of atomic hydrogen at the spacial position x along the membrane thickness. The concentration of atomic hydrogen is related to the partial pressure of hydrogen by Sievert's law, in equilibrium conditions:

$$C_H = S\sqrt{P_{H_2}} \tag{22}$$

where S is the sorption coefficient of hydrogen in the metal lattice. If the adsorbed hydrogen is in equilibrium with the gas phase at both membrane surfaces, the combination of equations (21) and (22) and subsequent integration along the membrane thickness results in the following equation:

$$J_{H_2} = \frac{P_{Pd,H_2}}{\delta}\left(\sqrt{P_{H_2,retentate}} - \sqrt{P_{H_2,permeate}}\right) \tag{23}$$

Equation (23) is only valid for defect free membranes. In order to account for the mass transport through defects equation (19) can be used. [4] For now it will be assumed that the permeation of hydrogen through the Pd-Ag membrane is controlled by the diffusion of atomic hydrogen in the Pd lattice ($x = 0.5$), for the temperature range used in this project. The dependency of the permeability of the membrane on the temperature is typically described by equation (20), as already mentioned.

The permeation tests performed for each temperature at different hydrogen trans-membrane partial pressure differences were used in order to obtain P_{Pd,H_2}, x and further $E_{a,Pd}$. In Figure 8 it is presented the flux of hydrogen through the Pd-Ag membrane as a function of the difference between the square roots of the hydrogen partial pressure in the retentate and permeate sides.

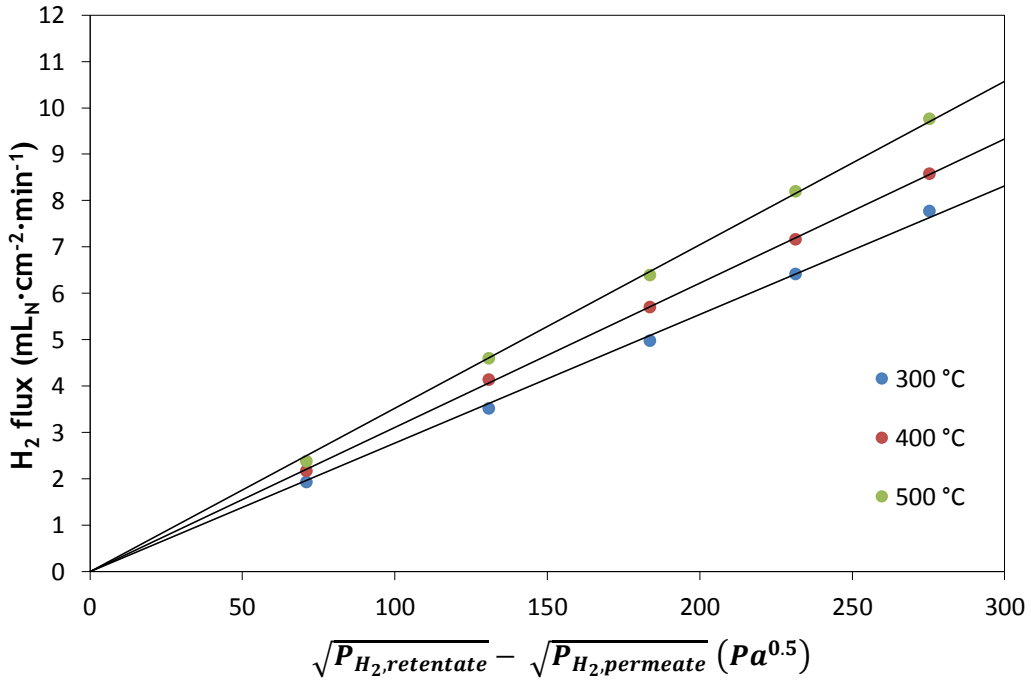

Figure 8 - Hydrogen flux through the Pd-Ag membrane as a function of the difference between the square roots of the hydrogen partial pressure in the retentate and permeate sides.

As can be seen there is a direct proportionality between the hydrogen flux through the Pd-Ag membrane and the difference between the square roots of the hydrogen partial pressure in the retentate and permeate sides. The result of 0.5 for the pressure exponent in equation (19) was obtained by comparing the linear regressions for a pressure exponent of 1 and 0.5, being that for a pressure exponent of 0.5 the fitting was better (data presented in Appendix B).

In order to know exactly the value of the pressure exponent a continuous stirred-tank reactor (CSTR) approach was considered for the permeation system. In this approach it is assumed that the membrane system is completely back-mixed and the gradient of hydrogen permeation along the membrane is constant, in other words, the hydrogen partial pressure doesn't change along the membrane (which was experimentally verified).

The overall molar balance can be expressed as follows:

$$n_{H_2,retentate} = n_{H_2,in} - n_{H_2,permeate} \tag{24}$$

where $n_{H_2,retentate}$ is the molar flow of H_2 in the retentate outlet, $n_{H_2,in}$ is the molar flow of H_2 fed to the reactor and $n_{H_2,permeate}$ is the molar flow of H_2 in the permeate outlet.

The partial pressure of hydrogen in the retentate is equal to the total pressure in the retentate since a feed stream of pure hydrogen was used during the permeation tests. The

predicted total flux of hydrogen through the membrane ($J'_{H_2,calc.}$) is written in the form of a Sievert's type equation:

$$J'_{H_2,calc.} = k_{Pd} \left(P^x_{H_2,retentate} - P^x_{H_2,permeate}\right) L \quad (25)$$

where L is the membrane length and k_{Pd} is the membrane constant and combines all the properties of the membrane as follows:

$$k_{Pd} = \frac{P_{Pd,H_2}}{\delta} \pi d_t \quad (26)$$

being that d_t is the diameter of the membrane tube [2].

The flux of hydrogen through the membrane for different trans-membrane hydrogen partial pressure differences was then compared with the value of the total flux calculated with equation (25) and divided by the membrane's area. The following data fitting procedure was used:

- The independent parameters k_{Pd} and x are given initial values;
- For each experimental data point equation (25) is solved using the initial values attributed to the two parameters previously mentioned and the calculated flux is then compared with the measured flux value;
- All the data points with varying hydrogen partial pressure differences in the membrane are solved in the same way for a fixed temperature;
- The relative error, defined in equation (27), in the flux prediction over all the measurement points is then minimised in the two independent parameters using the generalized reduced gradient nonlinear solving method of the solver tool of Microsoft Excel for a two parameter nonlinear constrained ($0.5 \leq x \leq 1.0$) minimisation;

$$\varepsilon = \sum_{i=1}^{number\ of\ data\ points} \frac{\left(\frac{J'_{H_2,calc.}}{\pi d_t L} - J_{H_2}\right)^2}{\left(J_{H_2}\right)^2} \quad (27)$$

- This procedure is repeated for the measurements at different temperatures.

In Table 6 there are presented for each temperature the values of the two independent parameters that allow a minimum relative error in the flux prediction over all the measurement points (the parity plots are presented in Appendix C).

As can be seen from 300 to 400 °C the value of x increases and from 400 to 500 °C it decreases again, which is somehow unexpected. Also the permeability of the membrane, which was expected to be higher at 500 °C, presents itself lower than for lower temperatures.

Table 6 - Results of error minimization.

Temperature (°C)	x	k_{Pd} (mol·m^{-1}·s^{-1}·Pa^{-x})	$P_{Pd,}$(mol·m^{-1}.s^{-1}·Pa^{-x})	ε (%)
300	0.58	1.976×10^{-6}	3.145×10^{-9}	5.306×10^{-2}
400	0.54	3.915×10^{-6}	6.231×10^{-9}	$7{,}989 \times 10^{-2}$
500	0.61	1.667×10^{-6}	2.652×10^{-9}	5.560×10^{-2}

This curious effect could be explained by the possible existence of some external mass transfer limitations from the gas phase to the Pd surface on the feed side at 500 °C. However, since these results were obtained for a pure H_2 feed this means that the external mass transfer limitations can be excluded. In order to understand how rough could be to consider a pressure exponent of 0.5, the data fitting procedure previously mentioned was repeated for an initial value of x in the neighborhood of 0.5 for all the temperatures. The results obtained are presented in Table 7 (the parity plots are presented in Appendix C).

Table 7 - Results of error minimization in the neighbourhood of $x = 0.5$.

Temperature (°C)	x	k_{Pd} (mol·m^{-1}·s^{-1}·Pa$^{-0.5}$)	$P_{Pd,}$(mol·m^{-1}.s^{-1}·Pa$^{-0.5}$)	ε (%)
300	0.5	5.978×10^{-6}	9.514×10^{-9}	1.613×10^{-1}
400	0.5	6.830×10^{-6}	1.087×10^{-8}	1.049×10^{-1}
500	0.5	7.598×10^{-6}	1.209×10^{-8}	2.339×10^{-1}

It is possible to conclude that although 0.5 is not the value that allows the attainment of the lowest relative errors, it is still a very good approximation since the relative errors obtained for the three temperatures are still very low (lower than the percentual unit). This way it can be concluded that the permeation of H through the Pd-Ag membrane is indeed the rate limiting step. Also, in order to be able to use the Arrhenius-type dependency in equation (20), with the aim of calculating the apparent activation energy and the pre-exponential factor for the permeability, x is considered to be 0.5 for all temperatures so that the units of the membrane permeability don't change with temperature.

In order to check the reproducibility of the results obtained for this Pd-Ag membrane a comparison of the permeation parameters between some typically literature reported Pd-Ag membranes and the Pd-Ag membrane characterized in this work is presented in Table 8.
By analysing Table 8 it is possible to realise that the values obtained in this work for the apparent activation energy and pre-exponential factor are in good agreement with other experimental results reported in the literature for Pd-Ag membranes. This can also be verified in Figure 9.

Table 8 - Apparent activation energy and pre-exponential factor for hydrogen permeation through the dense Pd-Ag membrane used in this work and taken from the literature.

$E_{a,Pd}$ (kJ·mol^{-1})	P^0_{Pd,H_2} (mol·m^{-1}·s^{-1}·Pa$^{-0.5}$)	Reference
2.93	1.50×10^{-8}	[36]
4.40	2.38×10^{-8}	This work
6.30	5.58×10^{-8}	[37][a]
6.60	7.73×10^{-8}	[38]

[a] - It's not the original work.

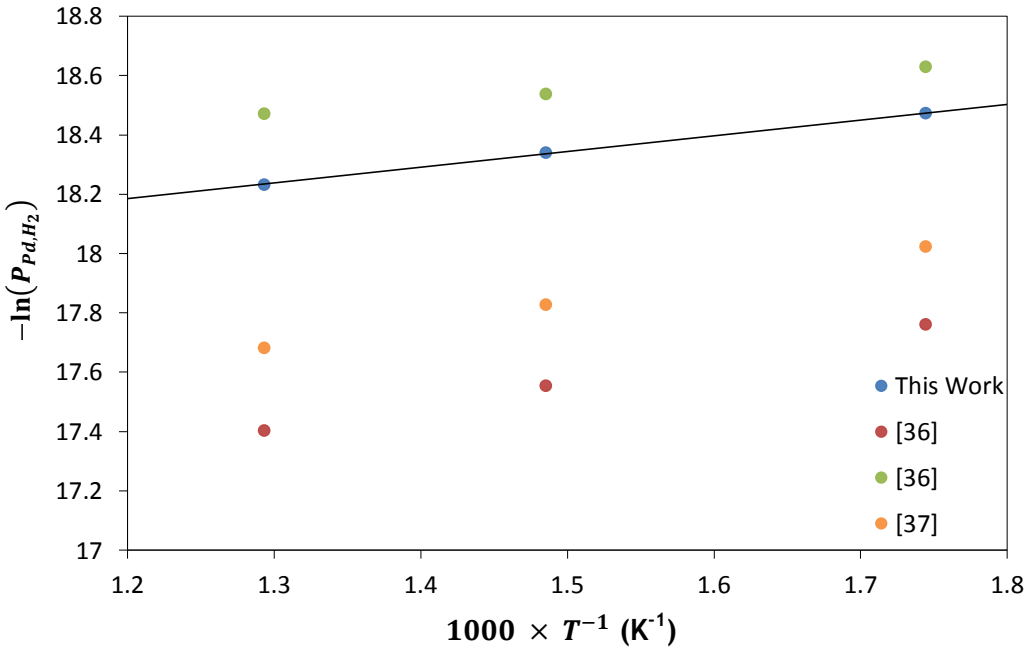

Figure 9 - Comparison between the Arrhenius plot obtained in this work and others reported in the literature. The line represents the regression of the data of this work with equation (20).

The flow of N_2 through the membrane was also measured in order to obtain the H_2/N_2 ideal selectivity. For all temperatures and a trans-membrane N_2 partial pressure difference of 2.5 bar there was no N_2 passing through the membrane. It can therefore be concluded that the Pd-Ag membrane presents infinite H_2/N_2 ideal selectivity.

The poisoning effect of CO on the Pd-Ag membrane was also accessed. In Figure 10 it is shown the variation of the hydrogen flux through the Pd-Ag membrane, for different hydrogen trans-membrane partial pressure differences, as a function of the concentration of CO.

As can be observed in Figure 10 the poisoning effect of CO on the Pd-Ag membrane is not negligible. As the concentration of CO in the feed increases the permeability of the

membrane decreases. Moreover a special behaviour can be verified: for lower concentrations of CO in the feed the decrease of the H_2 flux through the Pd-Ag membrane is higher than the one obtained for further equal additions of CO. Gallucci et al. [39] also reported a similar poisoning effect of CO for Pd-Ag membranes. This CO inhibition effect can be explained by the combination of surface effects at low CO concentrations and dilution effects for increasing CO concentrations. [39] This effect was also reported by Miguel et al. [28], being that in their case the inhibition effect was even higher because of the lower temperatures used (200-300 ˚C). Also it can be seen in Figure E.1 that there is a good agreement between these results and the Sieverts-Langmuir model.

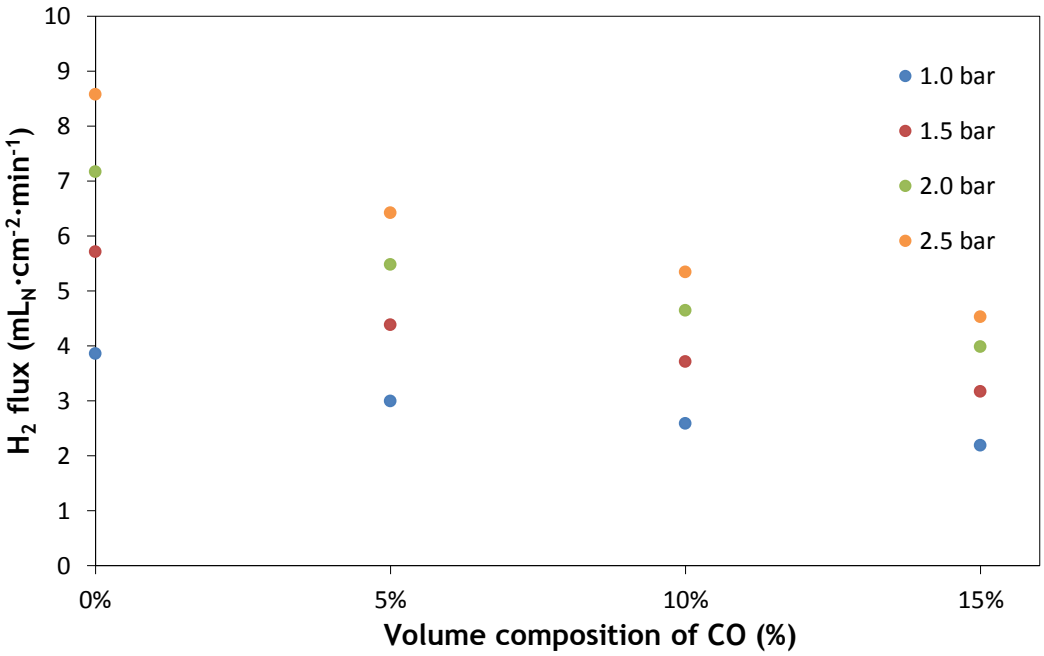

Figure 10 - H_2 flux as a function of the CO concentration in the feed for different H_2 trans-membrane partial pressure differences at 400 ˚C.

A similar analysis was done for both thin Pd membranes. As can be seen by the results presented in Appendix A these membranes are approximately 10 times more permeable to H_2 than the Pd-Ag membrane previously characterized. Also, for these membranes it was concluded that the permeation of H_2 is more controlled by the adsorption of H_2 at the Pd surface and dissociation into atomic hydrogen than by the diffusion of H through the metal lattice. Also for the thicker Pd membrane, which was tested at a lower temperature, the adsorption process is more rate limiting. This behaviour was expected due to the exothermic nature of the adsorption process. This was also verified by Patil [2]. Despite the higher permeability, the thin Pd membranes showed low H_2/N_2 ideal selectivies and started showing high N_2 trans-membrane flows after a short period of time. These N_2 flows happened most probably due to some leaks in the seal between the porous zone and the dense zone. It is

therefore concluded that there is still a long way to go regarding the sealing between the porous zone and the dense zone in this type of membranes.

The poisoning effect of CO and CO_2 was also analysed and the results are presented in Appendix A. It is possible to verify that the permeability of these membranes to H_2 is not so highly affected as the one of the thick Pd-Ag membrane. The effect of CO_2 on the trans-membrane flow of H_2 was found to be quite similar to the one of CO.

3.2 WGS Reaction Tests in a Packed Bed Membrane Reactor

After the permeation tests performed with the aim of characterizing the Pd-Ag membrane, the Pt-based catalyst described in Appendix D was introduced inside the Pd-Ag membrane and the WGS reaction was performed inside the PBMR.

3.2.1 Experimental set-up

The set-up used to perform the WGS tests is the same that was used for the permeation tests with some slight changes. In this case, due to the need of feeding steam to the PBMR, a steam generator was used. After the reactor retentate outlet a steam condenser was used being that the cold utility used was water with ice. The condensed water was then collected in a metallic container. The tube that goes from the steam generator to the reactor was isolated with glass wool and aluminium foil and continuously heated up by means of 2 tracing lines in order to avoid steam condensation before the reactor. Also, a one-way valve was used before the reactor in order not to allow steam going into the feed section main tube. Finally the bottom reactor inlet that is connected to the permeate side was opened and N_2 was used as sweep gas. The flow of N_2 was controlled by a mass flow controller (Brooks Smart Mass Flow, model 5850S). The described set-up is presented schematically in Figure 11.

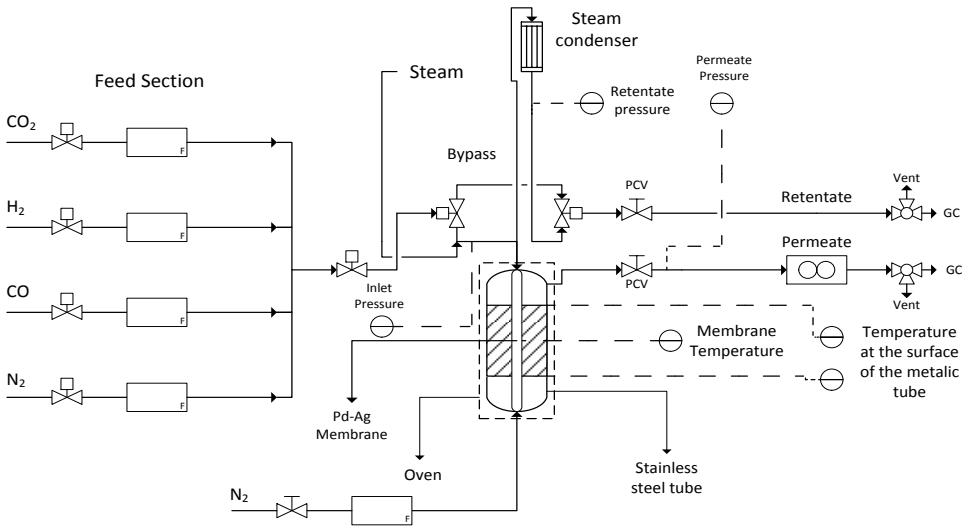

Figure 11 - Scheme of the experimental set-up for the WGS reaction tests in a PBMR.

3.2.2 Experiments performed

The 0.5Pt/6CeTiO$_2$ catalyst supplied by CSIC whose main characteristics are presented in Appendix D was introduced inside the Pd-Ag membrane tube (retentate side) and the WGS reaction was performed under the conditions presented in Table 9. Before performing the WGS tests inside the PBMR, the catalyst was activated in a packed bed reactor (PBR) in order to avoid permeation of H_2. The activation procedure consisted on heating the catalyst from room temperature up to 500 °C at 5 °C/min under N_2 flow. Then the calcination was performed at that temperature under O_2 flow for 30 minutes. After calcination the catalyst was cooled down to room temperature under N_2 flow and then heated up again up to 220 °C at 5°C/min under N_2 flow and was finally reduced under a 10 vol.% H_2/N_2 flow for 30 minutes. After the reduction, the catalyst was cooled down to room temperature under N_2 flow.

After being activated, 3.5 g of catalyst were diluted with quartz particles of similar size (150-350 μm) in order to avoid temperature gradients inside the bed due to the exothermicity of the WGS reaction (effect verified in other works). After being diluted the catalyst was introduced inside the Pd-Ag membrane tube (positioned in the membrane zone). On the sections of the tube where there was no membrane, only diluent particles were introduced. In order to avoid fluidization, a small amount of glass wool was introduced on the top of the bed. In order to avoid re-oxidation of the catalyst, when the WGS tests were not being performed the catalyst was kept under N_2 flow.

During the WGS reaction tests inside the PBMR the following feed gas volumetric composition was used: 5.56% CO, 36.54% H_2O, 26.55% H_2 and 15.69% CO_2 balanced with N_2, which simulates a typical reformate feed. In Table 9 are presented the conditions that were analysed for the WGS reaction performed inside the Pd-Ag PBMR.

Table 9 - Overview of the operating conditions investigated.

Temperature (˚C)	Retentate pressure (bar)	GHSV ($L_N \cdot kg_{cat.}^{-1} \cdot h^{-1}$)	H_2O/CO ratio
300-400	3.5	14736-20696	4.7-6.5

At first no sweep gas was used and the partial pressure of H_2 in the permeate side was kept at 1 bar. However, in such conditions there was almost no permeation of H_2 due to the combination of the CO poisoning effect on the membrane and the dilution of H_2. In order to increase the driving force in the membrane and thus increase the permeating flux of H_2, a flow of 345 $mL_N \cdot min^{-1}$ of N_2 was used to sweep the H_2 in the permeate side.

After the MR tests, the Pd-Ag membrane was replaced by a stainless steel tube in order to simulate the operation of a PBR for subsequent comparison with the MR performance.

3.2.3 Results and discussion

During the WGS reaction tests performed inside the PBMR the effect of the operating conditions on both CO conversion (X_{CO}) and H_2 recovery (Re_{H_2}) was analysed. Both parameters were calculated using equations 28 and 29:

$$X_{CO} = 1 - \frac{Q_{CO,out}^{Retentate}}{Q_{Co,in}^{Retentate}} \tag{28}$$

$$Re_{H_2} = \frac{Q_{H_2,out}^{Permeate}}{Q_{H_2,out}^{Permeate} + Q_{H_2,out}^{Retentate}} \tag{29}$$

where $Q_{CO,out}^{Retentate}$ and $Q_{Co,in}^{Retentate}$ are the volumetric flows of CO at the retentate outlet and inlet respectively and $Q_{H_2,out}^{Permeate}$ and $Q_{H_2,out}^{Retentate}$ are the volumetric flows of H_2 at the permeate and retentate outlets respectively. For all the graphics presented in this section, each data point results from the average of at least three experiments.

3.2.3.1 Influence of the reaction temperature

The reaction temperature was varied between 300 and 400 ˚C while the pressure in the retentate side and the GHSV were kept at a constant value of 3.5 bar and 14736 $L_N \cdot kg_{cat}^{-1} \cdot h^{-1}$ respectively. The feed composition was kept as follows: 5.56% CO, 36.54% H_2O, 26.55% H_2 and 15.69% CO_2 balanced with N_2. The permeate side was kept under a sweep gas flow rate of 345 $mL_N \cdot min^{-1}$. The thermodynamic equilibrium conversion of CO represented by the dotted line in Figure 12 was calculated using equation 4 for the simulated reformate gas composition used.

For the PBR it is observed that the conversion of CO is in general relatively close to the equilibrium one. For all the range of temperatures studied the conversion of CO in the PBR is below the equilibrium conversion. However, for increasing temperatures the CO conversion obtained inside the PBR gets closer to the thermodynamic limit. This can be explained by the fact that for higher temperatures the kinetics of the Pt-based catalyst is highly improved, as shown in Figure 12, and the thermodynamics of the WGS reaction is on the other hand not favoured due to its exothermicity (lower equilibrium conversions for higher temperatures).

Regarding the Pd-Ag PBMR there is a noticeable enhancement of the conversion of CO beyond the equilibrium boundaries for all temperatures. There is in particular a higher shift of the CO conversion for higher temperatures because of the higher permeability of the Pd-Ag membrane and consequent higher recovery of H_2 (Figure 13), despite the lower amount of H_2

in the retentate side due to the lower conversion of CO. Still, for higher temperatures the CO conversion is lower because of the thermodynamic constraints of the WGS reaction.

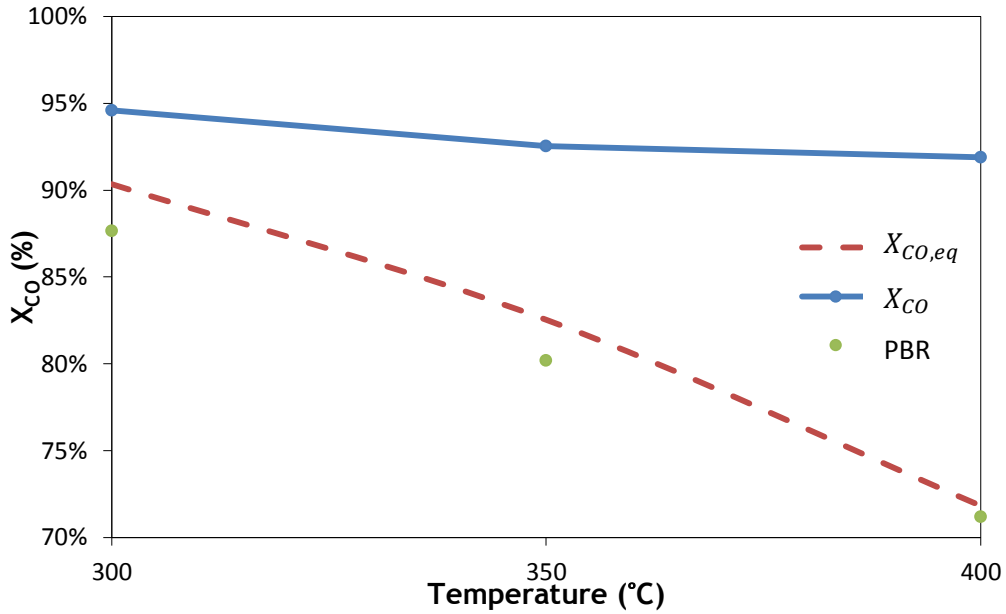

Figure 12 - Influence of the reaction temperature on the CO conversion for the WGS reaction over the 0.5Pt/6CeTiO$_2$ catalyst in the PBR and in the Pd-Ag PBMR.

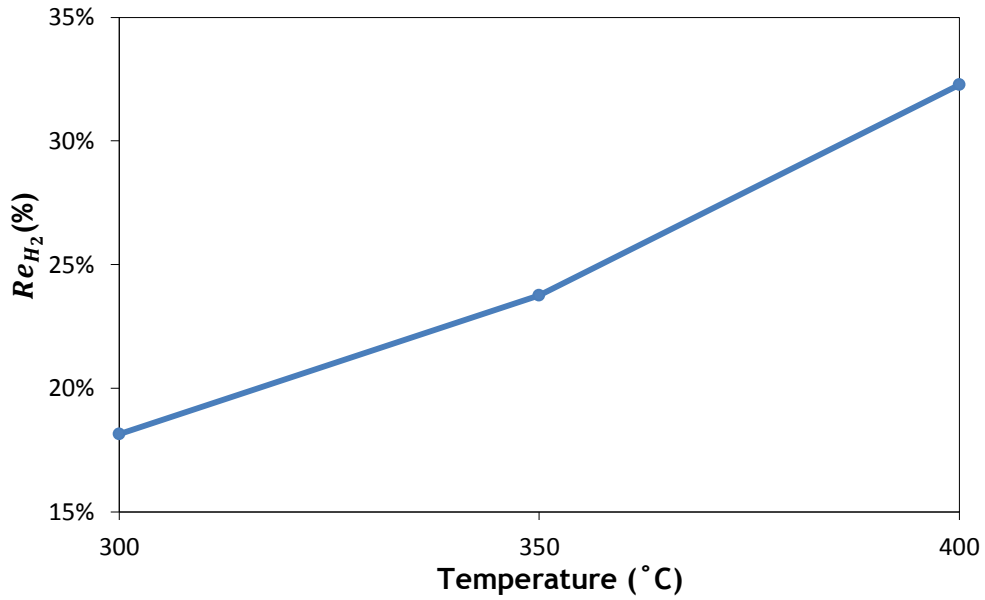

Figure 13 - Influence of the reaction temperature on the H_2 recovery for the WGS reaction over the 0.5Pt/6CeTiO$_2$ catalyst in the Pd-Ag PBMR.

A balance between the CO conversion and the H_2 recovery should be seeked. Low temperatures benefit the CO conversion but don't favour the recovery of H_2. High temperatures on the other hand benefit the recovery of H_2 however, lower CO conversions are obtained due to thermodynamic limitations. These trends for the CO conversion and H_2 recovery were also verified by Mendes [4] and Bi et al. [40]. In this case however, the Pd-Ag

membrane used is much more permeable for temperatures around 400 ˚C and so a higher increase in the H_2 recovery is verified for temperatures above 350 ˚C. Also for increasing temperatures the decrease in the CO conversion is quite small.

Having all these considerations in mind, it is possible to conclude that for temperatures around 400 ˚C the enhancement of the H_2 recovery completely outweighs the decrease of the CO conversion and so, this would be the optimum operation temperature neighbourhood within the analysed range for this Pd-Ag PBMR system.

With the aim of knowing how to improve even further the performance of Pd-Ag PBMR, the influence of other important parameters was studied at 400 ˚C.

3.2.3.2 Influence of the GHSV

The influence of the GHSV on the CO conversion and H_2 recovery was studied for a constant temperature and pressure of 400 ˚C and 3.5 bar respectively. A N_2 flow rate of 345 $mL_N \cdot min^{-1}$ was used as sweep gas in the permeate side. The gas stream fed to the reactor had the following volume composition: 5.56% CO, 36.54% H_2O, 26.65% H_2 and 15.69% CO_2 balanced with N_2. In order to vary the GHSV, the feed flow rate was varied while keeping the amount of catalyst constant. The GHSV was varied between 14736 and 20696 $L_N \cdot kg_{cat.}^{-1} \cdot h^{-1}$. In Figure 14 and 15 is presented the variation of the CO conversion and H_2 recovery respectively with the GHSV.

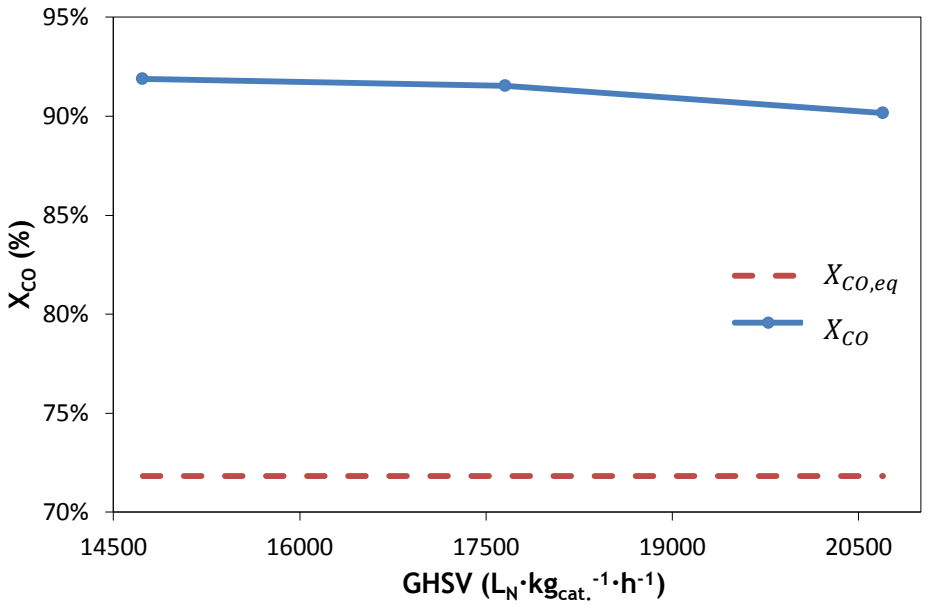

Figure 14 - Influence of the GHSV on the CO conversion for the WGS reaction over the $0.5Pt/6CeTiO_2$ catalyst in the Pd-Ag PBMR.

In this case the performance of the PBR wasn't analysed since the enhancement of the CO conversion from the PBR to the Pd-Ag PBMR was already demonstrated in the previous section. By analysing Figure 14 it is possible to conclude that the use of the Pd-Ag MR allows

once again the achievement of CO conversions well above the thermodynamic equilibrium. Also it is possible to notice that by increasing the GHSV and thus reducing the residence time of the gas inside the reactor the conversion of CO decreases slightly, being that the shift on the conversion is also higher for lower GHSVs. Increasing GHSVs affect negatively the H_2 recovery as well, as can be observed in Figure 15. However, this decrease on the H_2 recovery is also very small. It is consequently concluded that increasing GHSVs affect negatively both CO conversion and H_2 recovery due to the above mentioned lower residence time of the gas inside the reactor, however this negative effect is not very pronounced.

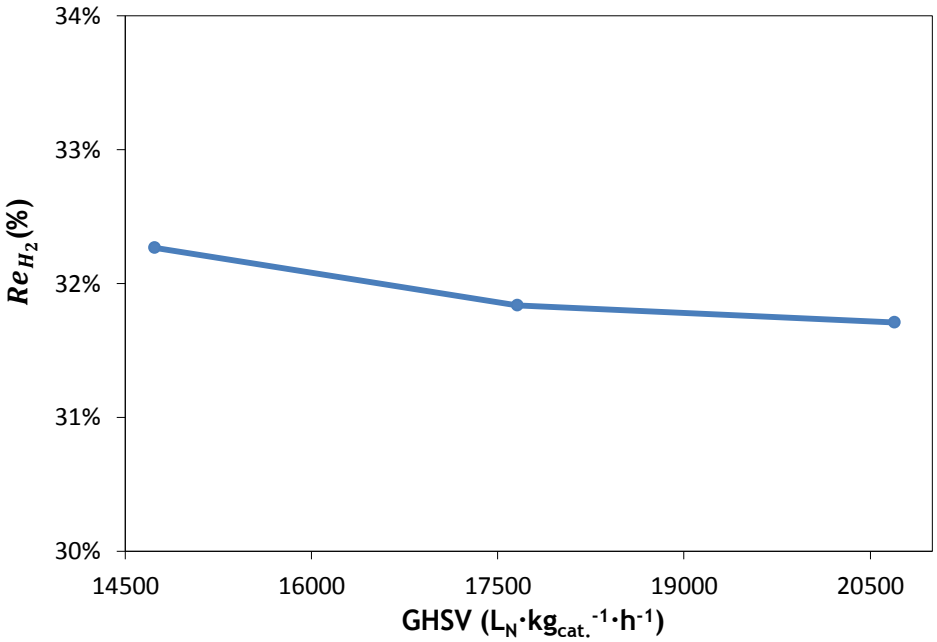

Figure 15 - Influence of the GHSV on the H_2 recovery for the WGS reaction over the 0.5Pt/6CeTiO$_2$ catalyst in the Pd-Ag PBMR.

This happens because for higher temperatures the Pt-based catalyst kinetics is favored, resulting in CO conversions that are close or equal to the equilibrium one and also because the permeation of H_2 through the Pd-Ag membrane is higher for higher temperatures.

This negative effect of the GHSV on both CO conversion and H_2 recovery is in line with what have been reported in the literature. Mendes [4] and Bi et al. [40] also obtained lower CO conversions and H_2 recoveries for higher GHSVs. In fact, Bi et al. also obtained only a slight decrease of the CO conversion while increasing the GHSV. In terms of H_2 recovery both works reported a significant decrease for increasing GHSVs. However, both of them presented such results for temperatures below the one used in this work, which means lower membrane permeability and higher sensitivity to CO poisoning and less favored kinetics which leads to CO conversions bellow the equilibrium one.

It possible to conclude that higher GHSVs have a negative impact on both CO conversion and H_2 recovery. However, this negative effect is more pronounced for lower temperatures due to the reasons previously mentioned. For this case, since a relatively high temperature was used, the effect of increasing GHSVs on both CO conversion and H_2 recovery was quite small. Still, independently of the operating temperature lower GHSVs are always preferable. In this project it wasn't possible to use lower velocities due to pratical limitations.

3.2.3.3 Influence of the H_2O/CO ratio

The influence of the H_2O/CO ratio was accessed as well due to the diversity of WGS feeds from different reforming processes and hydrocarbon feedstocks and the versatility that it demands from MRs. Also, since at the industrial level the WGS reaction is normally performed in the presence of excess of steam in order to favor the equilibrium shift, which means higher cost regarding H_2O evaporation, the study of the reactants ratio effect on the MR performance gains relevance.

In this work the H_2O/CO ratio was varied between 4.7 and 6.5 by changing only the H_2O volume composition (26.02-36.54%) while keeping the same CO amount. Both operating temperature and pressure were kept constant at 400 °C and 3.5 bar respectively. A N_2 flow rate of 345 $mL_N \cdot min^{-1}$ was used as sweep gas in the permeate side. The GHSV used was 14736 $L_N \cdot kg_{cat.}^{-1} \cdot h^{-1}$.

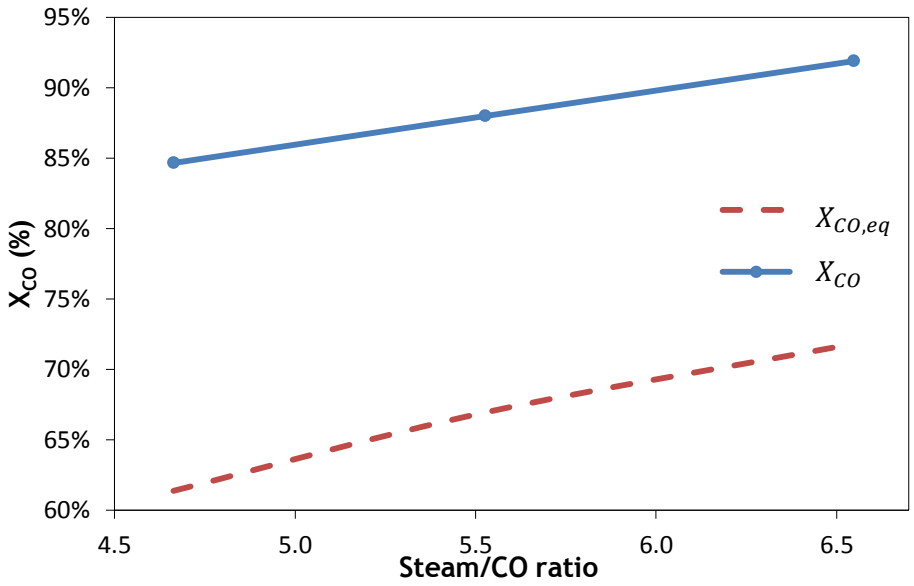

Figure 16 - Influence of the H_2O content in the feed on the CO conversion for the WGS reaction over the 0.5Pt/6CeTiO$_2$ catalyst in the Pd-Ag PBMR.

By analysing Figure 16 it is possible to conclude that higher H_2O/CO ratios lead to higher CO conversions (above the equilibrium conversion for all the analysed range). Also it

can be noticed that for lower H_2O/CO ratios the shift on the CO conversion is higher. It is also possible to see that for operating conversions beyond the thermodynamic equilibrium, the MR system behaves in accordance to the Le Chatelier's principle (dotted line in Figure 16). Also it has been seen in chapter 2.4 that normally the Pt-based catalysts reported in the literature highly depend on the H_2O content since there is normally competition between H_2O and H_2 regarding the adsorption on the free active sites. Considering this it can be concluded that the kinetics is favored for higher steam content and so higher CO conversions are obtained. However, the characterization of the catalyst provided is not in agreement with what has been reported in the literature and so it contradicts the higher CO conversions obtained for higher H_2O amounts. It is then possible that the kinetic results provided are somehow deceiving about the true behavior of the catalyst used. In terms of H_2 recovery it is positively affected by the increase of the H_2O/CO ratio (Figure 17) due to the higher amount of H_2 produced in the retentate side. This increase of both CO conversion and H_2 recovery for increasing H_2O/CO ratios has been verified and reported by many authors (Mendes; Bi et al.; Basile et al. [41]).

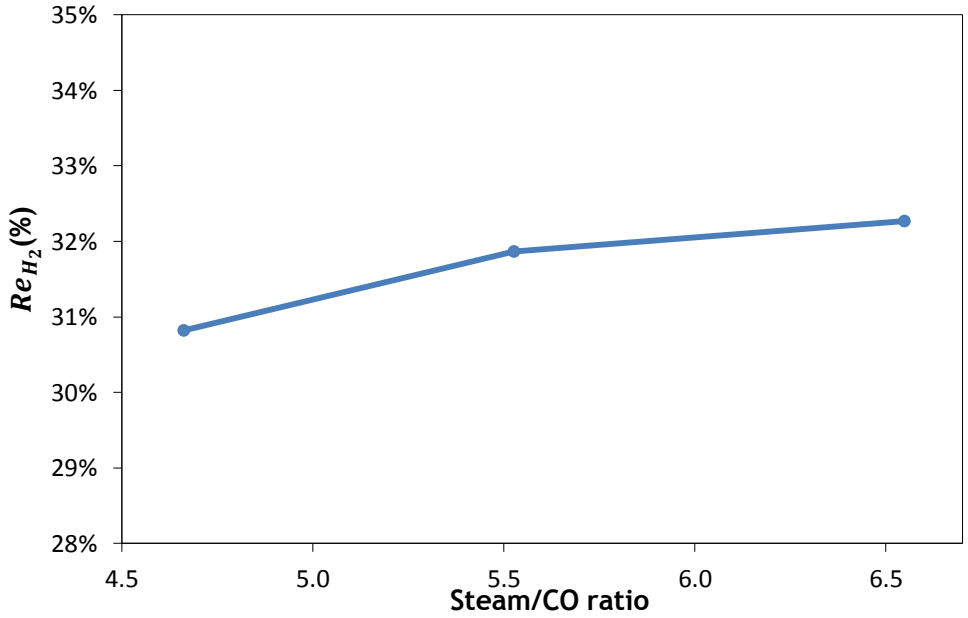

Figure 17 - Influence of the H_2O content in the feed on the H_2 recovery for the WGS reaction over the $0.5Pt/6CeTiO_2$ catalyst in the Pd-Ag PBMR.

It is therefore concluded that higher H_2O/CO ratios lead to higher CO conversions, consequently leading for higher amounts of H_2 in the retentate side and so higher H_2 recoveries. If higher H_2O/CO ratios had been used an even higher enhancement of the Pd-Ag PBMR performance would have been achieved. However, it would be pointless since the H_2O/CO ratios that are normally used at the industrial scale are close to 7 and the main goal is to reduce it even further in order to reduce the costs associated to H_2O evaporation.

It can be concluded that a MR can be used to reduce the amount of steam needed to obtain reasonable conversions.

3.2.3.4 Influence of the H_2 partial pressure difference in the membrane

During the experimental campaign the operating pressure in the retentate side was always kept at 3.5 bar. However, the pressure in the permeate side was varied. As already mentioned, in the beginning of the experimental campaign the partial pressure of H_2 in the permeate side was kept at 1 bar. However, it was verified that there was almost no H_2 permeation due to the very small driving force. In order to solve this inconvenient a flow rate of 345 $mL_N \cdot min^{-1}$ of N_2 was used to sweep the H_2 in the permeate side and consequently increase the driving force by decreasing the partial pressure of H_2 in the permeate. The sweep gas was used in the co-current mode. This way it was possible to recover between 18.14 and 32.27% of the total H_2 in the MR and to obtain conversions of CO ranging between 84.68 and 94.60%.

Although there were not performed WGS reaction tests inside the Pd-Ag PBMR for different specific H_2 partial pressure differences in the membrane at 400 °C it is possible to conclude, based on the situation previously mentioned that, by increasing the H_2 partial pressure difference in the membrane the permeation of H_2 through the Pd-Ag membrane is improved. This enhancement on the H_2 recovery on its hand shifts of the thermodynamic equilibrium towards higher conversions of CO. Also, if a higher flow rate of sweep gas had been used higher H_2 recoveries and consequently higher CO conversions would have been obtained. However that was not possible due to mechanical reasons regarding the Pd-Ag membrane. Also, because of the relatively low H_2 partial pressure difference in the membrane the changes in the different parameters didn't have much effect on the CO conversion and H_2 recovery (almost constant results except for the H_2O/CO ratio). This almost unchanged behavior might suggest that the conversions obtained are close to the maximum ones that could've been obtained for the driving force used. The same thing can be said for the H_2 recovery since it was verified that for the driving force used, the maximum amount of H_2 that could have permeated is lower than the total amount of H_2 inside the PBMR. In other words, a recovery of 100% could have never been obtained for the driving force used and so the H_2 recoveries obtained are close to the maximum that could have been obtained. As already mentioned before, if it was possible to use higher sweep gas flows (higher driving forces) the CO conversion obtained would be higher as well as the H_2 recovery. In alternative, instead of sweep gas it could also have been used a vacuum pump in the permeate side. Also, the effect of the changes in the different parameters would be more significant in terms of both CO conversion and H_2 recovery.

The activity of the catalyst during the experimental campaign was also measured on a daily basis for a base case and the verification of its activity is presented in Appendix E.

3.3 Validation of Both 1D and 2D Phenomenological Models

3.3.1 Models description

During this dissertation project another Masters student developed in Delphi 7 a 1D and a 2D model that describe the performance of a PBMR for the SRM. These models can easily be adapted in order to be used for the simulation the WGS reaction instead of the SRM.

The phenomenological 1D pseudo-homogeneous PBMR model encompasses the following main assumptions:

- Radial temperature gradients inside the PBMR are considered for via overall wall-to-bed heat transfer coefficients;
- Radial concentration profiles are neglected (absence of concentration polarization);
- External mass and heat transfer limitations are neglected;
- The size of the particles is sufficiently small so that both intra-particle mass and heat transfer limitations and external mass and heat transfer limitations from the gas bulk to the catalyst surface can be neglected.

The phenomenological 2D pseudo-homogeneous PBMR model includes the following main assumptions:

- The transport of mass and energy in the gas phase is described as convective flow with superimposed axial and radial dispersion;
- Homogeneous gas phase reactions are neglected considering the relatively low temperatures;
- The size of the particles is sufficiently small so that both intra-particle mass and heat transfer limitations and external mass and heat transfer limitations from the gas bulk to the catalyst surface can be neglected;
- The gas bulk can be described as an ideal Newtonian fluid.

3.3.2 Validation of the 1D and 2D phenomenological models

The experimental results previously presented and discussed in this Masters thesis were used to validate both 1D and 2D existing pseudo-homogeneous PBMR phenomenological models.

Before considering the WGS reaction inside the PBMR, the permeation of H_2 through the Pd-based membrane in the presence of CO at 400 °C was simulated using both 1D and 2D models for the conditions studied in section 3.1. However, it was observed that both models

over predict significantly the permeating flux of H_2. In order to make both models more realistic, the CO poisoning effect on the Pd-Ag membrane was taken into consideration by using equation 30 proposed by Barbieri et al. [42] for the permeating flux of H_2 through the Pd-Ag membrane:

$$J_{H_2} = \left[\left(1 - \alpha(T)\frac{K_{CO}p_{CO}}{1+K_{CO}p_{CO}}\right)\frac{P_{Pd,H_2}}{\delta}\right]\left(\sqrt{p_{H_2,retentate}} - \sqrt{p_{H_2,permeate}}\right) \quad (30)$$

where α is the H_2 permeance reduction factor, K_{CO} is the Langmuir's adsorption constant for CO and p_{CO} is the partial pressure of CO. The values used for α and K_{CO} are presented in Table 10. The calculation of these parameters is presented in Appendix F.

Table 10 - Values of the parameters of the Sierverts-Langmuir's model equation.

α	K_{CO} (kPa^{-1})
0.6794	0.037

Since normally a bigger difference between the experimental results and the models predictions is found for a H_2 partial pressure in the feed of 3.5 bar, a comparison between the experimental results and the models predictions for this H_2 partial pressure in the feed is presented in Figure 18.

As can be seen, both 1D and 2D model over predict significantly the H_2 flux that permeates through the membrane in the presence of CO. However, when the Sieverts-Langmuir's model equation is included in both 1D and 2D models the predicted H_2 fluxes are quite close to the ones obtained experimentally. Also, the 1D model accounting for CO poisoning presents closer predictions for the retentate side pressure considered than the 2D model accounting also for CO poisoning. However, these results are somehow deceiving since the average relative error between the predictions of the 2D model and the experimental results is lower than the one obtained for the 1D model. In fact, the average of the relative errors between the predicted H_2 fluxes using the 2D model with Sieverts-Langmuir's model equation and the ones obtained experimentally in section 3.1 is 3.33%, while for the 1D model with Sieverts-Langmuir's model equation the average relative error is 5.43%. It is possible to conclude that by including the Sieverts-Langmuir's model equation in both 1D and 2D models, the enhancement on the quality of the prediction of the permeating H_2 flux through the Pd-Ag membrane is considerable. It is also verified that the 2D model prediction is slightly more accurate than the 1D model one. This difference is due to the concentration polarization effect considered by the 2D model.

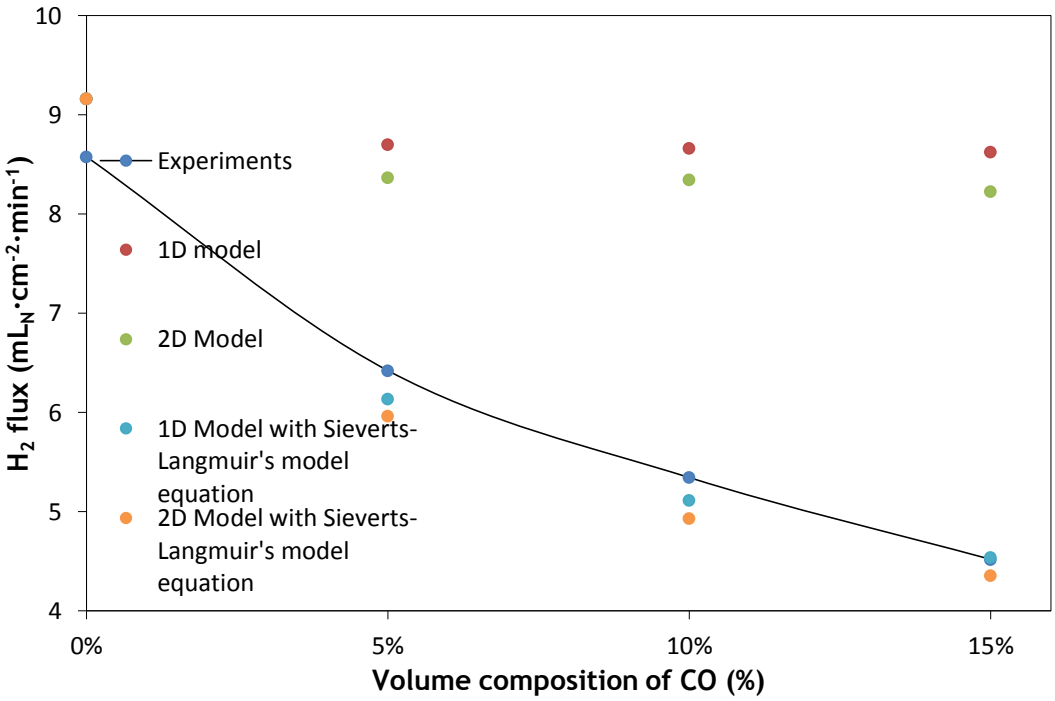

Figure 18 - Comparison of the H_2 permeating flux obtained using the 1D and 2D models and 1D and 2D models with Sieverts-Langmuir's model equation with the experimental one for a H_2 partial pressure in the retentate side of 3.5 bar at 400 ˚C.

The quantification of the impact of both concentration polarization and CO poisoning effects on the predicted H_2 flux through the Pd-Ag Membrane was done and it's presented in Appendix G. It was concluded that in order to predict accurately the permeation of H_2 through the Pd-Ag membrane for a feed composition that is not pure H_2, the concentration polarization effect has to be taken into consideration since it was shown that it is not negligible. If CO is also present in the retentate side, then its poisoning effect on the Pd-Ag membrane has to be considered as well.

Regarding the validation of both models for the WGS reaction inside the Pd-Ag PBMR, it was not possible to be done due to time limitations.

4 Conclusions

In this project a highly H_2 permeable Pd-Ag membrane and a highly active $0.5Pt/6CeTiO_2$ catalyst were combined to form a PBMR. The effect of temperature, GHSV, and H_2O/CO ratio on the conversion of CO and H_2 recovery through the membrane was analysed. Also although the effect of different trans-membrane pressure differences was not intentionally tested, some observations regarding the influence of this parameter on both CO conversion and H_2 recovery were done.

For the PBMR system studied in this work, it was possible to verify that higher CO conversions are achieved at lower temperatures where the thermodynamics of the WGS reaction is favored. On the other hand higher temperatures favor the recovery of H_2 because of the enhancement of the permeability of the Pd-Ag membrane to H_2. Both these effects were combined inside the reaction/separation system and it was concluded that although the CO conversion is lower for higher temperatures, the shift of the equilibrium was higher than for lower temperatures due to the higher H_2 recoveries obtained at higher temperatures. In other words, the advantages of the PBMR system compared to the PBR are much more explored at higher temperatures. It was also concluded that lower GHSVs improve the performance of the PBMR however, this improvement is less noticed at higher temperatures due to the favored kinetics and H_2 permeation. Regarding the H_2 partial pressure difference in the membrane, it was verified that for higher driving forces (sweep gas in the permeate side) the recovery of H_2 was much higher than the one obtained while keeping the partial pressure of H_2 in the permeate side at atmospheric pressure. In fact, for this last configuration sometimes no H_2 was recovered. Also, the influence of the concentration of H_2O in the feed was analysed and it was concluded that for higher H_2O compositions the CO conversion is enhanced and so more H_2 is produced thus resulting in higher H_2 recoveries. Also, for lower steam/CO ratios the attainment of reasonable CO conversions was verified proving once again that MRs are potential candidates to allow reducing the amount of steam needed. For this work, the conditions that allowed the best performance of the PBMR were as follows: 400 °C, 3.5 bar total pressure in the retentate with a flow of 345 $mL_N \cdot min^{-1}$ of sweep gas in the permeate, a GHSV of 14736 $L_N \cdot kg_{cat.}^{-1} \cdot h^{-1}$ and a H_2O/CO ratio of 6.5. However, some of these parameters (GHSV and H_2 partial pressure difference in the membrane) can be further improved in order to improve the overall performance of the Pd-Ag PBMR system. In this work such improvements were not possible due to practical limitations. In particular, the H_2 partial pressure difference used was relatively low and so the effect of the changes of the different parameters on the CO conversion and H_2 recovery was very small. This almost unchanged behavior suggests that the obtained CO conversions and H_2 recoveries are close to the

maximum ones that could have been obtained for the driving force used. A solution for this limitation would be to use either higher sweep gas flow rates or a vacuum pump.

Regarding the suitability of the H_2 feed produced for being directly fed to a PEMFC, it was concluded that the purity of the H_2 feed produced is acceptable to be directly fed to a PEMFC since in principle no poisoning of the anode would occur.

The validation of both 1D and 2D models for the permeation of H_2 through the Pd-Ag membrane was done. It was concluded that by including the Sieverts-Langmuir's model equation that describes the CO poisoning of Pd-Ag membranes in both 1D and 2D models, the relative error between the predicted flow and the actual one was highly decreased. Also, the quantification of the contribution of the concentration polarization effect and CO poisoning of the membrane on the H_2 permeating flow was done. It was verified that the CO poisoning of the membrane has a much higher effect on the flux of H_2 that permeates through the membrane. However, the concentration polarization effect shall not be neglected. In fact, minimum variations of 8.3% of the H_2 flux permeating through the Pd-Ag membrane caused by the concentration polarization effect were verified. Higher concentration polarization was verified for lower concentrations of CO due to the lower poisoning effect and thus higher permeability of the membrane that allows a higher mass transport from the gas bulk to the membrane wall.

5 Overall evaluation of this work

5.1 Achieved Goals

The main goal of this project was to analyse experimentally the permeation of H_2 through a thin Pd membrane and incorporate it inside a PBMR in order to perform the experimental study of its performance. Also, the validation of both 1D and 2D phenomenological models for the permeation of H_2 and the WGS reaction was intended.

In fact two thin Pd membranes were initially tested however, it was not possible to finish the minimum necessary tests for their characterization. Finally a 50 μm thick Pd-Ag membrane was characterized and introduced together with the already characterized $0.5Pt/6CeTiO_2$ catalyst inside the PBMR system. The experimental study of the influence of some of the most important parameters on the performance of the PBMR system was also successfully done. Finally, the validation of both 1D and 2D models for the permeation of H_2 through the Pd-Ag membrane was done however, the validation of these models for the WGS reaction carried inside a PBMR system was not possible due to time limitations.

5.2 Limitations and Future Work

The first big limitation encountered during this project was the relatively low durability of the thin Pd membranes since it wasn't even possible to perform all the necessary tests for their full characterization. The low H_2/N_2 ideal selectivities obtained for these membranes is also a very limiting aspect since it makes it impossible for them to be used to purify the H_2 that is to be used in PEMFCs. Since these thin Pd membranes are so promising in terms of industrial application due to their low thickness (low cost), it would be very pertinent to keep looking for ways to increase both the H_2/N_2 ideal selectivity and durability of these membranes. It would also be very interesting to incorporate them inside a MR in a more advanced stage in order to see how their higher permeability to H_2 would affect the performance of a PBMR, for example, for the WGS reaction.

In terms of the operating conditions tested for the WGS reaction in the PBMR, there were some practical limitations regarding the minimum feed flow rate possible to use, the maximum sweep gas flow possible to use due to mechanical limitations of the membrane or the fact that the set-up was not prepared to use a vacuum pump and the instability of the steam generator used, especially for lower flows. If it was possible to surpass these limitations, a better performance of the PBMR for the WGS reaction would be achieved. Also a verification of the kinetic tests for the $0.5Pt/6CeTiO_2$ catalyst should be done and if

necessary the characterization of the catalyst regarding the effect of each component on the kinetics should be repeated.

Regarding the validation of both 1D and 2D phenomenological models, since only the permeation of H_2 through the Pd-Ag membrane was validated due to time constraints, it would be very interesting to also validate the performance of the PBMR for the WGS reaction predicted by both models.

5.3 Final Appreciation

The combination of both experimental and modeling work during this project made it much more reliable since each component supported the other (for the permeation of H_2 through the Pd-Ag membrane). It was also very interesting, from the experimental point of view, to work with this kind of systems and understand the practical limitations to which they are normally associated. Finally, it was very challenging trying to avoid/solve the many practical problems that kept appearing on a daily basis during this project.

6 References

1. http://www.ucsusa.org/clean_energy/our-energy-choices/a-short-history-of-energy.html, consulted on 1st of May of 2013.
2. Patil, C.S.: 2005, "Membrane reactor technology for ultrapure hydrogen production.", PhD thesis, University of Twente.
3. Wawrzinek, K., Keller, C., 2007. "Industrial hydrogen production & technology", 2nd International workshop on functional materials for mobile hydrogen storage, Karlsruhe research center.
4. Mendes, D.: 2010, "Use of Pd-Ag Membrane Reactors in the Water-Gas Shift Reaction", PhD thesis, Faculty of Engineering – University of Porto.
5. Mendes, D., A. Mendes, L. M. Madeira, A. Iulianelli, J. M. Sousa and A. Basile (2010). "The water-gas shift reaction: from conventional catalytic systems to Pd-based membrane reactors—a review." Asia-Pacific Journal of Chemical Engineering **5**(1): 111-137.
6. http://w3.chem.tue.nl/en/the_department/research_groups/multiphase_reactors/introduction/, consulted on 27th of March of 2013.
7. http://www.making-hydrogen.com/history-of-hydrogen.html, consulted on 16th of May of 2013.
8. http://www.webelements.com/hydrogen/history.html, consulted on 16th of May of 2013.
9. http://www.schydrogen.org/documents/Factsheets/factSheet_history.pdf, consulted on 16th of May of 2013.
10. Tiemersma, T. P., C. S. Patil, M. v. Sint Annaland and J. A. M. Kuipers (2006). "Modelling of packed bed membrane reactors for autothermal production of ultrapure hydrogen." Chemical Engineering Science **61**(5): 1602-1616.
11. Kalamaras, C. M., P. Panagiotopoulou, D. I. Kondarides and A. M. Efstathiou (2009). "Kinetic and mechanistic studies of the water–gas shift reaction on Pt/TiO_2 catalyst." Journal of Catalysis **264**(2): 117-129.
12. Roh, H.-S., H. S. Potdar, D.-W. Jeong, K.-S. Kim, J.-O. Shim, W.-J. Jang, K. Y. Koo and W. L. Yoon (2012). "Synthesis of highly active nano-sized (1 wt.% Pt/CeO2) catalyst for water gas shift reaction in medium temperature application." Catalysis Today **185**(1): 113-118.
13. González, I. D., R. M. Navarro, W. Wen, N. Marinkovic, J. A. Rodriguéz, F. Rosa and J. L. G. Fierro (2010). "A comparative study of the water gas shift reaction over platinum catalysts supported on CeO_2, TiO_2 and Ce-modified TiO_2." Catalysis Today **149**(3-4): 372-379.
14. Maroño, M., J. M. Sánchez and E. Ruiz (2010). "Hydrogen-rich gas production from oxygen pressurized gasification of biomass using a Fe–Cr Water Gas Shift catalyst." International Journal of Hydrogen Energy **35**(1): 37-45.
15. Maroño, M., E. Ruiz, J. M. Sánchez, C. Martos, J. Dufour and A. Ruiz (2009). "Performance of Fe–Cr based WGS catalysts prepared by co-precipitation and oxi-precipitation methods." International Journal of Hydrogen Energy **34**(21): 8921-8928.
16. Mahadevaiah, N., P. Singh, B. D. Mukri, S. K. Parida and M. S. Hegde (2011). "$Ce_{0.67}Fe_{0.33}O_{2-\delta}$ and $Ce_{0.65}Fe_{0.33}Pt_{0.02}O_{2-\delta}$: New water gas shift (WGS) catalysts." Applied Catalysis B: Environmental **108-109**(0): 117-126.

17. Zhang, L., J.-M. M. Millet and U. S. Ozkan (2009). "Deactivation characteristics of Fe–Al–Cu water-gas shift catalysts in the presence of H_2S." Journal of Molecular Catalysis A: Chemical **309**(1–2): 63-70.

18. Gamboa-Rosales, N. K., J. L. Ayastuy, A. Iglesias-González, M. P. González-Marcos and M. A. Gutiérrez-Ortiz (2012). "Oxygen-enhanced WGS over ceria-supported Au-Co_3O_4 bimetallic catalysts." Chemical Engineering Journal **207–208**(0): 49-56.

19. Sakurai, H., T. Akita, S. Tsubota, M. Kiuchi and M. Haruta (2005). "Low-temperature activity of Au/CeO_2 for water gas shift reaction, and characterization by ADF-STEM, temperature-programmed reaction, and pulse reaction." Applied Catalysis A: General **291**(1–2): 179-187.

20. Jeong, D.-W., H. S. Potdar, J.-O. Shim, W.-J. Jang and H.-S. Roh (2013). "H2 production from a single stage water–gas shift reaction over Pt/CeO_2, Pt/ZrO_2, and Pt/$Ce_{(1-x)}Zr_{(x)}O_2$ catalysts." International Journal of Hydrogen Energy **38**(11): 4502-4507.

21. Phatak, A. A., N. Koryabkina, S. Rai, J. L. Ratts, W. Ruettinger, R. J. Farrauto, G. E. Blau, W. N. Delgass and F. H. Ribeiro (2007). "Kinetics of the water–gas shift reaction on Pt catalysts supported on alumina and ceria." Catalysis Today **123**(1–4): 224-234.

22. Radhakrishnan, R., R. R. Willigan, Z. Dardas and T. H. Vanderspurt (2006). "Water gas shift activity and kinetics of Pt/Re catalysts supported on ceria-zirconia oxides." Applied Catalysis B: Environmental **66**(1–2): 23-28.

23. Denkwitz, Y., A. Karpenko, V. Plzak, R. Leppelt, B. Schumacher and R. J. Behm (2007). "Influence of CO_2 and H_2 on the low-temperature water–gas shift reaction on Au/CeO_2 catalysts in idealized and realistic reformate." Journal of Catalysis **246**(1): 74-90.

24. Leppelt, R., B. Schumacher, V. Plzak, M. Kinne and R. J. Behm (2006). "Kinetics and mechanism of the low-temperature water–gas shift reaction on Au/CeO_2 catalysts in an idealized reaction atmosphere." Journal of Catalysis **244**(2): 137-152.

25. Koryabkina, N. A., A. A. Phatak, W. F. Ruettinger, R. J. Farrauto and F. H. Ribeiro (2003). "Determination of kinetic parameters for the water–gas shift reaction on copper catalysts under realistic conditions for fuel cell applications." Journal of Catalysis **217**(1): 233-239.

26. Rhodes, C. and G. J. Hutchings (2003). "Studies of the role of the copper promoter in the iron oxide/chromia high temperature water gas shift catalyst." Physical Chemistry Chemical Physics **5**(12): 2719-2723.

27. Barbieri, G., A. Brunetti, A. Caravella and E. Drioli (2011). "Pd-based membrane reactors for one-stage process of water gas shift." RSC Advances **1**(4): 651-661.

28. Miguel, C. V., A. Mendes, S. Tosti and L. M. Madeira (2012). "Effect of CO and CO2 on H_2 permeation through finger-like Pd–Ag membranes." International Journal of Hydrogen Energy **37**(17): 12680-12687.

29. Tosti, S., A. Basile, L. Bettinali, F. Borgognoni, F. Chiaravalloti and F. Gallucci (2006). "Long-term tests of Pd–Ag thin wall permeator tube." Journal of Membrane Science **284**(1–2): 393-397.

30. Mendes, D., S. Sá, S. Tosti, J. M. Sousa, L. M. Madeira and A. Mendes (2011). "Experimental and modeling studies on the low-temperature water-gas shift reaction in a dense Pd–Ag packed-bed membrane reactor." Chemical Engineering Science **66**(11): 2356-2367.

31. Santucci, A., F. Borgognoni, M. Vadrucci and S. Tosti (2013). "Testing of dense Pd–Ag tubes: Effect of pressure and membrane thickness on the hydrogen permeability." Journal of Membrane Science **444**(0): 378-383.

32. Peters, T. A., T. Kaleta, M. Stange and R. Bredesen (2011). "Development of thin binary and ternary Pd-based alloy membranes for use in hydrogen production." Journal of Membrane Science **383**(1–2): 124-134.

33. Gallucci, F., M. Van Sintannaland and J. A. M. Kuipers (2010). "Theoretical comparison of packed bed and fluidized bed membrane reactors for methane reforming." International Journal of Hydrogen Energy **35**(13): 7142-7150.

34. Mendes, D., V. Chibante, J.-M. Zheng, S. Tosti, F. Borgognoni, A. Mendes and L. M. Madeira (2010). "Enhancing the production of hydrogen via water–gas shift reaction using Pd-based membrane reactors." International Journal of Hydrogen Energy **35**(22): 12596-12608.

35. Marín, P., F. V. Díez and S. Ordóñez (2012). "Fixed bed membrane reactors for WGSR-based hydrogen production: Optimisation of modelling approaches and reactor performance." International Journal of Hydrogen Energy **37**(6): 4997-5010.

36. Okazaki, J., T. Ikeda, D. A. P. Tanaka, K. Sato, T. M. Suzuki and F. Mizukami (2011). "An investigation of thermal stability of thin palladium–silver alloy membranes for high temperature hydrogen separation." Journal of Membrane Science **366**(1–2): 212-219.

37. Tosti, S., M. Fabbricino, A. Moriani, G. Agatiello, C. Scudieri, F. Borgognoni and A. Santucci (2011). "Pressure effect in ethanol steam reforming via dense Pd-based membranes." Journal of Membrane Science **377**(1–2): 65-74.

38. Ackerman, F. J. and G. J. Koskinas (1972). "Permeation of hydrogen and deuterium through palladium-silver alloys." Journal of Chemical & Engineering Data **17**(1): 51-55.

39. Gallucci, F., F. Chiaravalloti, S. Tosti, E. Drioli and A. Basile (2007). "The effect of mixture gas on hydrogen permeation through a palladium membrane: Experimental study and theoretical approach." International Journal of Hydrogen Energy **32**(12): 1837-1845.

40. Bi, Y., H. Xu, W. Li and A. Goldbach (2009). "Water–gas shift reaction in a Pd membrane reactor over $Pt/Ce_{0.6}Zr_{0.4}O_2$ catalyst." International Journal of Hydrogen Energy **34**(7): 2965-2971.

41. Basile, A., E. Drioli, F. Santell, V. Violante, G. Capannelli and G. Vitulli (1996). "A study on catalytic membrane reactors for water gas shift reaction." Gas Separation & Purification **10**(1): 53-61.

42. Barbieri, G., F. Scura, F. Lentini, G. De Luca and E. Drioli (2008). "A novel model equation for the permeation of hydrogen in mixture with carbon monoxide through Pd–Ag membranes." Separation and Purification Technology **61**(2): 217-224.

Appendix A - Results of the Permeation Tests for the Thin Pd Membranes

A.1 - Experiments Performed for the Thin Pd Membranes

For the thin Pd membranes supplied by TECNALIA group the experimental conditions presented in Table A.1 were investigated before they started presenting N_2 flows from the retentate to the permemeate side. Besides the conditions presented in Table A.1, the flow of N_2 through the membranes was also measured for a N_2 partial pressure difference of 2.0 and 2.5 bar for the 3.5-4.0 and 4.0-5.0 μm thick membranes respectively in order to obtain the H_2/N_2 ideal selectivity. The set of experiments performed for the thinner membrane was the one that was being studied by a PhD student when this project started.

A.2 - Results Obtained

In Figures A.1 and A.2 is presented the flux of H_2 through the 3.5-4.0 and 4.0-5.0 μm thick Pd membranes respectively for different H_2 partial pressure differences in the membrane and different H_2 compositions in the feed (for the case of the thinner membrane).

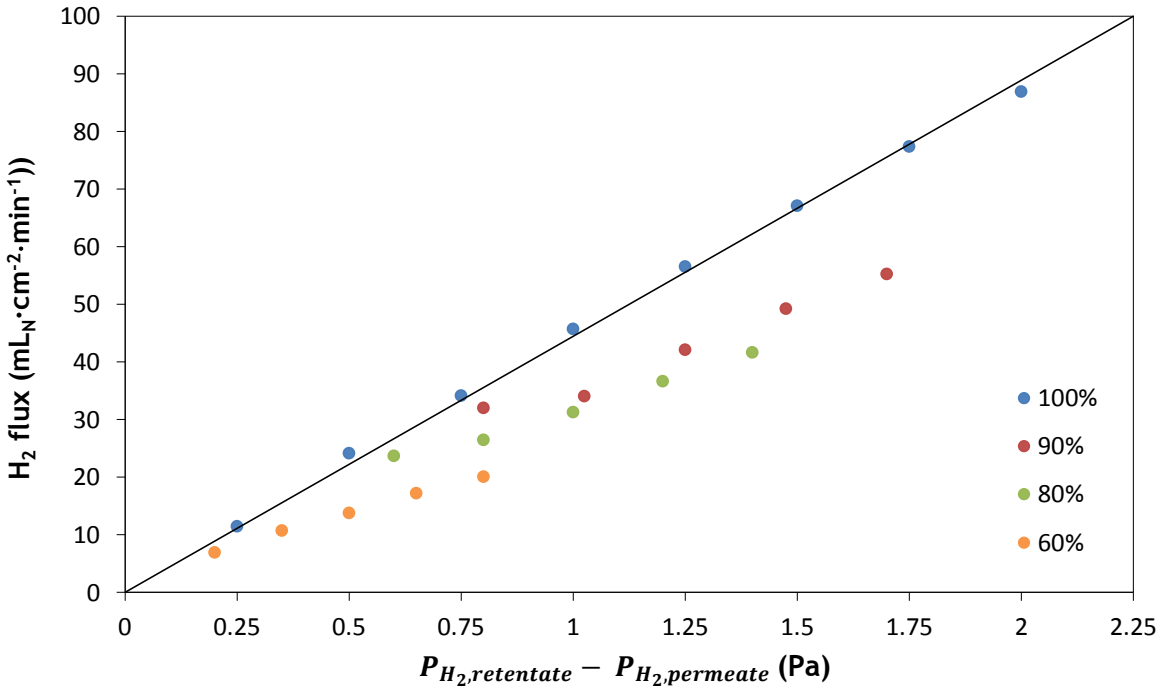

Figure A.1 - Flux of H_2 through the 3.5-4.0 μm thick Pd membrane as a function of the H_2 trans-membrane partial pressure difference for different H_2 volume compositions at 400 ˚C.

Table A.1 – Overview of the conditions investigated before the detection of N_2 leaks.

Temperature (°C)	Pd membrane thickness (μm)	Feed flow ($mL_N \cdot min^{-1}$)	Trans-membrane H_2 partial pressure difference (bar)	H_2 concentration (volume %)	N_2 concentration (volume %)	CO concentration (volume %)	CO_2 concentration (volume %)	Number of data points
		1516	0.25-2	100	0	0	0	8
		1516	0.8-1.7	90	10	0	0	5
		1516	0.6-1.4	80	10	0	0	5
		2021	0.2-0.8	60	40	0	0	5
		3536	0.2	40	60	0	0	1
400	3.5-4.0	2021	0.2-0.8	60	30	10	0	5
		2021	0.2-0.8	60	20	20	0	5
		2021	0.2-0.8	60	10	30	0	5
		2021	0.2-0.8	60	30	0	10	5
		2021	0.2-0.8	60	20	0	20	5
		2021	0.2-0.8	60	10	0	30	5
300	4.0-5.0	202-1010	0.5-2.5	100	0	0	0	5

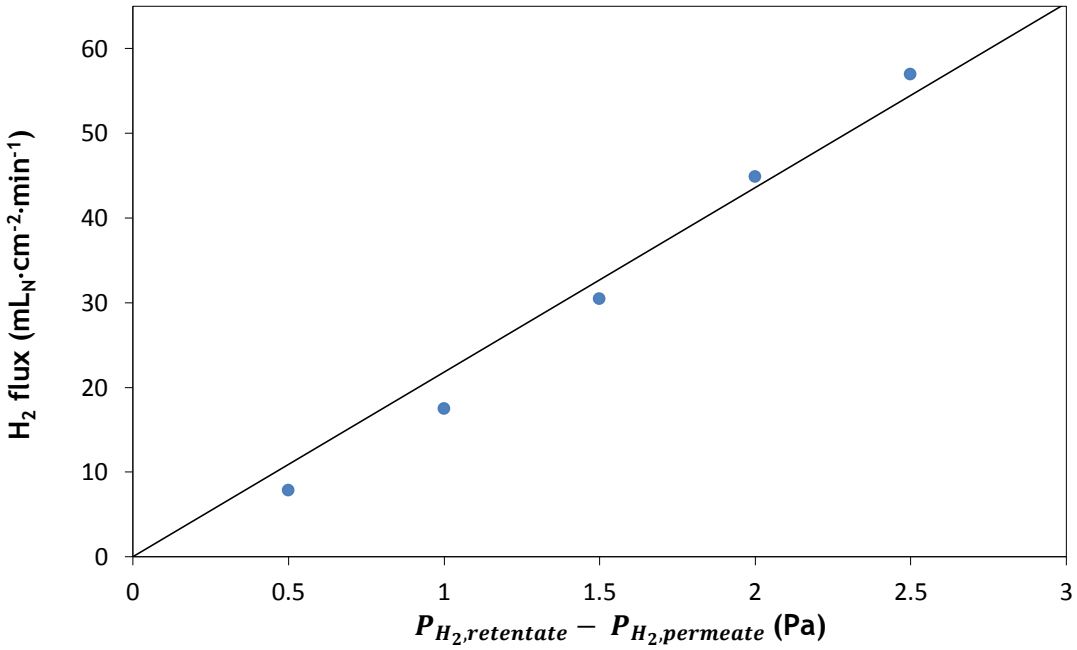

Figure A.2 - Flux of H_2 through the 4.0-5.0 μm thick Pd membrane as a function of the H_2 trans-membrane partial pressure difference at 300 ˚C.

The first thing that can be noticed by analysing Figures A.1 and A.2 is that the fluxes of H_2 that permeate through both membranes are around 10 times higher than the ones obtained for the Pd-Ag membrane. This higher permeation is due to the lower thickness of these membranes. For the thinnest membrane it can be observed that for a pure H_2 feed the H_2 flux that passes through the membrane is directly proportional to the H_2 partial pressure difference in the membrane. By comparing both regressions presented in Figure A.3 and A.4 it is possible to see that indeed a value of 1 for the pressure exponent allows a better data fitting than 0.5. For the thicker membrane a pressure exponent of 1 also allows a better fitting, as observed in Figures A.5 and A.6, however the data fitting for both pressure exponent values is quite poorer than the one for the previous membrane.

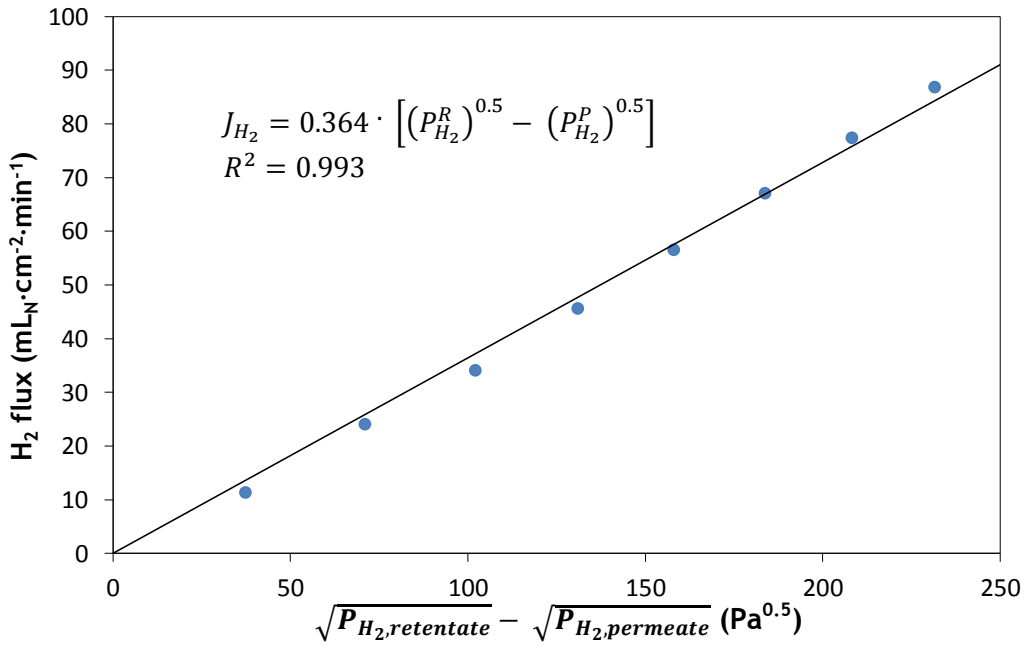

Figure A.3 - Linear regression of the H_2 flux through the 3.5-4.0 μm thick Pd membrane as a function of the difference between the square roots of the hydrogen partial pressure in the retentate and permeate sides at 400 ˚C.

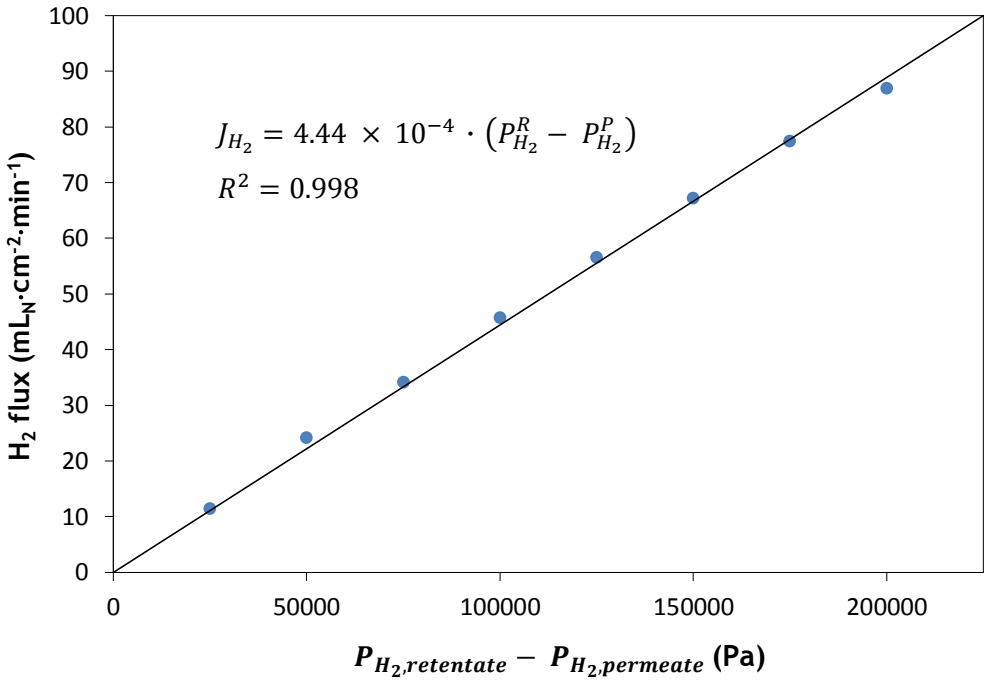

Figure A.4 - Linear regression of the H_2 flux through the 3.5-4.0 μm thick Pd membrane as a function of the difference between the H_2 partial pressure in the retentate and permeate sides at 400 ˚C.

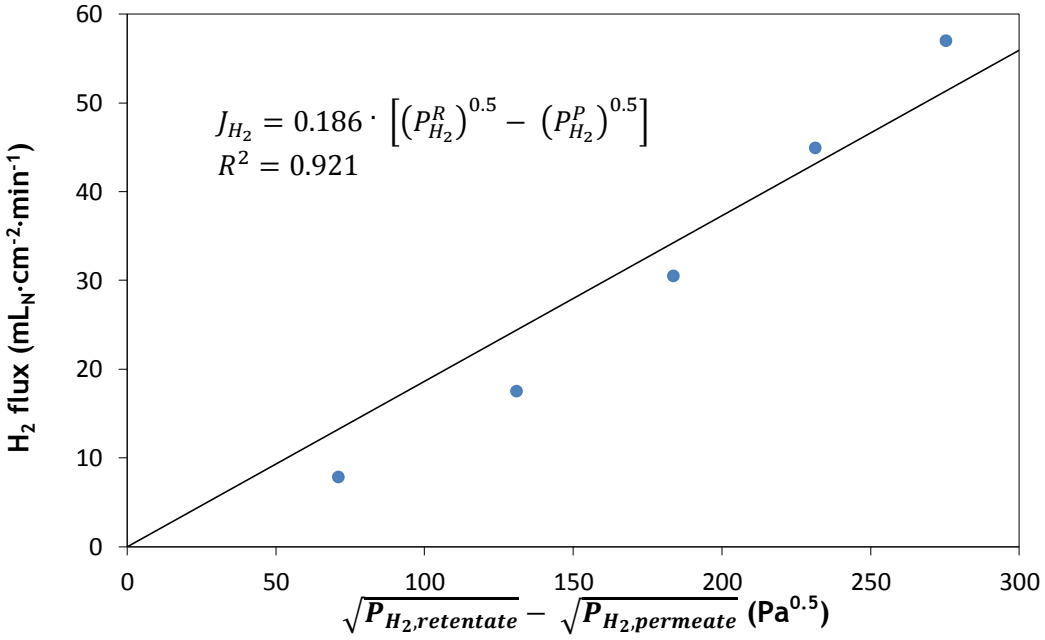

Figure A.5 - Linear regression of the H_2 flux through the 4.0-5.0 μm thick Pd membrane as a function of the difference between the square roots of the hydrogen partial pressure in the retentate and permeate sides at 300 ˚C.

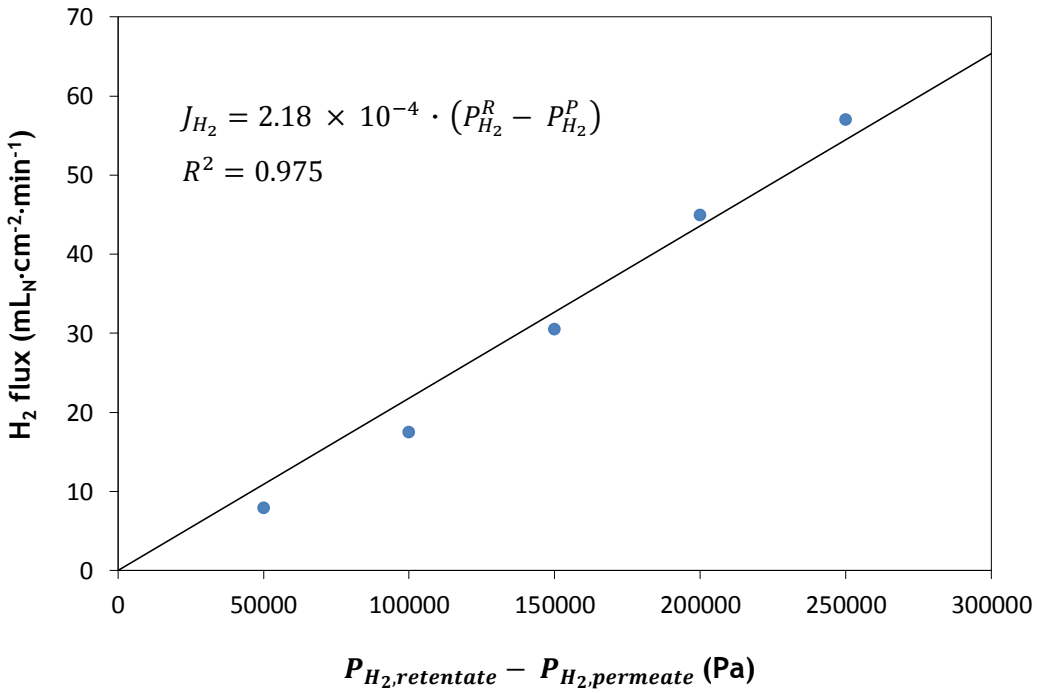

Figure A.6 - Linear regression of the H_2 flux through the 3.5-4.0 μm thick Pd membrane as a function of the difference between the H_2 partial pressure in the retentate and permeate sides at 400 ˚C.

In order to find the optimum value of the pressure exponent the CSTR approach was once again considered and the data fitting procedure used in section 3.1.3 was used. In Tables A.2 and A.3 there are presented for the 3.5-4.0 and 4.0-5.0 μm thick Pd membranes respectively the values of the two independent parameters that allow a minimum relative error in the flux prediction over all the measurement points for a pure H_2 feed.

Table A.2 - Results of error minimisation for the 3.5-4.0 μm thick Pd membrane.

Temperature (°C)	x	k_{Pd} (mol·m^{-1}·s^{-1}·Pa^{-x})	P_{Pd,H_2}(mol·m^{-1}.s^{-1}·Pa^{-x})	ε (%)
400	0.85	6.994×10^{-7}	8.349×10^{-11}	2.829×10^{-1}

Table A.3 - Results of error minimisation for the 4.0-5.0 μm thick Pd membrane.

Temperature (°C)	x	k_{Pd} (mol·m^{-1}·s^{-1}·Pa^{-x})	P_{Pd,H_2}(mol·m^{-1}.s^{-1}·Pa^{-x})	ε (%)
300	1.00	4.169×10^{-8}	5.972×10^{-12}	10.54 %

It can be concluded that indeed for these thin membranes the permeation of H_2 is more controlled by the adsorption of H_2 on the Pd surface and dissociation into atomic hydrogen than the Pd-Ag membrane. In fact, for the thicker membrane the value of the pressure exponent indicates that the permeation of H_2 is exclusively controlled by the adsorption and subsequent dissociation of H_2 on the Pd surface. However, the error obtained for this value of x is quite high (much higher than the ones obtained for the other 2 membranes) meaning that even considering a pressure exponent of 1 is still a quite rough approximation. Since it wasn't possible to perform permeation tests for different temperatures due to the appearance of N_2 leaks, it was not possible to calculate the apparent activation energy and pre-exponential factor for hydrogen permeation through these thin membranes. For these membranes the N_2 flow through the membrane was also measured for a feed of pure N_2. For the thinner membrane the N_2 flux measured at 400 °C for a N_2 pressure difference of 2.0 bar was 0.019 mL_N·min^{-1}·cm^{-2} and for the thicker Pd membrane it was 0.073 mL_N·min^{-1}·cm^{-2} at 300 °C and for a N_2 pressure difference of 2.50 bar. The ideal H_2/N_2 selectivities obtained were 4603 and 781 respectively, which are much lower than the one obtained for the Pd-Ag membrane.

The poisoning effect of CO and CO_2 was analysed as well. In Figure A.7 it is shown the variation of the hydrogen flux through the 3.5-4.0 μm thick Pd membrane, for different hydrogen trans-membrane partial pressure differences, as a function of the concentration of CO. In this case it is possible to observe once again that for lower concentrations of CO the decrease of the H_2 flux through the thin Pd membrane is higher than for the decrease

obtained for further equal additions of CO. In this case however, the dilution effect for higherconcentrations of CO in the feed wasn't felt because the total volume percentage of H_2 in the feed was kept constant (60%). As a matter of fact, for higher concentrations of CO there was a slight increase in the amount of H_2 permeating through the membrane.

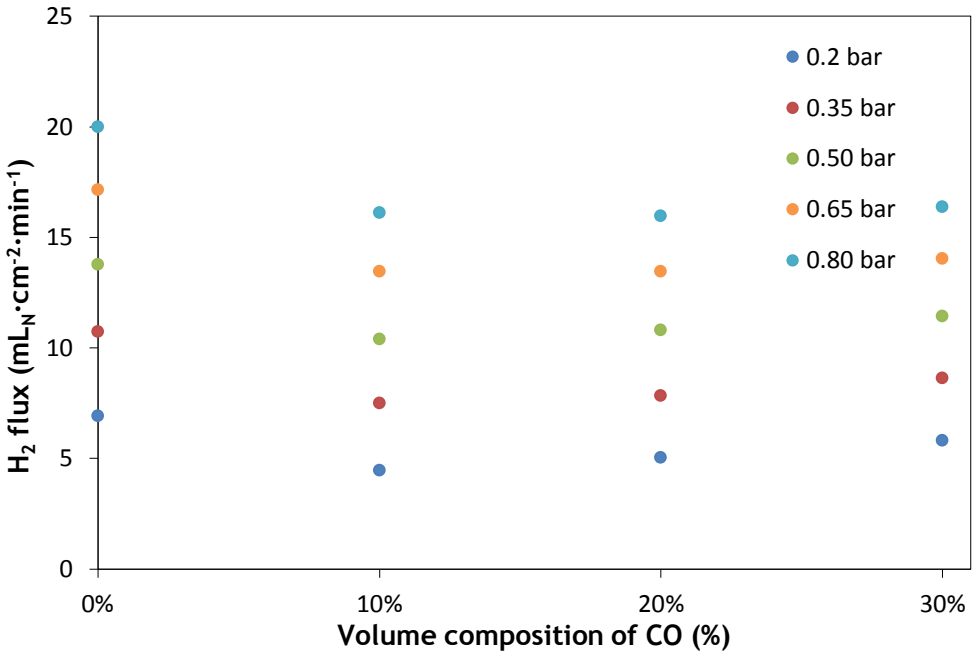

Figure A.7 - H_2 flux as a function of the CO concentration in the feed for different H_2 trans-membrane partial pressure differences at 400 ˚C for the 3.5-4.0 μm thick Pd membrane.

In Figure A.8 it is presented the poisoning effect of CO_2 on the H_2 flux that permeates through the thin Pd membrane.

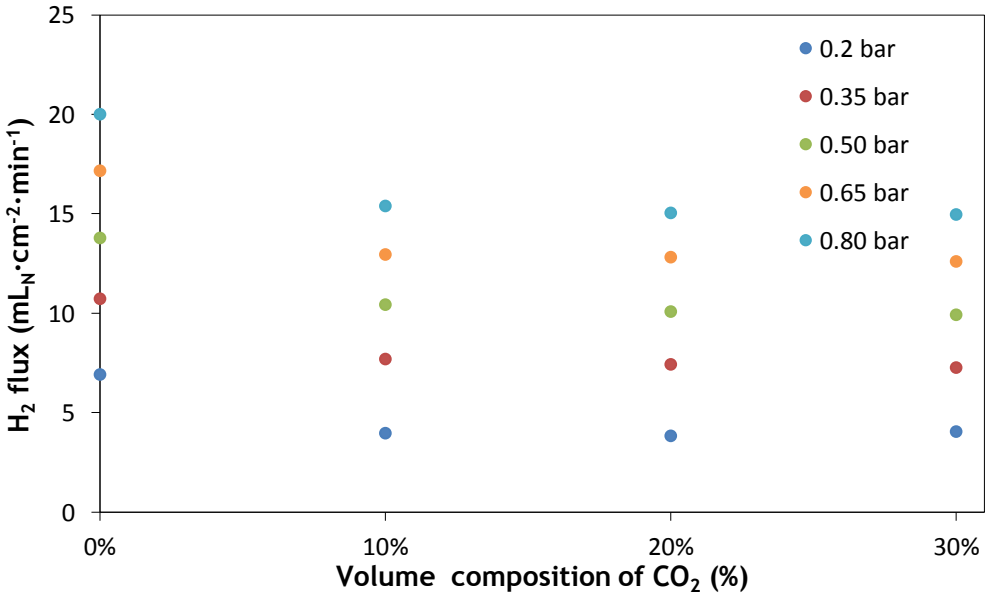

Figure A.8 - H_2 flux as a function of the CO_2 concentration in the feed for different H_2 trans-membrane partial pressure differences at 400 ˚C for the 3.5-4.0 μm thick Pd membrane.

By analysing Figure A.8 it is possible to verify that CO_2 affects the permeation of H_2 through the membrane in a similar way CO does.

Appendix B – Gas Chromatograph Calibration

In order to calibrate the gas chromatograph (GC) it is necessary to know approximately what will be the composition of the analysed streams during the membrane and PBMR tests. With that in mind the following calibrations in Table B.1 were done.

Table B.1 - Calibrations done for N_2, CO and CO_2.

Component	Volume Composition (%)
N_2	10-70
CO	0-10
CO_2	10-60

Due to some difficulties regarding the calibration for hydrogen, the composition in hydrogen was determined from the mass balance (difference from 100% on a dry basis).

For the calibrations, mixtures of the desired component and N_2 with known compositions were used. For the calibration of N_2 the second component used in the mixture was CO. After the measurements in the GC the chromatograms were reprocessed for the respective volume compositions of the desired component. In Tables B.2, B.3 and B.4 are presented the binary mixtures used for the calibration of the GC.

Table B.2 - Binary mixtures used for the calibration of N_2.

N_2 Volume Composition (%)	CO Volume Composition (%)
10	90
15	85
25	75
35	65
70	30

Table B.3 - Binary mixtures used for the calibration of CO.

CO Volume Composition (%)	N_2 Volume Composition (%)
2.5	97.5
5.0	95.0
7.5	92.5
10.0	90.0

Table B.4 - Binary mixtures used for the calibration of CO_2.

CO_2 Volume Composition (%)	N_2 Volume Composition (%)
10	90
15	85
25	75
35	65
45	55
60	40

For each composition of each component being calibrated at least three agreeing points were used for the respective calibration curves. The calibration curves obtained are presented in Figures B.1, B.2 and B.3.

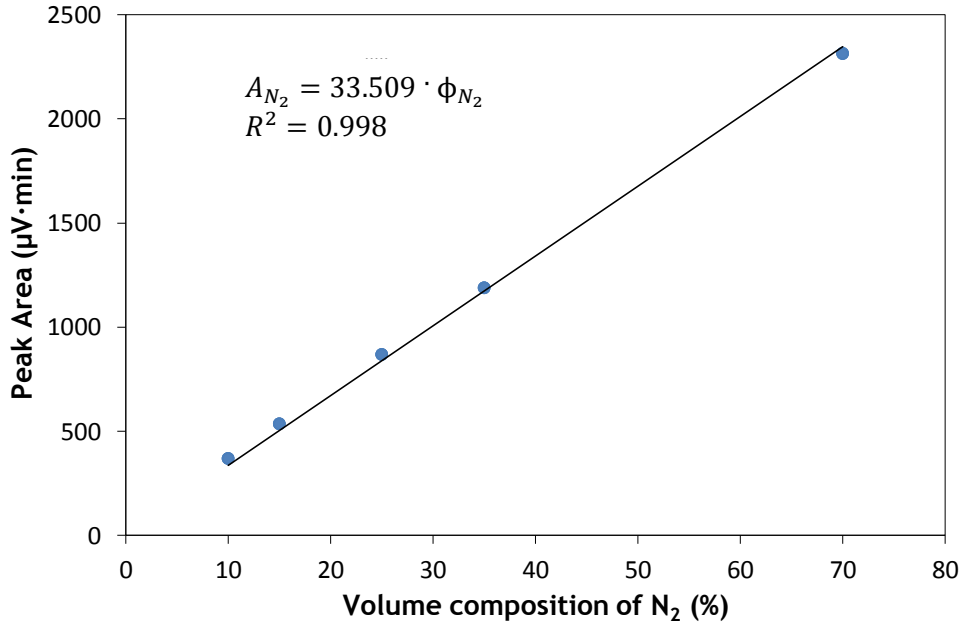

Figure B.1 - Calibration curve for N_2.

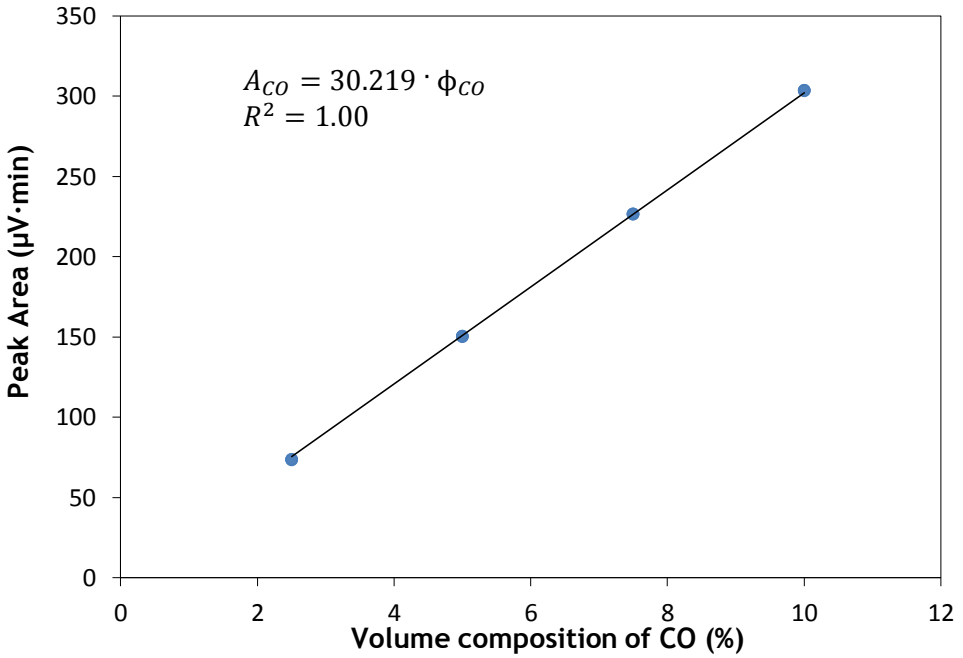

Figure B.2 - Calibration curve for CO.

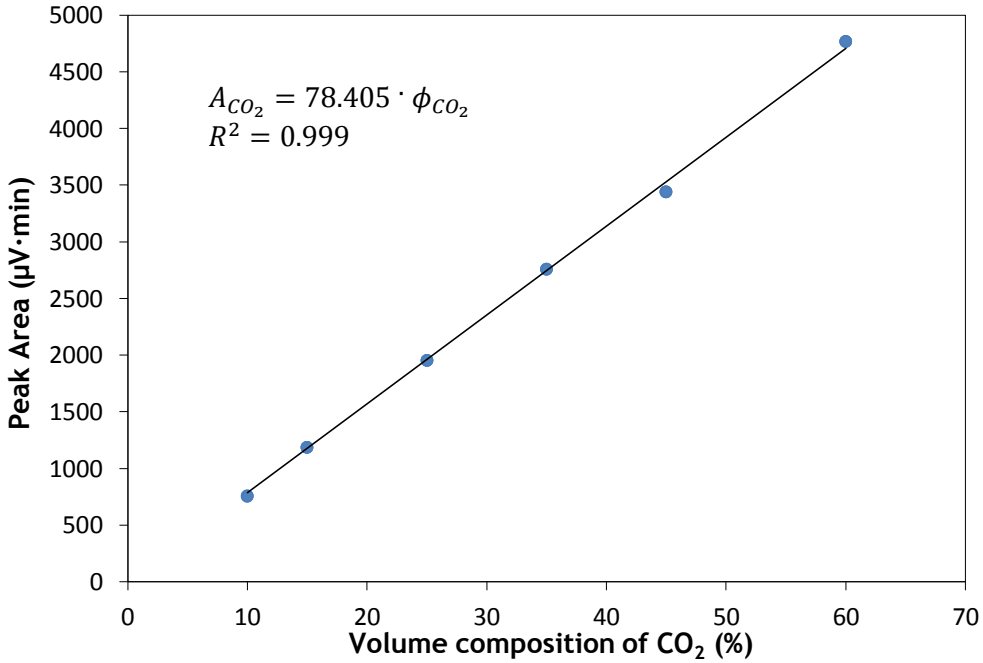

Figure B.3 - Calibration curve for CO_2.

All the measurements in the GC were done with all columns at 70 ˚C. In order to have results with the highest quality possible, during the night the GC was left in the cleaning mode with all columns at 180 ˚C in order to eliminate any residues present in the columns. This way all the measurements of the following day would not be affected by possible remaining residues of the previous day.

Appendix C – Supporting Data for the Permeation Results of the Pd-Ag Membrane

C.1 – Regressions for $x = 0.5$ and $x = 1$

In order to find out which value of the pressure exponent, 0.5 or 1, best describes the permeation of H_2 through the Pd-Ag membrane, the H_2 flux through the membrane was represented as a function of the hydrogen partial pressure difference in the membrane for both values of the pressure exponent and then linear regressions were done. The linear regressions for both values of x at each temperature are presented below.

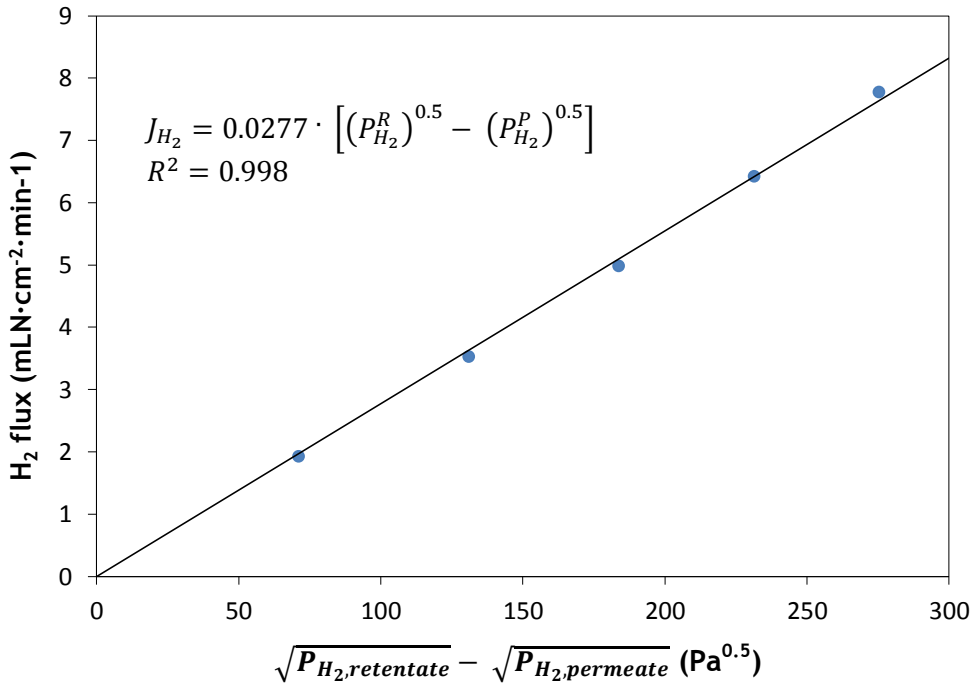

Figure C.1 - Linear regression of the hydrogen flux through the Pd-Ag membrane as a function of the difference between the square roots of the hydrogen partial pressure in the retentate and permeate sides at 300 ˚C.

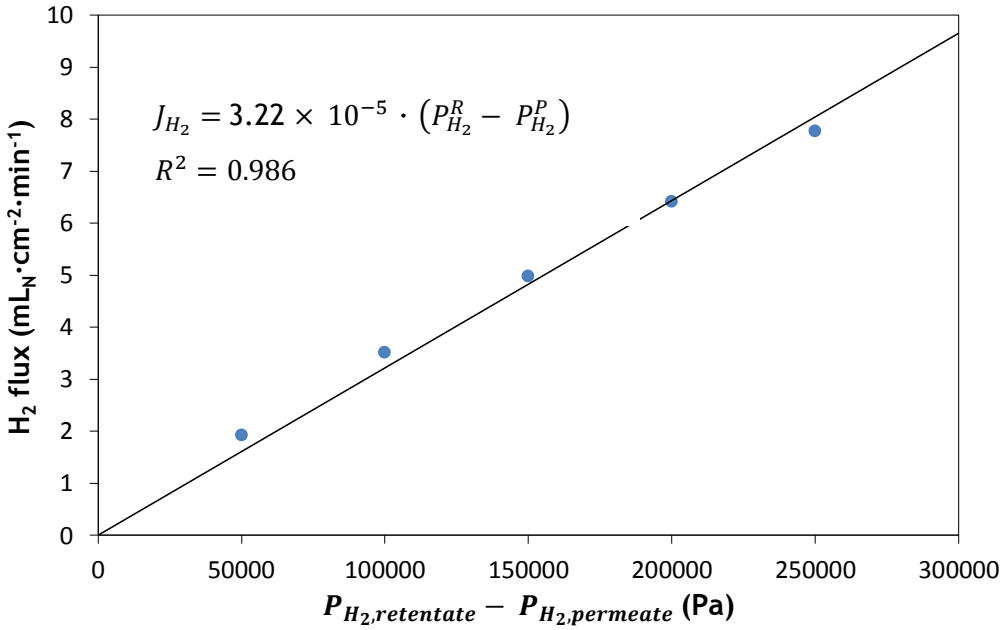

Figure C.2 - Linear regression of the hydrogen flux through the Pd-Ag membrane as a function of the difference between the hydrogen partial pressure in the retentate and permeate sides at 300 ˚C.

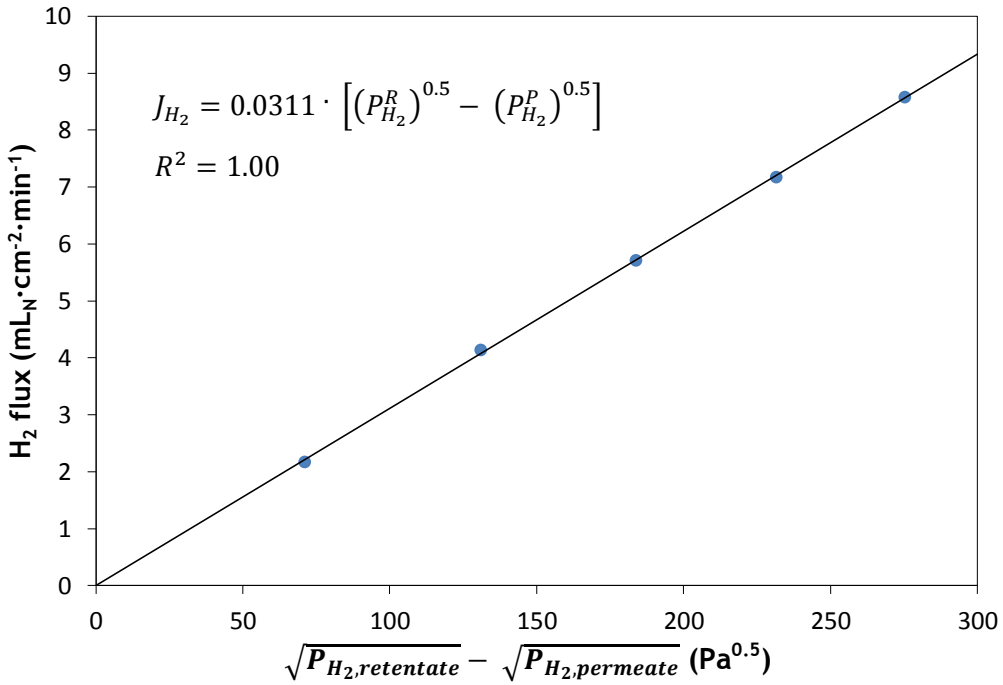

Figure C.3 - Linear regression of the hydrogen flux through the Pd-Ag membrane as a function of the difference between the square roots of the hydrogen partial pressure in the retentate and permeate sides at 400 ˚C.

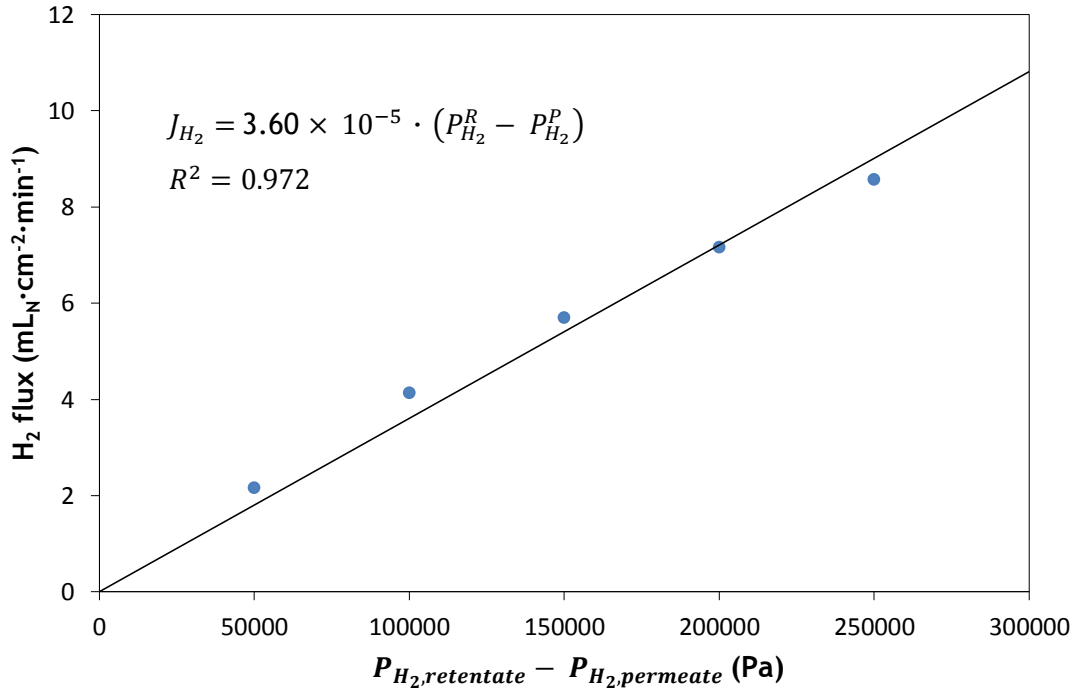

Figure C.4 - Linear regression of the hydrogen flux through the Pd-Ag membrane as a function of the difference between the hydrogen partial pressure in the retentate and permeate sides at 400 ˚C.

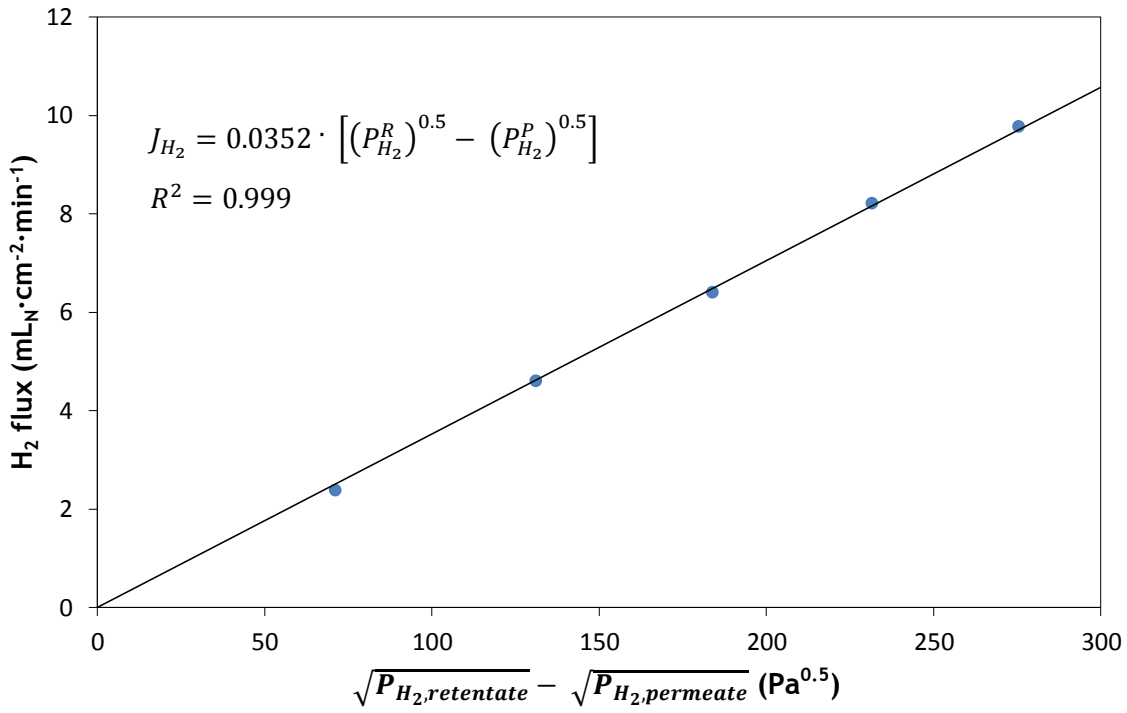

Figure C.5 - Linear regression of the hydrogen flux through the Pd-Ag membrane as a function of the difference between the square roots of the hydrogen partial pressure in the retentate and permeate sides at 500 ˚C.

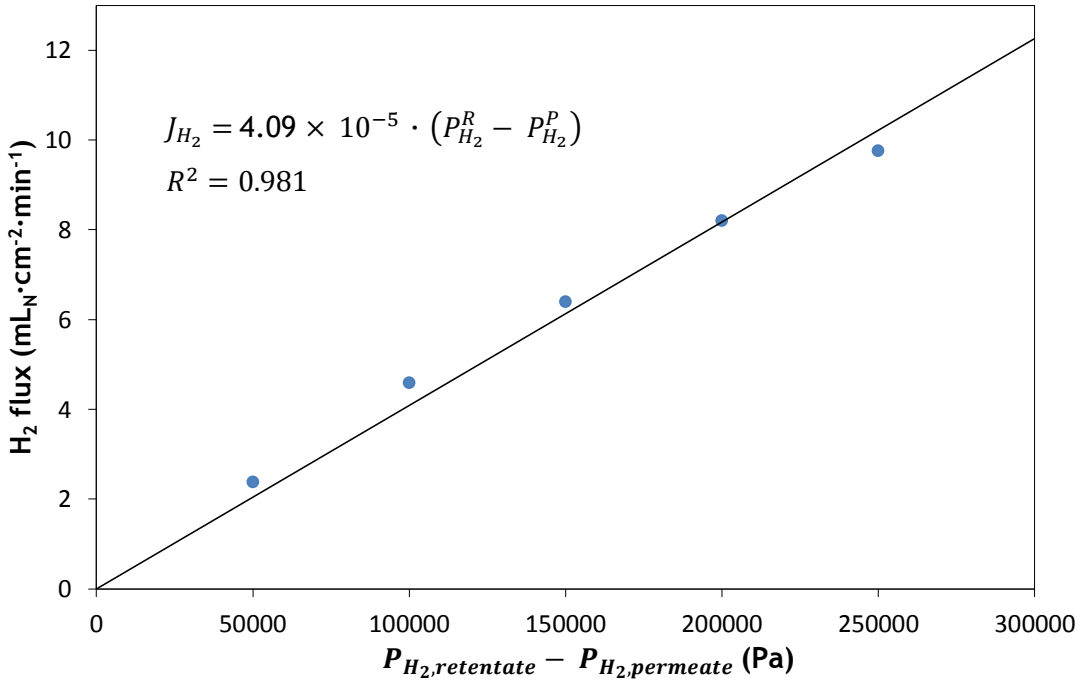

Figure C.6 - Linear regression of the hydrogen flux through the Pd-Ag membrane as a function of the difference between the hydrogen partial pressure in the retentate and permeate sides at 500 ˚C.

Indeed all the linear regressions for a pressure exponent of 0.5 showed a better fitting than the ones assuming a value of 1 for the pressure exponent.

C.2 – Comparison Between the Predicted Flux Values and the Measured Flux Values (Parity Plots)

The parity plots that relate the predicted fluxes of H_2 through the Pd-Ag membrane (for the pressure exponents that present the lowest relative errors and for 0.5) with the measured fluxes are presented below.

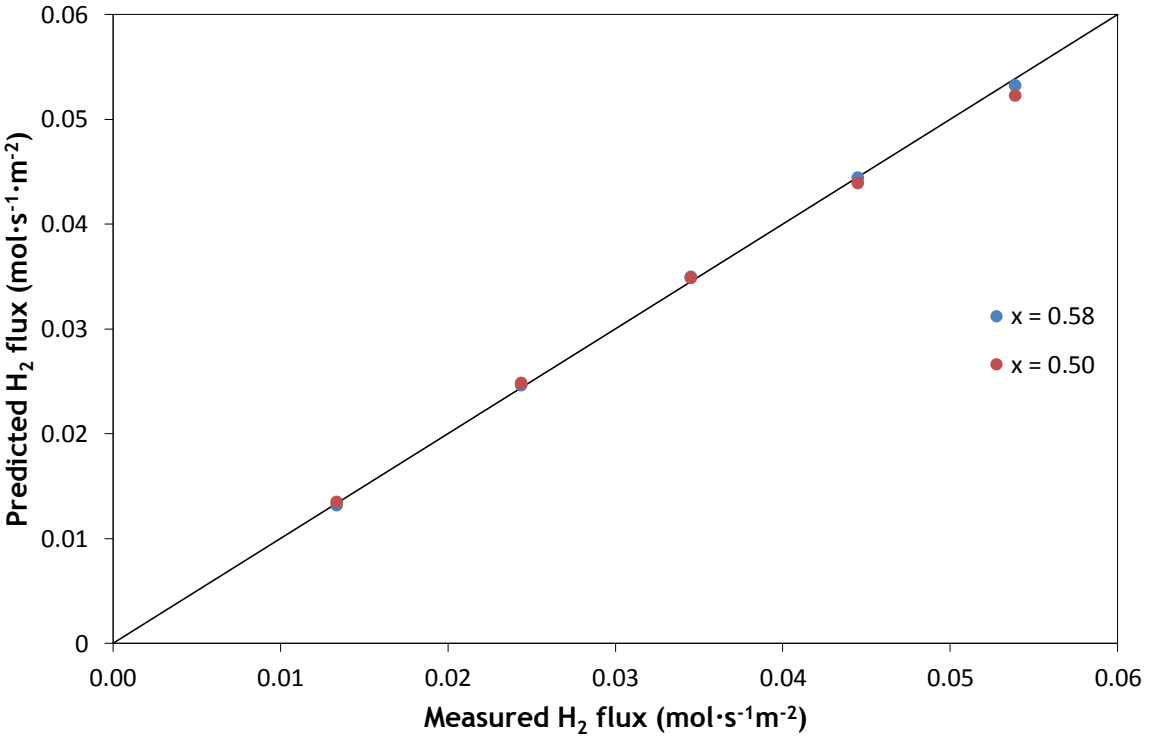

Figure C.7 - Comparison of the parity plots for x = 0.58 and x = 0.50 at 300 ˚C.

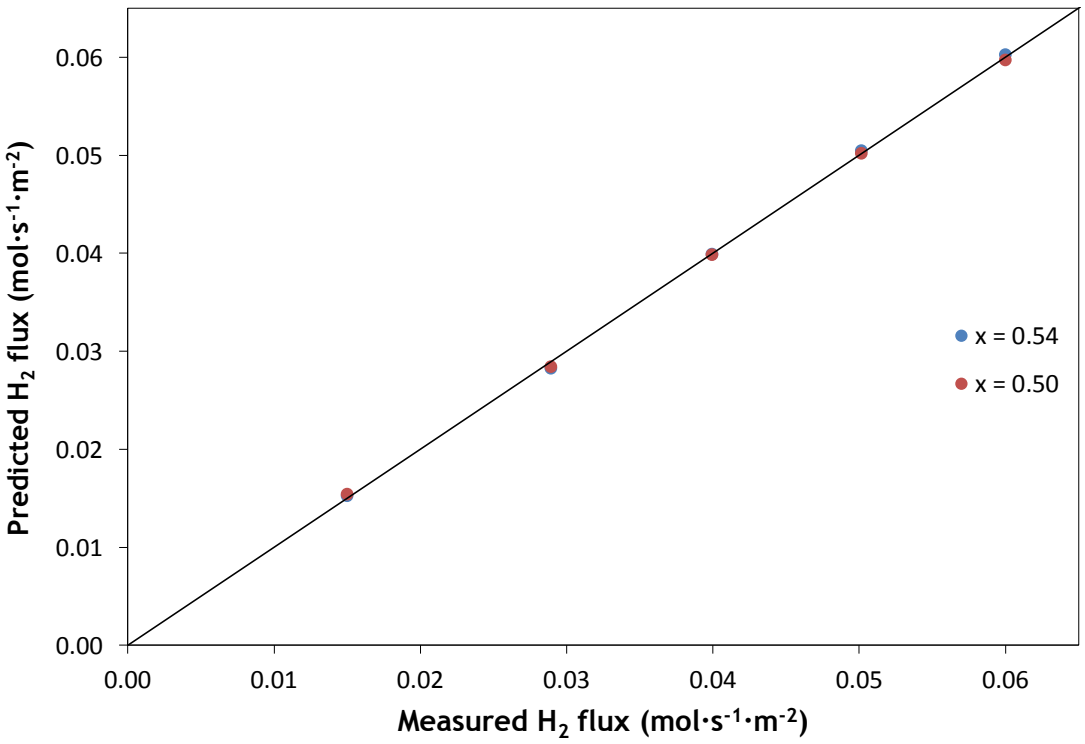

Figure C.8 - Comparison of the parity plots for x = 0.54 and x = 0.50 at 400 ˚C.

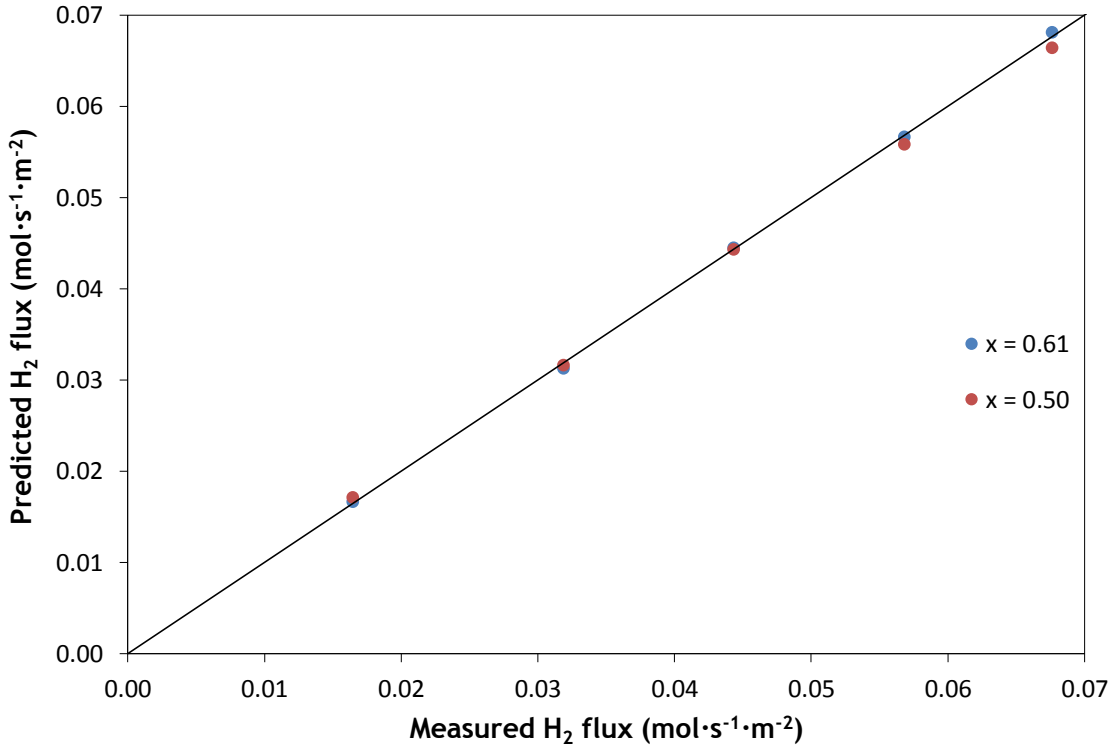

Figure C.9 - Comparison of the parity plots for x = 0.61 and x = 0.50 at 500 ˚C.

As can be seen in the parity plots the difference between the values of x that allow the attainment of the minimum relative error and 0.5 is very small. This proves once again that assuming that the pressure exponent is 0.5 is a good approximation.

Appendix D – Catalyst Characterization

Before performing the WGS reaction inside the PBMR it must be decided which catalyst is going to be used and measure the kinetic parameters for the WGS reaction on that catalyst under certain conditions, which are similar to the ones that are going to be used during the WGS reaction carried inside the PBMR. In this project a 0.5Pt/6CeTiO$_2$ catalyst with an average particle size between 150-350 μm was used for the reasons previously mentioned. Since this catalyst had already been characterized by a PhD student, only a brief summary of the kinetic parameters obtained is presented.

D.1 - Kinetics of the WGS Reaction on the 0.5Pt/6CeTiO$_2$ Catalyst

The effect of temperature on the activity of the Pt-based catalyst was firstly accessed being that it was observed that by increasing the temperature from 250 to 300 ˚C the reaction rate increased gradually and therefore an increase in the conversion of CO was observed, as shown in Figure D.1. It was also verified that the Pt-based catalyst becomes much more active for higher temperatures (Figure D.2).

In order to determine the apparent activation energy the Arrhenius plot presented in Figure D.3 was used.

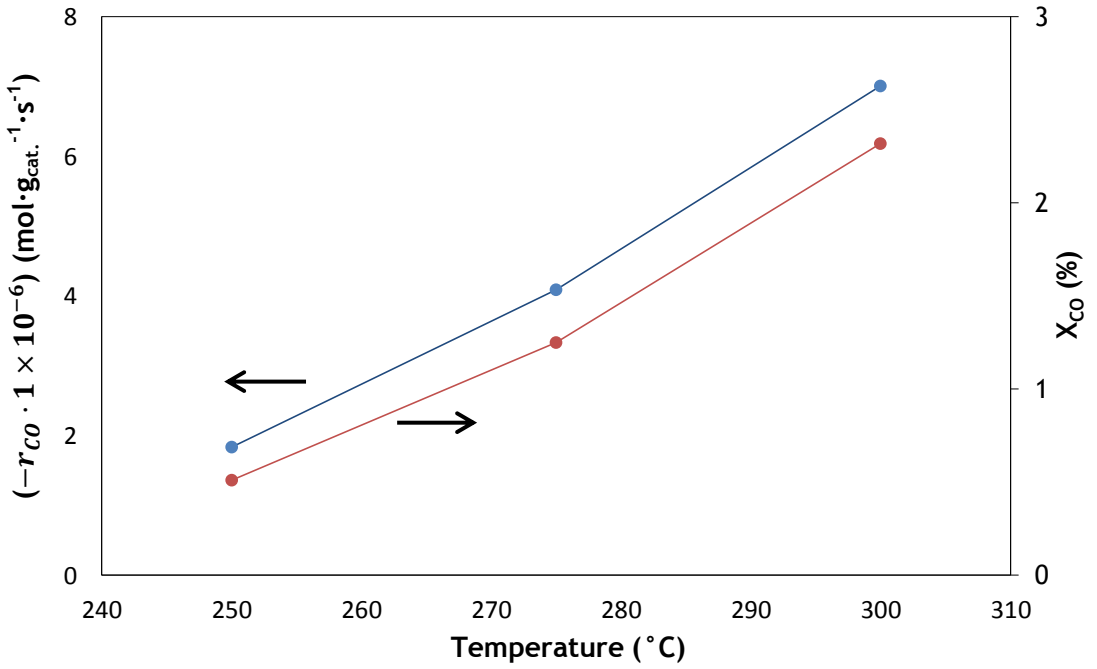

Figure D.1 - Effect of temperature on the activity of the 0.5Pt/6CeTiO$_2$ catalyst and on the X_{CO} for temperatures between 250 and 300 ˚C.

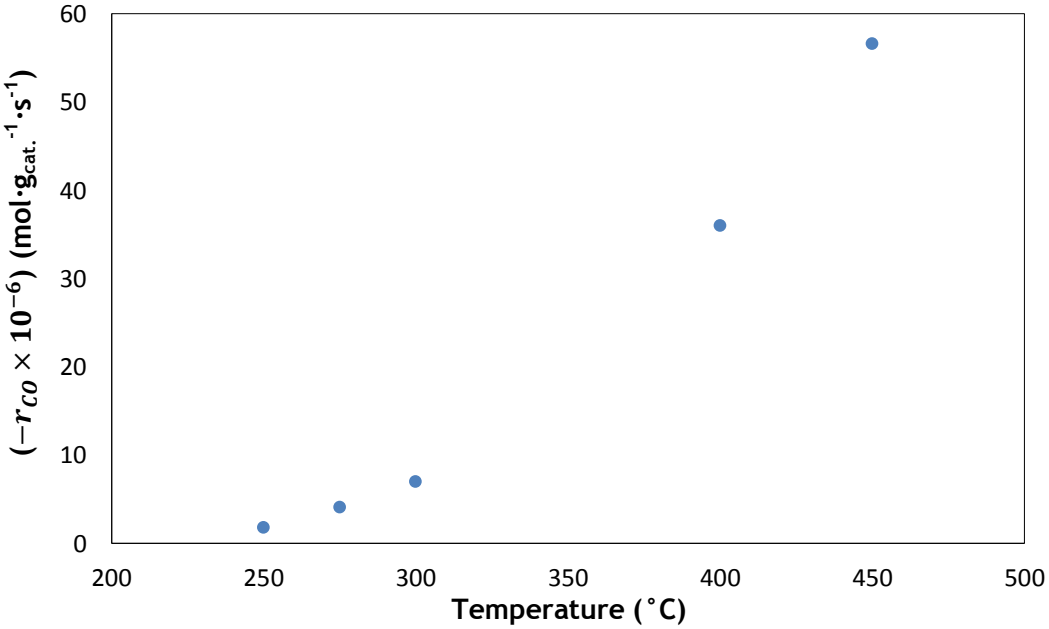

Figure D.2 - Effect of temperature on the activity of the 0.5Pt/6CeTiO$_2$ for temperatures between 250 and 450 ˚C.

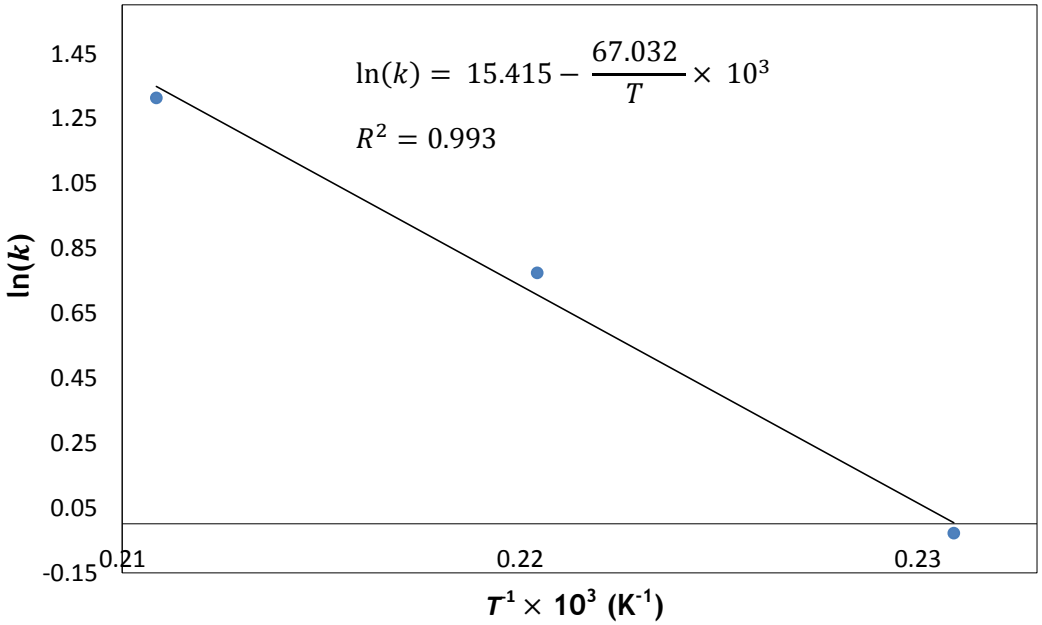

Figure D.3 - Arrhenius plot for the WGS reaction carried over the 0.5Pt/6CeTiO$_2$ catalyst for the temperature range between 250 and 300 ˚C and the following inlet gas volume composition: 5% CO, 7.5% CO_2, 40% H_2O and 35% H_2 balanced with N_2.

The apparent activation energy and pre-exponential factor can be obtained from the linear regression equation. The results for both parameters are presented in Table D.1.

Table D.1 - Apparent activation energy and pre-exponential factor (k_0) obtained for the WGS reaction over the 0.5Pt/6CeTiO$_2$ catalyst.

E_a (kJ·mol^{-1})	k_0 (s^{-1})
67	4.95×10^6

The effect of each intervenient in the WGS reaction on the activity of the Pt-based catalyst was also evaluated. In order to do this, the composition of the component whose effect was being analysed was changed while the composition of the other three components that participate in the WGS reaction was kept constant, for the same pressure and temperature. For each case a power type regression was used in order to determine the apparent partial reaction order for each component, as shown in Figures D.4, D.5, D.6 and D.7.

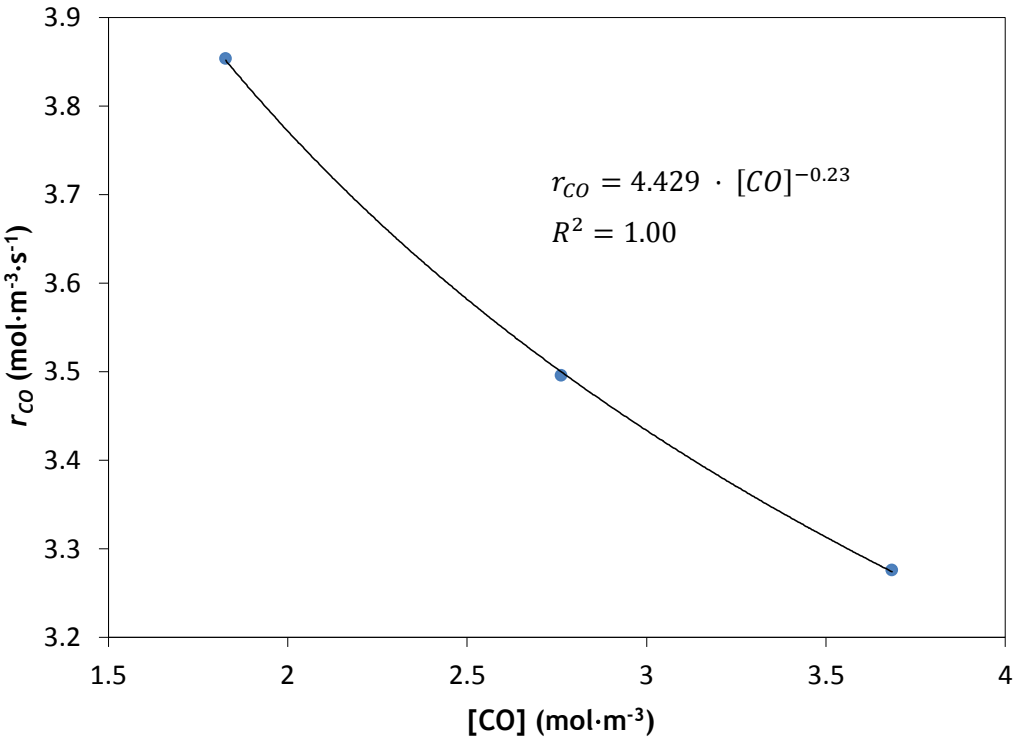

Figure D.4 - Determination of the apparent WGS reaction order for CO for the 0.5Pt/6CeTiO$_2$ catalyst at 275 ºC and 1 bar total pressure.

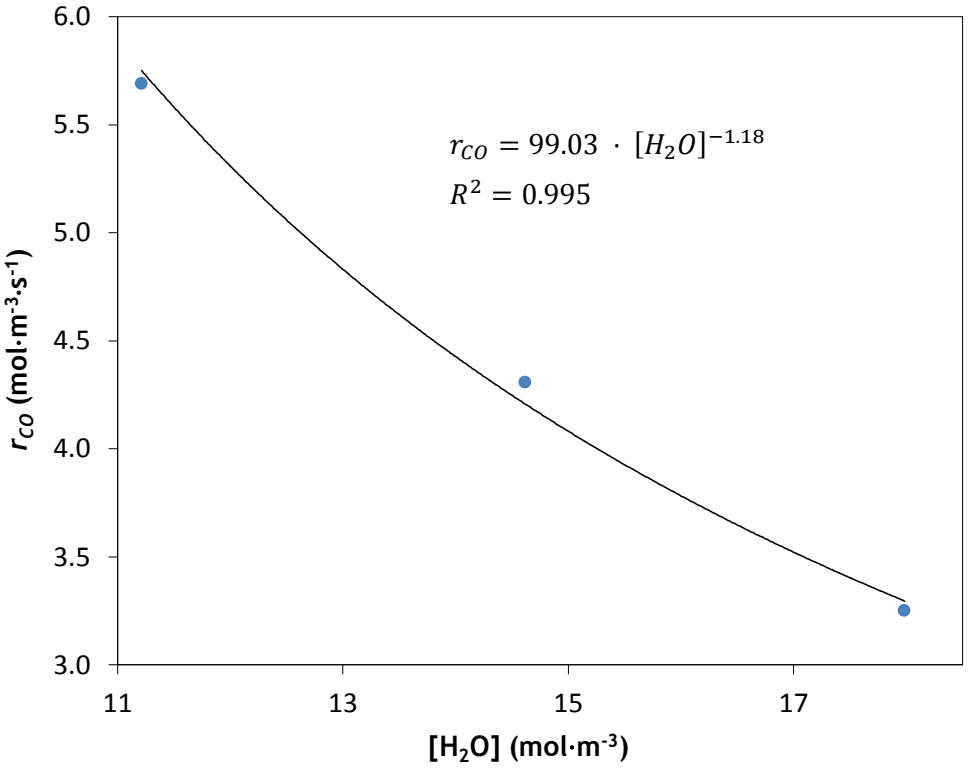

Figure D.5 - Determination of the apparent WGS reaction order for H_2O for the 0.5Pt/6CeTiO$_2$ catalyst at 275 ºC and 1 bar total pressure.

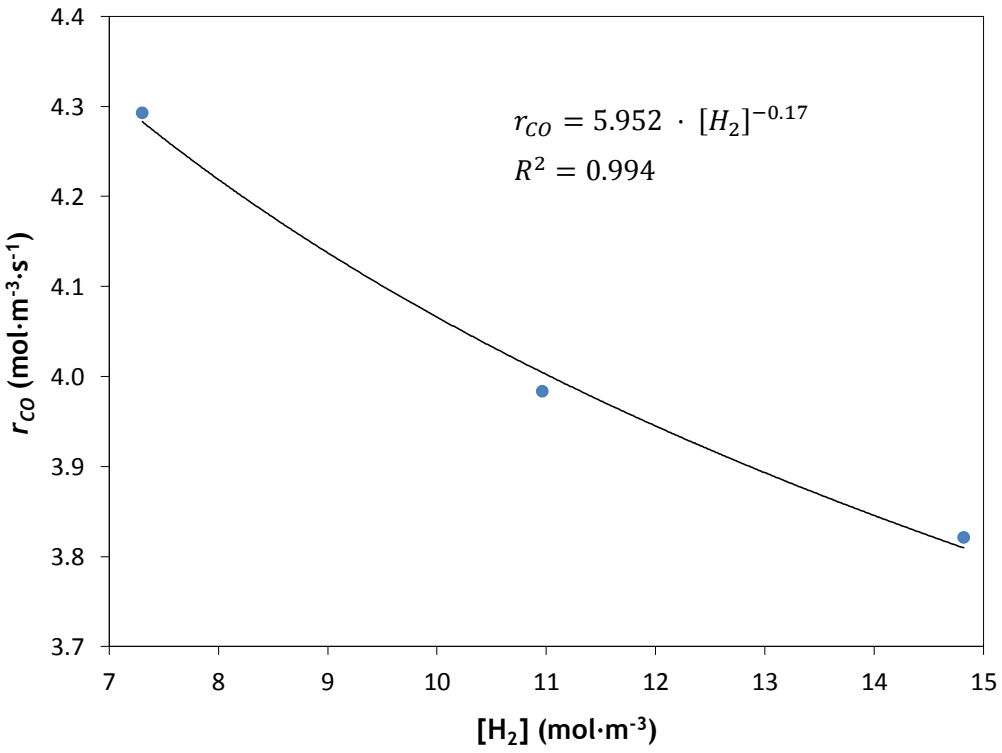

Figure D.6 - Determination of the apparent WGS reaction order for H_2 for the 0.5Pt/6CeTiO$_2$ catalyst at 275 ºC and 1 bar total pressure.

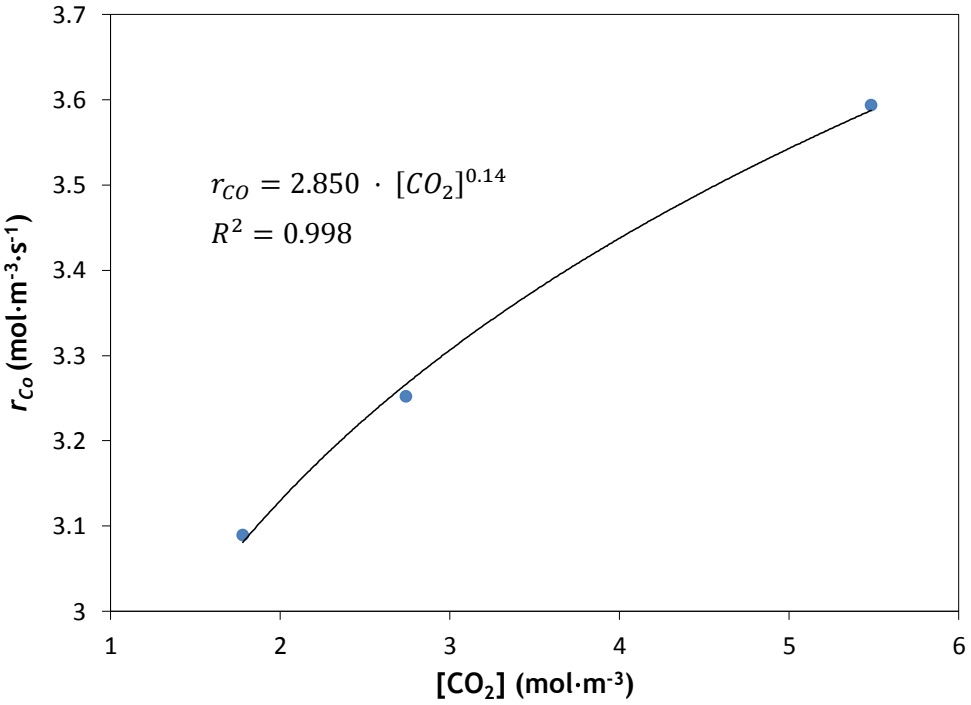

Figure D.7 - Determination of the apparent WGS reaction order for CO_2 for the 0.5Pt/6CeTiO$_2$ catalyst at 275 ºC and 1 bar total pressure.

In Table D.2 there are presented the apparent partial reaction orders obtained for the four components that participate in the WGS reaction.

Table D.2 - Apparent partial reaction orders obtained for the WGS reaction over the 0.5Pt/6CeTiO$_2$ catalyst at 275 ˚ and for a base volumetric composition of 5% CO, 7.5% CO_2, 40% H_2O and 35% H_2 balanced with N_2.

Reaction order			
CO[a]	**H_2O[b]**	**H_2[c]**	**CO_2[d]**
-0.23	-1.18	-0.17	0.14

[a] – Base volumetric composition except for CO (5-10%) and N_2 (balance).
[b] – Base volumetric composition except for H_2O (30-50%) and N_2 (balance).
[c] – Base volumetric composition except for H_2 (20-40%) and N_2 (balance).
[d] – Base volumetric composition except for CO_2 (5-15%) and N_2 (balance).

The apparent reaction orders were fitted to a power rate law expression as follows:

$$r = k\,[CO]^a[H_2O]^b[H_2]^c[CO_2]^d\,(1-\beta) \qquad \text{(D.1)}$$

where β that is the approach to equilibrium can be defined as follows:

$$\beta = \frac{[CO_2][H_2]}{K_{eq}[CO][H_2O]} \quad \text{(D.2)}$$

For each case the component concentration exponent obtained with the power type regression is the apparent WGS reaction order with respect to that component.

Appendix E – Verification of the Catalyst Activity

In order to know the catalytic activity for which each result was obtained, a specific test at specific conditions (base case) was performed every day before all the other WGS reaction measurements. The base case was performed at 350 °C, 3.5 bar in the retentate side and a sweep gas flow rate of 345 $mL_N \cdot min^{-1}$ in the permeate side. The GHSV was 14736 $L_N \cdot kg_{cat.}^{-1} \cdot h^{-1}$ and a 5.56% CO, 36.54% H_2O, 26.65% H_2 and 15.69% CO_2 balanced with N_2 volumetric feed composition was used. In Figure E.1 it is presented the conversion of CO obtained for the base case at the beginning of each day of the experimental campaign and for all the other tests performed in the respective days.

It can be seen day for the first two days of WGS experiments the activity of the catalyst was almost the same, while for the third day a decrease of almost 4% for the CO conversion of the base case was obtained. This might have influenced slightly the performance of the PBMR for the tests performed in the third day of experiments campaign (H_2O/CO ratios of 4.7 and 5.5). This lower activity could be simply explained by deactivation of the catalyst. However, there's another aspect that might have influenced this lower CO conversion. During the WGS tests, the steam that was going to the reactor was fed directly from the steam generator, which doesn't feed steam continuously. Because of this, sometimes it was difficult to obtain stable results, especially for lower flows of steam. It is then possible that this instability of the steam stream has caused this hypothetical apparent decrease of the catalyst activity. Furthermore before going to the reactor, the dry gas went to the steam tube and only went to the reactor when the pressure in the tube was higher than the one inside the reactor. This might have contributed as well to the instability of the steam stream fed to the reactor. Also, ideally this catalyst activity verification should be done in a PBR so that no hypothetical changes in the membrane would possibly affect the results obtained.

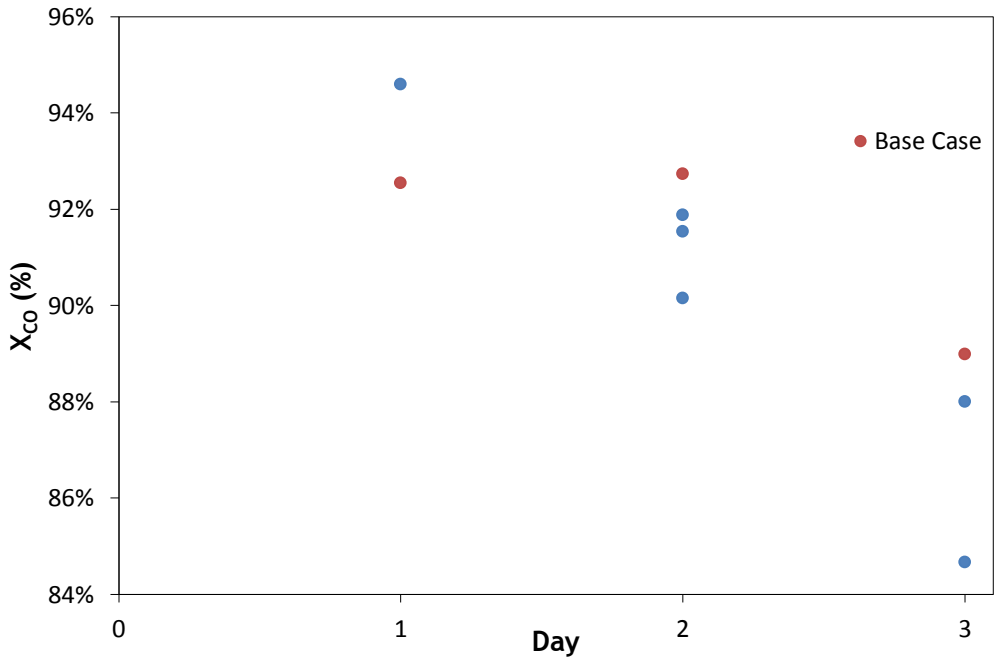

Figure E.1 - Conversion of CO obtained for the base case at the beginning of each day of the experimental campaign and for all the other measurements.

Appendix F – Determination of the Parameters of the Sieverts-Langmuir's Model Equation

In order to determine the parameters for the Sieverts-Langmuir's model equation the following equation for the correction factor was considered:

$$\text{Correction factor } (T,P) = \alpha(T)\frac{K_{CO}P_{CO}}{1+K_{CO}P_{CO}} = 1 - \frac{\text{S-L } H_2 \text{ permeance}}{\text{Sieverts } H_2 \text{ permeance}} \quad \text{(E.1)}$$

in which S-L H_2 permeance and Sieverts H_2 permeance are the permeances of the membrane to H_2 calculated using Sieverts-Langmuir's model equation in the presence of CO and Sieverts equation for a pure H_2 feed respectively. Initial values were attributed to both α and K_{CO} and the S-L H_2 permeance was calculated using equation B.1 for each CO partial pressure tested experimentally in section 3.1 at 400 °C. The relative error in the S-L H_2 permeance prediction over all the measurement points was then minimized in the independent parameters α and K_{CO} using the generalized reduced gradient nonlinear solving method of the solver tool of Microsoft Excel for a two parameter nonlinear unconstrained minimisation. Values of 0.6794 for α and 0.037 kPa^{-1} for K_{CO} were obtained after this minimisation procedure. For these values of the parameters, a minimum relative error of 1.13% was obtained. In Figure E.1 the variation of the H_2 permeance with the partial pressure of CO is presented and the comparison between the experimental data and the Sieverts-Langmuir model prediction is done.

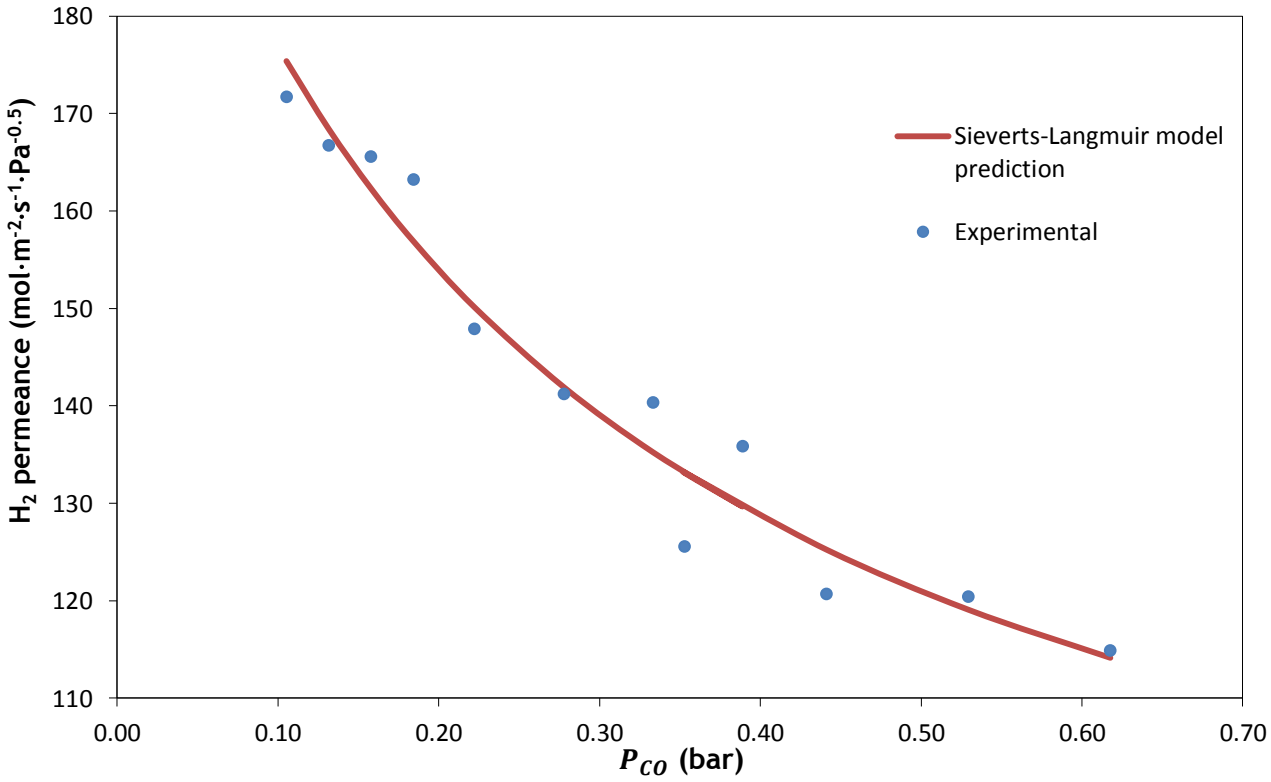

Figure F.1 - Relation between the H_2 permeance and the partial pressure of CO. Comparison between the experimental data and the Sieverts-Langmuir model prediction.

It is possible to see that there is a good agreement between the experimental data and the Sieverts-Langmuir model.

Appendix G – Quantification of the Impact of Both Concentration Polarization and CO Poisoning Effects on the Predicted H_2 flux through the Pd-Ag Membrane

With the aim of quantifying the impact of both CO poisoning and concentration polarization effects on the predicted H_2 flux through the Pd-Ag membrane, the following was done:

- The H_2 fluxes obtained with the 2D model with Sieverts-Langmuir's model equation were considered to be equal to the experimental ones at the same conditions;
- The H_2 fluxes obtained for the 1D and 2D models were then normalized.
- The difference between the normalized fluxes for the 1D model and the 2D model was considered to be due to concentration polarization and the difference between the normalized fluxes for the 2D model and the 2D model with the Sieverts-Langmuir's model equation was considered to be due to the CO poisoning effect on the Pd-Ag membrane;
- Finally, these differences were divided by the total flow difference between the 1D model and the 2D model with Sieverts-Langmuir's model equation and the relative H_2 permeating flux variations were obtained.

In Figures G.1, G.2 and G.3 there are presented the relative H_2 permeating flux variations due to the concentration polarization effect and the CO poisoning effect on the Pd-Ag membrane for different CO volumetric compositions in the feed and different H_2 partial pressure differences in the membrane. It is possible to conclude that for a constant H_2/CO feed composition, the concentration polarization effect becomes less noticed for increasing H_2 partial pressure differences in the membrane. This behavior is due to the fact that by increasing the partial pressure of H_2 in the retentate, the total pressure in the retentate increases as well and so a higher CO adsorption on the Pd-Ag membrane surface occurs. This higher adsorption of CO on the membrane leads to a higher decrease of the permeability of the membrane, thus decreasing the amount of H_2 that is transported from the gas bulk to the membrane wall and so a lower concentration polarization effect is observed. Also for increasing CO compositions the concentration polarization effect becomes less relevant while the poisoning effect of CO on the Pd-Ag membrane becomes more important. However, it can

be observed that for variations in the CO composition at lower CO concentrations the decrease of the concentration polarization effect is more noticeable than for equal variations at higher CO concentrations. This happens due to the higher adsorption of CO for lower concentrations and the consequent higher poisoning effect on the Pd-Ag membrane, as previously mentioned. Also, for higher CO concentrations the dilution effect (considered for both 1D and 2D models) starts gaining relevance over the membrane poisoning one.

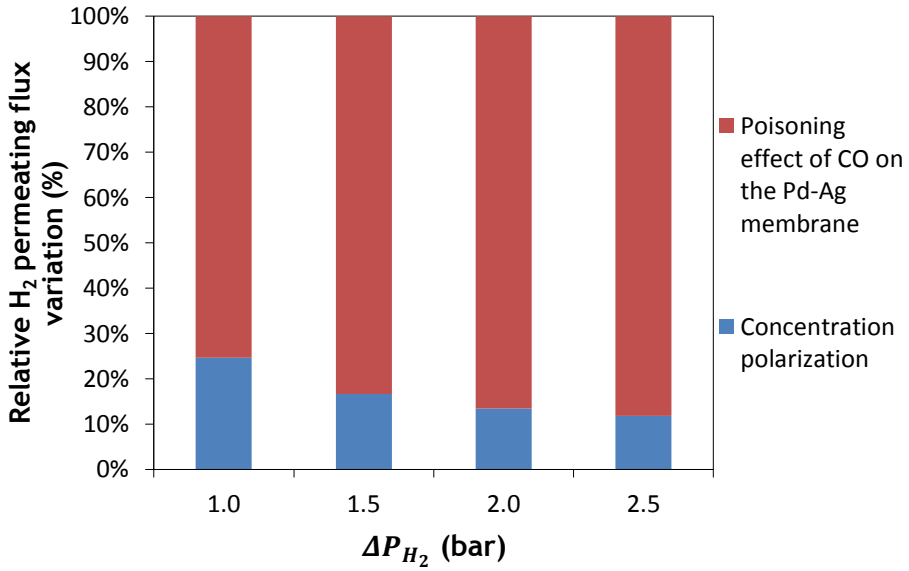

Figure G.1 - Relative effect of the concentration polarization and poisoning of the Pd-Ag membrane on the permeating flux of H_2 for a feed volumetric composition of 5% CO and 95% H_2 and different H_2 partial pressure differences in the membrane.

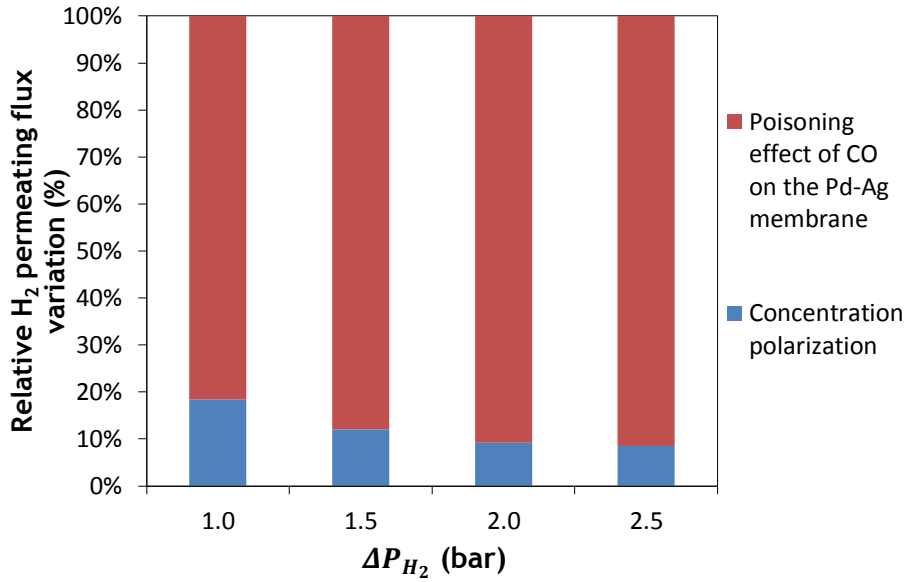

Figure G.2 - Relative effect of the concentration polarization and poisoning of the Pd-Ag membrane on the permeating flux of H_2 for a feed volumetric composition of 10% CO and 90% H_2 and different H_2 partial pressure differences in the membrane.

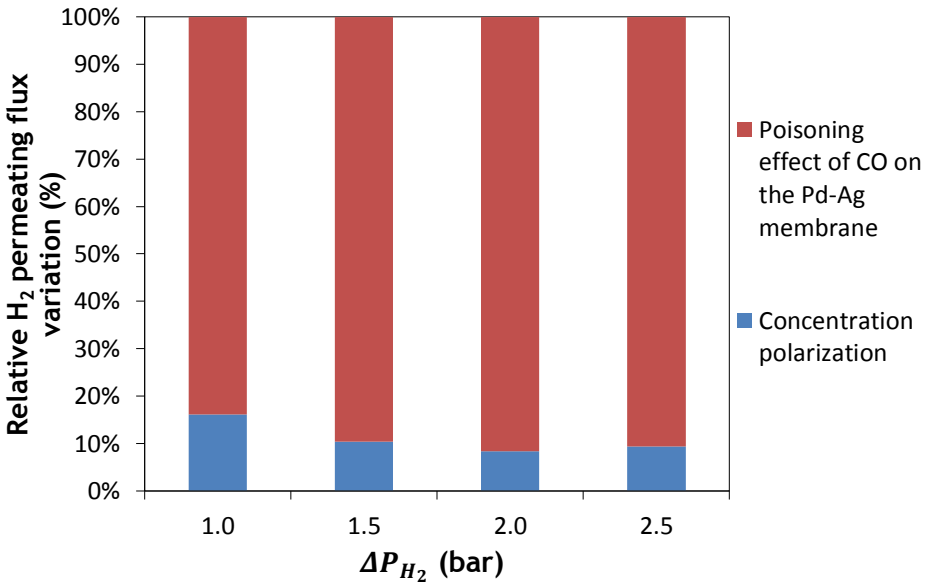

Figure G.3 - Relative effect of the concentration polarization and poisoning of the Pd-Ag membrane on the permeating flux of H_2 for a feed volumetric composition of 15% CO and 85% H_2 and different H_2 partial pressure differences in the membrane.